

Interpolation-Based Optimization for Enforcing ℓ_p -Norm Metric Differential Privacy in Continuous and Fine-Grained Domains

Chenxi Qiu

University of North Texas

Abstract

Metric Differential Privacy (mDP) generalizes Local Differential Privacy (LDP) by adapting privacy guarantees based on pairwise distances, enabling context-aware protection and improved utility. While existing optimization-based methods reduce utility loss effectively in coarse-grained domains, optimizing mDP in fine-grained or continuous settings remains challenging due to the computational cost of constructing dense perturbation matrices and satisfying pointwise constraints.

In this paper, we propose an *interpolation-based* framework for optimizing ℓ_p -norm mDP in such domains. Our approach optimizes perturbation distributions at a sparse set of anchor points and interpolates distributions at non-anchor locations via log-convex combinations, which provably preserve mDP. To address privacy violations caused by naive interpolation in high-dimensional spaces, we decompose the interpolation process into a sequence of one-dimensional steps and derive a corrected formulation that enforces ℓ_p -norm mDP by design. We further explore joint optimization over perturbation distributions and privacy budget allocation across dimensions. Experiments on real-world location datasets demonstrate that our method offers rigorous privacy guarantees and competitive utility in fine-grained domains, outperforming baseline mechanisms.

1 Introduction

Privacy-preserving data sharing is increasingly important in applications such as location-based services (LBSs), mobility prediction, and user modeling. These applications highly depend on fine-grained data representations, which are also required to comply with stringent privacy constraints. Standard mechanisms like *Local Differential Privacy (LDP)* [15] enforce uniform privacy across all input pairs, often introducing excessive noise and degrading utility, especially in spatial, continuous, or structured domains. *Metric Differential Privacy (mDP)* [9] addresses this limitation by relaxing LDP

through a distance-aware formulation: It requires stronger indistinguishability for nearby records and permits weaker guarantees for distant ones. This flexibility enables improved privacy-utility trade-offs and has been applied to protect geo-location data [3], word embeddings [20], speech [22], and image data [13, 16].

Since the introduction of mDP [9], numerous *pre-defined noise mechanisms* have been proposed to enforce distance-based privacy guarantees. Notably, the planar Laplace mechanism [3] achieves ℓ_2 -based geo-indistinguishability by adding two-dimensional noise scaled to the sensitivity of location queries, while the Exponential Mechanism (EM) [11] selects outputs based on a fixed utility function that favors locations closer to the true input. These methods are efficient and well-suited for continuous and fine-grained domains. However, their fixed noise distributions often lead to suboptimal privacy-utility trade-offs, as they fail to account for direction-dependent or context-specific variations in utility.

To address the limitations of pre-defined noise mechanisms, recent work has explored *optimization-based* approaches, most notably *linear programming (LP)*, to directly optimize the perturbation distribution by minimizing expected utility loss subject to mDP constraints [6, 23, 29]. However, LP-based formulations are typically restricted to coarse-grained domains: solving them over continuous or fine-grained spaces is computationally prohibitive. A common workaround is to discretize the domain (e.g., using uniform grids or road-map features), which improves tractability but weakens formal guarantees: discretization can overestimate distances between nearby records, thereby loosening the effective mDP constraints and overlooking fine-grained privacy leakage [10].

To balance utility and efficiency, hybrid methods combine optimization with pre-defined noise. For instance, *Bayesian remapping* [10] post-processes outputs of a fixed mechanism via Bayes' rule to improve utility; *ConstOPT* [23] and *LR-Geo* [30] reduce complexity by constraining the search space (e.g., locality- or structure-aware parameterizations). Nonetheless, these approaches have notable limitations: Bayesian remapping depends on fixed noise priors and cannot guarantee

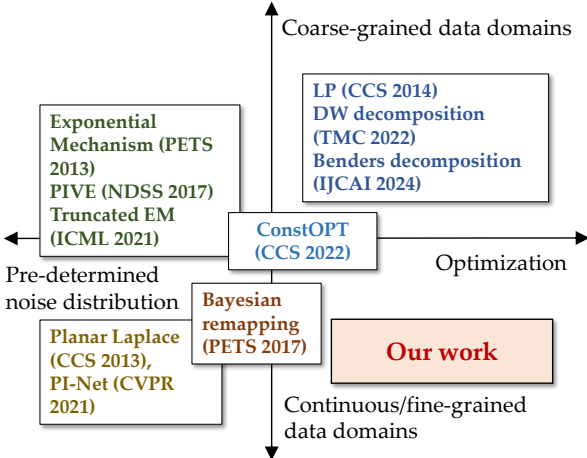


Figure 1: Related works vs. our work.

Example works in the figure: EM [9], Planar Laplace [3], LP [6], PI-Net (Laplace) [13], PIVE (EM-based) [37], Danzig-Wolfe (DW) decomposition (LP-based) [31], Benders decomposition (LP-based) [29], ConstOPT (EM+LP) [23], Bayesian Remapping [10], Truncated EM [8].

tee global optimality, while ConstOPT and LR-Geo *still incur* substantial computational overhead and remain tied to discretization, which limits scalability and can compromise strict mDP enforcement in fine-grained or continuous domains.

Fig. 1 situates prior mDP methods along two axes, domain granularity and mechanism design, and shows that most either (i) rely on pre-defined perturbation distributions suited to continuous spaces or (ii) perform optimization only after coarse discretization. This reveals a clear gap: scalable, optimization-based mechanisms that operate efficiently in continuous/fine-grained domains.

Our contributions. In this paper, we take a first step toward addressing this gap by introducing a new *interpolation-based* framework for optimizing mDP in continuous or fine-grained domains under general ℓ_p -norm distance metrics (e.g., ℓ_1 , ℓ_2 , ℓ_∞). The flexibility of ℓ_p -norms allows our method to accommodate diverse applications. Our framework consists of three main steps: (1) partitioning the N -dimensional secret domain into disjoint cells and selecting their corners as *anchor records* to approximate the full domain; (2) solving an *Anchor Perturbation Optimization (APO)* problem to compute the optimal perturbation probabilities at these anchor points; and (3) interpolating the perturbation probabilities for non-anchor records using a *log-convex function*, specifically a weighted geometric mean of the anchor probabilities, which ensures smooth and privacy-preserving transitions across the domain.

Naively applying log-convex interpolation in high dimensions does not by itself enforce ℓ_p -mDP: because the ℓ_p norm is convex for $p \geq 1$, combining anchor-wise bounds during

interpolation can enlarge the effective distance and thus violate the *global Lipschitz condition* required by mDP [24]. We avoid this by decomposing the N -dimensional interpolation into axis-aligned, one-dimensional log-convex steps (**Definition 3**). For each axis we establish a one-dimensional Lipschitz bound (**Propositions 1–2**), then distribute a total privacy budget across coordinates using a dimension-wise composition rule (**Theorem 1**; e.g., $\sum_\ell \epsilon_\ell^{p/(p-1)} \leq \epsilon^{p/(p-1)}$ for $p > 1$). We combine the per-axis interpolants through a product construction (**Definition 6**) and show that the resulting mechanism satisfies a global Lipschitz guarantee with respect to the ℓ_p metric (**Theorem 2**). After normalization, this yields a valid high-dimensional perturbation mechanism that preserves the target mDP guarantee up to a small constant-factor slack quantified in our analysis.

Moreover, to minimize utility loss within this framework, we formulate the *Anchor Perturbation Optimization (APO)* problem, which jointly optimizes the perturbation probabilities at anchor points and the allocation of dimension-wise privacy budgets. Due to the non-convex nature of the APO objective, we propose a tractable linear approximation, termed *Approx-APO*, and provide theoretical bounds on its optimality gap relative to the original formulation.

We evaluate our method on real-world road network datasets from Rome, New York City, and London [1], considering both the ℓ_2 norm (Euclidean distance) and the ℓ_1 norm (Manhattan distance) for measuring spatial proximity. Experimental results show that our approach enforces strictly stronger privacy guarantees (0% mDP violations) than coarse-grained LP-based mechanisms [6, 23], while consistently achieving lower utility loss compared to pre-defined noise mechanisms (e.g., EM [8, 11], Laplace [3], and *Truncated EM* [8]), and hybrid methods (e.g., ConstOPT [23] and Bayesian remapping [10]).

Our main contribution can be summarized as follows:

- ▷ We propose a novel interpolation-based framework for enforcing ℓ_p -norm mDP in continuous and fine-grained domains, bridging the gap between rigorous privacy guarantees and practical utility.
- ▷ We introduce a dimension-wise composition strategy for ℓ_p -mDP and design a log-convex interpolation mechanism, proving its theoretical validity under (ϵ, d_p) -mDP (**Theorems 1–2** and **Proposition 3**).
- ▷ We formulate the *Anchor Perturbation Optimization (APO)* problem, which jointly optimizes anchor perturbations and privacy budget allocation, and propose a linear approximation with provable optimality bounds.
- ▷ Across mobility datasets from Rome, New York City, and London, our method shows zero observed mDP violations in fine-grained settings and consistently achieves lower utility loss than competing approaches.

The remainder of the paper is organized as follows. Section 2 introduces the preliminaries of mDP optimization. Section 3 outlines the overall framework, while Sections 4 and 5 present the algorithmic design for one-dimensional and multi-dimensional interpolation, respectively. Section 6 evaluates the performance of the proposed algorithm. Section 7 discusses related work, and Section 8 concludes the paper.

2 Preliminaries

In this section, we introduce the *formal definition* of the ℓ_p -norm mDP (Section 2.2), describe the *perturbation optimization framework* (Section 2.2), and highlight the *limitations* of existing optimization-based approaches (Section 2.3). A summary of the key notations used throughout the paper is provided in Appendix A.

2.1 ℓ_p -norm mDP

Local Differential Privacy (LDP) enforces the same level of *indistinguishability* for every pair of inputs, regardless of how similar they are [15]. *Metric differential privacy* (mDP), also called *Lipschitz privacy* [24], d_X -privacy [18], or *smooth DP* [14], generalizes this idea by tying the privacy guarantee to a distance over the input space: nearby inputs must be harder to distinguish than far-apart ones. Originally proposed for location privacy [3], mDP naturally extends to high-dimensional continuous domains via distance-aware privacy control.

We consider a continuous (or fine-grained) secret domain $\mathcal{X} \subseteq \mathbb{R}^N$, where each record $\mathbf{x}_a \in \mathcal{X}$ is a vector $\mathbf{x}_a = [x_{a,1}, \dots, x_{a,N}]$. Similarity between $\mathbf{x}_a, \mathbf{x}_b \in \mathcal{X}$ is measured by the ℓ_p distance

$$d_p(\mathbf{x}_a, \mathbf{x}_b) := \left(\sum_{\ell=1}^N |x_{a,\ell} - x_{b,\ell}|^p \right)^{1/p}, \quad (1)$$

which yields a flexible family of metrics (e.g., $\ell_1, \ell_2, \ell_\infty$) to capture task-specific sensitivity.

Definition 1 (Lipschitz bound and continuity w.r.t. d_p). *Let $f : \mathcal{X} \rightarrow \mathbb{R}$ and let d_p be the ℓ_p distance on \mathbb{R}^N with $p \in [1, \infty]$. We say f satisfies an (ϵ, d_p) -Lipschitz bound between $\mathbf{x}_a, \mathbf{x}_b \in \mathcal{X}$ if*

$$|f(\mathbf{x}_a) - f(\mathbf{x}_b)| \leq \epsilon d_p(\mathbf{x}_a, \mathbf{x}_b). \quad (2)$$

we say f is (ϵ, d_p) -Lipschitz continuous if the bound in (2) holds for all $\mathbf{x}_a, \mathbf{x}_b \in \mathcal{X}$.

Definition 2 $((\epsilon, d_p)$ -metric differential privacy (mDP)). *Let $\mathcal{X} \subseteq \mathbb{R}^N$ be the secret (input) domain and let \mathcal{Y} denote the perturbation (output) domain. A randomized mechanism $\mathcal{M} : \mathcal{X} \rightarrow \mathcal{Y}$ is said to satisfy (ϵ, d_p) -mDP (or ℓ_p -norm mDP) if,*

▷ for each element $\mathbf{y} \in \mathcal{Y}$, the log-probability function $f_{\mathbf{y}}(\mathbf{x}) := \ln \Pr[\mathcal{M}(\mathbf{x}) = \mathbf{y}]$ of the output is (ϵ, d_p) -Lipschitz continuous, i.e., $\forall \mathbf{x}_a, \mathbf{x}_b \in \mathcal{X}$

$$|\ln \Pr[\mathcal{M}(\mathbf{x}_a) = \mathbf{y}] - \ln \Pr[\mathcal{M}(\mathbf{x}_b) = \mathbf{y}]| \leq \epsilon d_p(\mathbf{x}_a, \mathbf{x}_b), \quad (3)$$

▷ and $\forall \mathbf{x} \in \mathcal{X}$, the normalization constraint of its perturbation probability is satisfied, i.e.,

$$\sum_{\mathbf{y} \in \mathcal{Y}} \Pr[\mathcal{M}(\mathbf{x}) = \mathbf{y}] = 1. \quad (4)$$

Threat Model. We assume an adversary that observes the obfuscated output $\mathbf{y} \in \mathcal{Y}$ released by the mechanism \mathcal{M} and attempts to infer the user's true input $\mathbf{x} \in \mathcal{X}$. The adversary may have arbitrary auxiliary knowledge about the domain \mathcal{X} (e.g., road networks, prior distributions) and the mechanism \mathcal{M} , but does not control \mathcal{M} . The (ϵ, d_p) -mDP guarantee ensures that the likelihood ratio between any two possible inputs $\mathbf{x}_a, \mathbf{x}_b$ is bounded in proportion to their distance $d_p(\mathbf{x}_a, \mathbf{x}_b)$, thereby limiting the adversary's ability to distinguish between nearby inputs.

2.2 Perturbation Discretization and Optimization

While pre-defined noise mechanisms can enforce mDP over continuous domains, they do not explicitly optimize for utility. Optimization-based methods address this by minimizing utility loss, but exact solutions in continuous or fine-grained spaces are computationally intractable. To enable tractable optimization, prior work discretizes the input domain into a finite set of representative points. For instance, [6, 33] partition geographic regions into uniform grids and represent each cell by its centroid. Similarly, [29, 31] project raw locations onto road network features (e.g., intersections and junctions) to define a discrete optimization space.

Formally, let $\hat{\mathcal{X}} \subset \mathcal{X}$ denote the finite set of representative records obtained by discretizing the continuous domain \mathcal{X} . Let $p(\mathbf{x})$ be the prior distribution over \mathcal{X} , representing the probability that the secret record is located at $\mathbf{x} \in \mathcal{X}$. We consider the case that perturbation domain \mathcal{Y} is discrete, and model the randomized mechanism \mathcal{M} as a stochastic *perturbation matrix* $\mathbf{Z} = \{z(\mathbf{y}_k \mid \hat{\mathbf{x}}_i)\}_{(\hat{\mathbf{x}}_i, \mathbf{y}_k) \in \hat{\mathcal{X}} \times \mathcal{Y}}$, where each entry $z(\mathbf{y}_k \mid \hat{\mathbf{x}}_i)$ denotes the probability of reporting output $\mathbf{y}_k \in \mathcal{Y}$ given input $\hat{\mathbf{x}}_i \in \hat{\mathcal{X}}$, i.e., $z(\mathbf{y}_k \mid \hat{\mathbf{x}}_i) = \Pr[\mathcal{M}(\hat{\mathbf{x}}_i) = \mathbf{y}_k]$. The Lipschitz bound constraint in Eq. (3) is then enforced over all pairs of records in the discretized domain $\hat{\mathcal{X}}$, and corresponds to the following set of linear constraints:

$$z(\mathbf{y}_k \mid \hat{\mathbf{x}}_i) - e^{\epsilon d_p(\hat{\mathbf{x}}_i, \hat{\mathbf{x}}_j)} z(\mathbf{y}_k \mid \hat{\mathbf{x}}_j) \leq 0, \quad \forall \hat{\mathbf{x}}_i, \hat{\mathbf{x}}_j \in \hat{\mathcal{X}}, \forall \mathbf{y}_k \in \mathcal{Y}. \quad (5)$$

We define $\mathcal{L}(\hat{\mathbf{x}}_i, \mathbf{y}_k)$ as the utility loss incurred when the mechanism reports \mathbf{y}_k while the true input lies in the region of \mathcal{X}

represented by the discretized point $\hat{\mathbf{x}}_i$; let $p(\hat{\mathbf{x}}_i)$ denote the prior probability that the true input lies in that region (i.e., the probability mass of the cell corresponding to $\hat{\mathbf{x}}_i$, with $\sum_i p(\hat{\mathbf{x}}_i) = 1$). Then, the expected utility loss caused by the perturbation matrix \mathbf{Z} can be represented by

$$\mathcal{L}(\mathbf{Z}) = \sum_{\hat{\mathbf{x}}_i \in \hat{\mathcal{X}}} \sum_{\mathbf{y}_k \in \mathcal{Y}} p(\hat{\mathbf{x}}_i) z(\mathbf{y}_k | \hat{\mathbf{x}}_i) \mathcal{L}(\hat{\mathbf{x}}_i, \mathbf{y}_k). \quad (6)$$

Consequently, the goal of the *mDP optimization* problem is to minimize the expected utility loss $\mathcal{L}(\mathbf{Z})$ subject to the constraints imposed by mDP (*Lipschitz bound* and *normalization* constraints). This can be formulated as the following *linear programming (LP)* problem:

$$\min \quad \mathcal{L}(\mathbf{Z}) \quad (7)$$

$$\text{s.t.} \quad z(\mathbf{y}_k | \hat{\mathbf{x}}_i) - e^{\epsilon d_p(\hat{\mathbf{x}}_i, \hat{\mathbf{x}}_j)} z(\mathbf{y}_k | \hat{\mathbf{x}}_j) \leq 0, \quad (8)$$

$$\forall \hat{\mathbf{x}}_i, \hat{\mathbf{x}}_j \in \hat{\mathcal{X}}, \forall \mathbf{y}_k \in \mathcal{Y} \text{ (Lipschitz bound)}$$

$$\sum_{\mathbf{y}_k \in \mathcal{Y}} z(\mathbf{y}_k | \hat{\mathbf{x}}_i) = 1, \forall \hat{\mathbf{x}}_i \in \hat{\mathcal{X}} \text{ (Normalization)} \quad (9)$$

$$z(\mathbf{y}_k | \hat{\mathbf{x}}_i) \geq 0, \forall \hat{\mathbf{x}}_i \in \hat{\mathcal{X}}, \forall \mathbf{y}_k \in \mathcal{Y} \quad (10)$$

where the *non-negativity constraint* in Eq. (10) enforces that each individual probability is non-negative [32].

2.3 Limitations of Discretization-Based mDP Enforcement

While discretization-based methods significantly reduce the computational cost of solving LPs, they do not ensure strict compliance with mDP in continuous domains or high-resolution settings. The key limitation arises from distance overestimation: discretized representative points (e.g., grid cell centers) may misrepresent the true distance between original inputs, especially when records lie near cell boundaries. This can lead to relaxed mDP constraints that are satisfied by the mechanism, but fail to hold for the underlying continuous/fine-grained domain.

Fig. 2 illustrates this limitation. Suppose that a user moves from location \mathbf{x}_a to a nearby location \mathbf{x}_b in an adjacent grid cell, and let $\hat{\mathbf{x}}_i$ and $\hat{\mathbf{x}}_j$ denote the corresponding cell centers. Prior methods [6, 28, 33] discretize the domain by approximating each location with its cell center, so that $\Pr[\mathcal{M}(\mathbf{x}) = \mathbf{y}] = \Pr[\mathcal{M}(\hat{\mathbf{x}}) = \mathbf{y}]$, and they enforce $\frac{\Pr[\mathcal{M}(\hat{\mathbf{x}}_i) = \mathbf{y}]}{\Pr[\mathcal{M}(\hat{\mathbf{x}}_j) = \mathbf{y}]} \leq e^{\epsilon d_p(\hat{\mathbf{x}}_i, \hat{\mathbf{x}}_j)}, \forall \mathbf{y} \in \mathcal{Y}$. However, near cell boundaries one typically has $d_p(\hat{\mathbf{x}}_i, \hat{\mathbf{x}}_j) > d_p(\mathbf{x}_a, \mathbf{x}_b)$. Thus, the center-based enforcement is *weaker* than the true constraint: $\frac{\Pr[\mathcal{M}(\mathbf{x}_a) = \mathbf{y}]}{\Pr[\mathcal{M}(\mathbf{x}_b) = \mathbf{y}]} \leq e^{\epsilon d_p(\mathbf{x}_a, \mathbf{x}_b)}$ in Definition 2. Consequently, there may exist some \mathbf{y} such that $\frac{\Pr[\mathcal{M}(\mathbf{x}_a) = \mathbf{y}]}{\Pr[\mathcal{M}(\mathbf{x}_b) = \mathbf{y}]} \leq e^{\epsilon d_p(\hat{\mathbf{x}}_i, \hat{\mathbf{x}}_j)}$ but $> e^{\epsilon d_p(\mathbf{x}_a, \mathbf{x}_b)}$, which violates the Lipschitz bound between the true locations \mathbf{x}_a and \mathbf{x}_b . In essence, mDP requires that small changes in the input domain induce only $e^{\epsilon d_p}$ -bounded changes in output probabilities, an invariant that coarse discretization may fail to preserve.

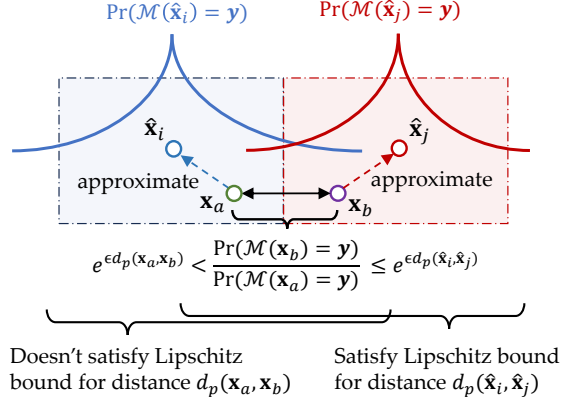


Figure 2: mDP based on approximated distance.

3 Framework

In this section, we introduce our interpolation-based framework for optimizing perturbation mechanisms under ℓ_p -norm mDP in continuous or fine-grained secret domains. As illustrated in Fig. 3, the framework consists of three main steps:

- ① **Domain partitioning:** The secret domain \mathcal{X} is partitioned into cells, with anchor records placed at each cell corner to serve as representative inputs for optimization.
- ② **Anchor perturbation optimization:** Perturbation distributions are optimized at anchor locations to minimize expected utility loss, subject to mDP constraints over the anchor set.
- ③ **Perturbation interpolation:** For non-anchor records, perturbation probabilities are inferred via interpolation from anchor distributions, while preserving mDP guarantees.

Intuition behind interpolation design. In Step ③, let \mathcal{C}_m denote a cell in the partitioned domain, and let $\hat{\mathcal{X}}_m$ denote the set of anchor points within \mathcal{C}_m . Suppose the perturbation distributions at these anchor points, denoted by $\mathbf{Z}_{\hat{\mathcal{X}}_m} = \{z(\mathbf{y}_k | \hat{\mathbf{x}}_j)\}_{(\hat{\mathbf{x}}_j, \mathbf{y}_k) \in \hat{\mathcal{X}}_m \times \mathcal{Y}}$, have already been optimized. The goal of the interpolation function f_{int} is to assign perturbation probabilities to each non-anchor record $\mathbf{x}_a \in \mathcal{C}_m$ such that mDP is satisfied between \mathbf{x}_a and any other record in the domain \mathcal{X} .

As defined by the Lipschitz bound (Eq. (3) in Definition 2), (ϵ, d_p) -mDP requires that the *log-probability* of outputs varies at most linearly with the ℓ_p -distance between inputs. This motivates the use of *log-convex interpolation*, which linearly interpolates log-probabilities to ensure smooth transitions in the output distribution. As a natural first attempt, we define the log-probability at a non-anchor point $\mathbf{x}_a \in \mathcal{C}_m$ as a convex combination of those at the anchor points:

$$\ln z(\mathbf{y}_k | \mathbf{x}_a) = \sum_{\hat{\mathbf{x}} \in \hat{\mathcal{X}}_m} \lambda_{\hat{\mathbf{x}}, \mathbf{x}_a} \ln z(\mathbf{y}_k | \hat{\mathbf{x}}),$$

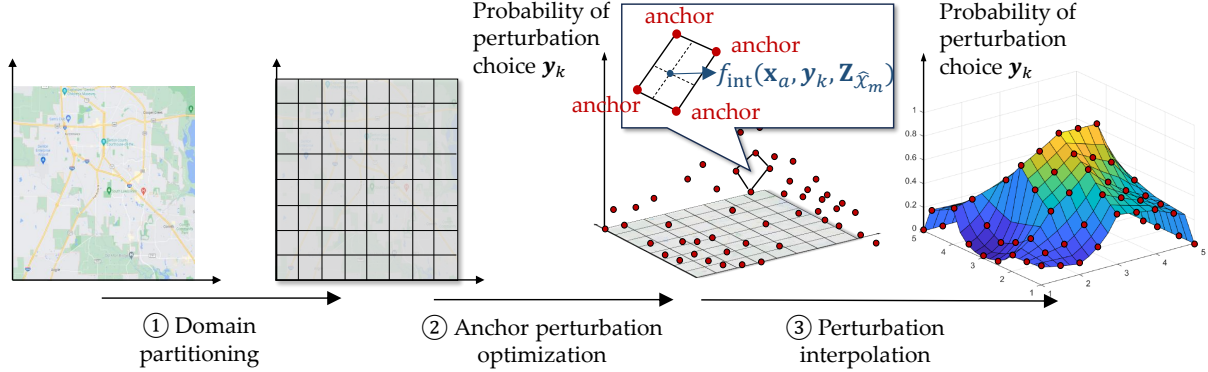


Figure 3: Framework of our method

where the convex coefficients $\lambda_{\hat{\mathbf{x}}, \mathbf{x}_a} \geq 0$ sum to one and reflect the relative position of \mathbf{x}_a within \mathcal{C}_m . Ideally, such interpolation would preserve mDP, i.e., if a reference point \mathbf{x}_b satisfies mDP with respect to each anchor in $\hat{\mathcal{X}}_m$, then it should also satisfy mDP with respect to the interpolated point \mathbf{x}_a . Formally, we would desire:

$$\underbrace{\left| \sum_{\hat{\mathbf{x}} \in \hat{\mathcal{X}}_m} \lambda_{\hat{\mathbf{x}}, \mathbf{x}_a} \ln z(\mathbf{y}_k | \hat{\mathbf{x}}) - \ln z(\mathbf{y}_k | \mathbf{x}_b) \right|}_{\text{Interpolated probability for } \mathbf{x}_a} \leq \varepsilon \cdot d_p(\mathbf{x}_a, \mathbf{x}_b). \quad (11)$$

However, this inequality does not generally hold in high dimensions due to the convexity of the ℓ_p -norm for $p \geq 1$. Specifically, the convex combination of anchor distances $\sum \lambda_{\hat{\mathbf{x}}, \mathbf{x}_a} d_p(\hat{\mathbf{x}}, \mathbf{x}_b)$ may exceed $d_p(\mathbf{x}_a, \mathbf{x}_b)$, leading to interpolated log-probabilities that violate the Lipschitz bound required by mDP. A formal analysis of this problem is provided in [Appendix E.1](#).

To overcome this issue, we factor the N -dimensional interpolation into a sequence of *one-dimensional, log-convex interpolations*, applied independently along each coordinate axis. In one dimension, the Lipschitz bound in Eq. (11) holds exactly (i.e., for $N = 1$), as formally established in [Propositions 1](#) and [2](#). We then construct the N -dimensional mechanism by multiplicatively composing the per-axis interpolators in [Definition 5](#) and normalizing to obtain a valid joint perturbation distribution in [Definition 6](#). The correctness of this composition is established by [Theorem 2](#) and [Proposition 3](#), which respectively show that the resulting mechanism is (ε, d_p) -Lipschitz continuous and satisfies (ε, d_p) -mDP over the entire N -dimensional domain \mathcal{X} .

Next, we first introduce the one-dimensional interpolation primitive in [Section 4](#), and then extend this construction to the multi-dimensional setting in [Section 5](#), following the three-step procedure outlined in Fig. 3 (Steps ①–③).

4 One-Dimensional Interpolation and Privacy Composition

Definition 3 (One-Dimensional Log-Convex Interpolation). Let $\mathbf{x}_i, \mathbf{x}_{i'} \in \mathcal{X}$ be two records that differ only in their ℓ th coordinate, with $x_{i',\ell} = x_{i,\ell} + \Delta_\ell$ for some $\Delta_\ell > 0$. For any intermediate point \mathbf{x}_a such that $x_{a,\ell} \in [x_{i,\ell}, x_{i',\ell}]$ and all other coordinates match \mathbf{x}_i and $\mathbf{x}_{i'}$, define the convex coefficient $\lambda_{\mathbf{x}_i, \mathbf{x}_a}^\ell = \frac{x_{i',\ell} - x_{a,\ell}}{x_{i',\ell} - x_{i,\ell}}$. Then, the log-probability at \mathbf{x}_a is given by the log-convex interpolation:

$$\ln z(\mathbf{y}_k | \mathbf{x}_a) = \lambda_{\mathbf{x}_i, \mathbf{x}_a}^\ell \ln z(\mathbf{y}_k | \mathbf{x}_i) + (1 - \lambda_{\mathbf{x}_i, \mathbf{x}_a}^\ell) \ln z(\mathbf{y}_k | \mathbf{x}_{i'}), \quad (12)$$

which is written as $z(\mathbf{y}_k | \mathbf{x}_a) \xrightarrow{\text{logcvx}} (z(\mathbf{y}_k | \mathbf{x}_i), z(\mathbf{y}_k | \mathbf{x}_{i'}))$.

In [Propositions 1](#) and [2](#), we prove that the interpolation mechanism preserves (ε_ℓ, d_1) -Lipschitz continuity; that is, it is (ε_ℓ, d_1) -Lipschitz within each one-dimensional interval and across adjacent intervals.

Proposition 1 (Intra-Interval Validity). Let \mathbf{x}_i and $\mathbf{x}_{i'}$ be two records that differ only in their ℓ th coordinate, with $x_{i,\ell} < x_{i',\ell}$, and suppose their corresponding log-perturbation probabilities $\ln z(\mathbf{y}_k | \mathbf{x}_i)$ and $\ln z(\mathbf{y}_k | \mathbf{x}_{i'})$ satisfy the (ε, d_1) -Lipschitz bound. Then, for any $\mathbf{x}_a, \mathbf{x}_b \in \mathcal{X}$ such that $x_{a,\ell}, x_{b,\ell} \in [x_{i,\ell}, x_{i',\ell}]$ and all other coordinates are identical to those of \mathbf{x}_i , if the interpolated values $\hat{z}(\mathbf{y}_k | \mathbf{x}_a)$ and $\hat{z}(\mathbf{y}_k | \mathbf{x}_b)$ are calculated by

$$\hat{z}(\mathbf{y}_k | \mathbf{x}_a) \xrightarrow{\text{logcvx}} (z(\mathbf{y}_k | \mathbf{x}_i), z(\mathbf{y}_k | \mathbf{x}_{i'})), \quad (13)$$

$$\hat{z}(\mathbf{y}_k | \mathbf{x}_b) \xrightarrow{\text{logcvx}} (z(\mathbf{y}_k | \mathbf{x}_i), z(\mathbf{y}_k | \mathbf{x}_{i'})), \quad (14)$$

then $\ln \hat{z}(\mathbf{y}_k | \mathbf{x}_a)$ and $\ln \hat{z}(\mathbf{y}_k | \mathbf{x}_b)$ also satisfy the (ε, d_1) -Lipschitz bound between \mathbf{x}_a and \mathbf{x}_b . This property is illustrated in Fig. 4(a).

Proposition 2 (Across-Interval Validity). Let $\mathbf{x}_i, \mathbf{x}_{i'}, \mathbf{x}_j, \mathbf{x}_{j'}$ be four records that differ only in their ℓ th coordinate, with

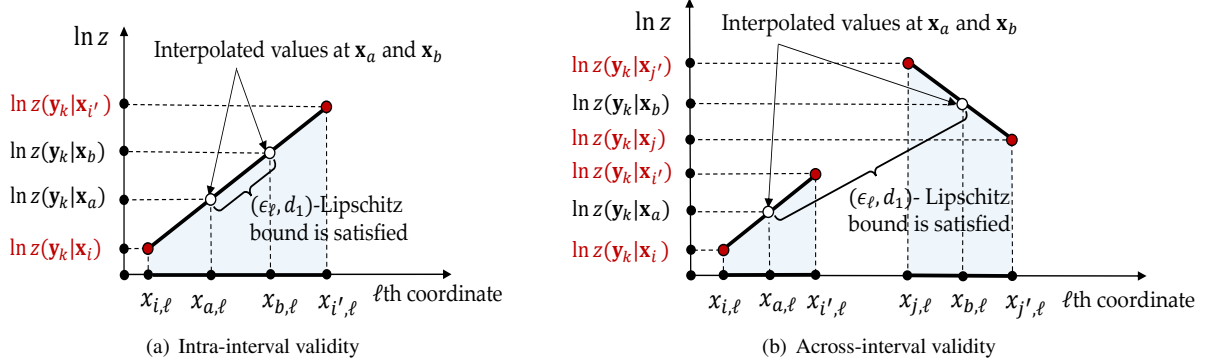


Figure 4: Illustration of Proposition 1 and Proposition 2.

$x_{i,\ell} < x_{i',\ell} \leq x_{a,\ell} < x_{b,\ell} < x_{j',\ell}$. Suppose that each pair of log-perturbation probabilities $\ln z(\mathbf{y}_k | \mathbf{x}_i)$, $\ln z(\mathbf{y}_k | \mathbf{x}_{i'})$, $\ln z(\mathbf{y}_k | \mathbf{x}_j)$, and $\ln z(\mathbf{y}_k | \mathbf{x}_{j'})$ satisfy (ϵ, d_1) -Lipschitz bound.

Let \mathbf{x}_a and \mathbf{x}_b be two additional records that differ from the above four points only in the ℓ th coordinate, with $x_{a,\ell} \in [x_{i,\ell}, x_{i',\ell}]$ and $x_{b,\ell} \in [x_{j,\ell}, x_{j',\ell}]$. If the corresponding interpolated values $\hat{z}(\mathbf{y}_k | \mathbf{x}_a)$ and $\hat{z}(\mathbf{y}_k | \mathbf{x}_b)$ are defined via log-convex interpolation as:

$$\hat{z}(\mathbf{y}_k | \mathbf{x}_a) \xrightarrow{\text{logcvx}} (\ln z(\mathbf{y}_k | \mathbf{x}_i), \ln z(\mathbf{y}_k | \mathbf{x}_{i'})) \quad (15)$$

$$\hat{z}(\mathbf{y}_k | \mathbf{x}_b) \xrightarrow{\text{logcvx}} (\ln z(\mathbf{y}_k | \mathbf{x}_j), \ln z(\mathbf{y}_k | \mathbf{x}_{j'})), \quad (16)$$

then the pair $(\hat{z}(\mathbf{y}_k | \mathbf{x}_a), \hat{z}(\mathbf{y}_k | \mathbf{x}_b))$ satisfies (ϵ, d_1) -Lipschitz bound between \mathbf{x}_a and \mathbf{x}_b . This property is illustrated in Fig. 4(b).

Propositions 1 and 2 establish that the one-dimensional log-convex interpolation is (ϵ, d_1) -Lipschitz along coordinate ℓ . In multi-dimensional domains, however, inputs typically differ along multiple coordinates simultaneously. To extend our interpolation framework while preserving an overall (ϵ, d_p) -Lipschitz guarantee, we must coordinate the privacy leakage across dimensions via per-coordinate budgets $\{\epsilon_\ell\}_{\ell=1}^N$. **Theorem 1** formalizes this by specifying how the $\{\epsilon_\ell\}$ compose to yield a mechanism that satisfies the (ϵ, d_p) -Lipschitz condition on \mathcal{X} , thereby providing the theoretical foundation for our high-dimensional interpolation scheme.

Theorem 1 (Dimension-wise Composition for Lipschitz Bound Condition). Let $f : \mathcal{X} \rightarrow \mathbb{R}$ be a mechanism that interpolates values in an N -dimensional space. Suppose that for each $\ell \in \{1, \dots, N\}$, f satisfies (ϵ_ℓ, d_1) -Lipschitz bound when the input records differ only in the ℓ th coordinate. If the parameters $\epsilon_1, \dots, \epsilon_N$ satisfy the following budget composition condition:

$$\sum_{\ell=1}^N \epsilon_\ell^{\frac{p}{p-1}} \leq \epsilon^{\frac{p}{p-1}}, \quad \text{for } p > 1, \quad (17)$$

$$\text{and} \quad \max_\ell \epsilon_\ell \leq \epsilon, \quad \text{for } p = 1, \quad (18)$$

then f is (ϵ, d_p) -Lipschitz continuous.

Proof Sketch. Fix $\mathbf{x}_a, \mathbf{x}_b \in \mathcal{X}$ and let $\Delta = \mathbf{x}_b - \mathbf{x}_a$, where $\Delta = [\Delta_1, \dots, \Delta_N]$. Construct an axis-aligned path that updates one coordinate at a time: $\mathbf{x}^{(0)} = \mathbf{x}_a$ and $\mathbf{x}^{(\ell)} = \mathbf{x}^{(\ell-1)} + \Delta_\ell \mathbf{e}_\ell$, where \mathbf{e}_ℓ is the ℓ th basis vector. Given that each one-dimensional step satisfies, for all $\mathbf{y}_k \subseteq \mathcal{Y}$,

$$|f(\mathbf{x}^{(\ell)}) - f(\mathbf{x}^{(\ell-1)})| \leq \epsilon_\ell |\Delta_\ell|. \quad (19)$$

Summing these bounds along the path gives

$$|f(\mathbf{x}_b) - f(\mathbf{x}_a)| \leq \sum_{\ell=1}^N \epsilon_\ell |\Delta_\ell|. \quad (20)$$

Let $p \in [1, \infty]$ and q be its dual exponent $(1/p + 1/q = 1)$. By Hölder's inequality, $\sum_{\ell=1}^N \epsilon_\ell |\Delta_\ell| \leq \|\epsilon\|_q \|\Delta\|_p$. Setting $\epsilon := \|\epsilon\|_q$ and $d_p(\mathbf{x}_a, \mathbf{x}_b) := \|\mathbf{x}_b - \mathbf{x}_a\|_p$ yields $\sum_{\ell=1}^N \epsilon_\ell |\Delta_\ell| \leq \epsilon d_p(\mathbf{x}_a, \mathbf{x}_b)$, and hence $|f(\mathbf{x}_b) - f(\mathbf{x}_a)| \leq \epsilon d_p(\mathbf{x}_a, \mathbf{x}_b)$, which is the desired (ϵ, d_p) -Lipschitz bound. A complete proof is provided in Appendix B.3. \square

Remark. **Theorem 1** ensures preservation of coordinate-wise Lipschitz bounds but does not guarantee that the interpolated values form a valid probability distribution (i.e., summing to one over \mathcal{Y}). In applications where \mathcal{M} represents a data perturbation mechanism (where the normalization constraint is required), we therefore apply a normalization step after interpolation to restore validity. In our construction, normalization can increase the effective Lipschitz bound (and thus the mDP budget) by up to a factor of 2, which will be further discussed in Section 5.2.

In **Corollary 1**, we instantiate **Theorem 1** for a normalized data-perturbation mechanism $\mathcal{M} : \mathcal{X} \rightarrow \mathcal{Y}$.

Corollary 1 (Dimension-wise Composition for mDP). Let \mathcal{M} be a mechanism that perturbs data in an N -dimensional space. Suppose that for each $\ell \in \{1, \dots, N\}$, \mathcal{M} satisfies (ϵ_ℓ, d_1) -mDP when the input records differ only in the ℓ th coordinate. If the parameters $\epsilon_1, \dots, \epsilon_N$ satisfy the budget

composition condition defined in Eqs. (17)(18), then \mathcal{M} is (ϵ, d_p) -mDP.

Discussion: Multi-attribute LDP as a special case of ℓ_p -norm mDP. Consider $\mathcal{X} \subseteq \mathcal{A}^N$ with Hamming distance $d_H(\mathbf{x}_a, \mathbf{x}_b) = \sum_{\ell=1}^N \mathbf{1}[x_{a,\ell} \neq x_{b,\ell}]$. A mechanism \mathcal{M} satisfies *multi-attribute ϵ -LDP* [4] if, for all $\mathbf{x}_a, \mathbf{x}_b \in \mathcal{X}$ and $\mathbf{y} \in \mathcal{Y}$,

$$\Pr[\mathcal{M}(\mathbf{x}_a) = \mathbf{y}] \leq e^{\epsilon d_H(\mathbf{x}_a, \mathbf{x}_b)} \Pr[\mathcal{M}(\mathbf{x}_b) = \mathbf{y}], \quad (21)$$

which is exactly (ϵ, d_H) -mDP.

Moreover, multi-attribute LDP can be seen as a limiting case of ℓ_p -mDP when $p \rightarrow \infty$ on binary domains. Assume $\mathcal{X} \subseteq \{0, 1\}^N$ (or more generally, that each coordinate difference is at most 1 after rescaling). Then

$$d_p(\mathbf{x}_a, \mathbf{x}_b) = \|\mathbf{x}_a - \mathbf{x}_b\|_\infty = \max_{\ell} |x_{a,\ell} - x_{b,\ell}| = \begin{cases} 1, & \mathbf{x}_a \neq \mathbf{x}_b, \\ 0, & \mathbf{x}_a = \mathbf{x}_b, \end{cases} \quad (22)$$

and per-coordinate distances reduce to

$$d_1(x_{a,\ell}, x_{b,\ell}) = |x_{a,\ell} - x_{b,\ell}| = \begin{cases} 1, & x_{a,\ell} \neq x_{b,\ell}, \\ 0, & x_{a,\ell} = x_{b,\ell}. \end{cases} \quad (23)$$

Under this metric, the pointwise mDP guarantee

$$\Pr[\mathcal{M}(\mathbf{x}_a) = \mathbf{y}] \leq e^{\epsilon d_p(\mathbf{x}_a, \mathbf{x}_b)} \Pr[\mathcal{M}(\mathbf{x}_b) = \mathbf{y}] \quad (24)$$

simplifies to the standard LDP bound

$$\Pr[\mathcal{M}(\mathbf{x}_a) = \mathbf{y}] \leq e^\epsilon \Pr[\mathcal{M}(\mathbf{x}_b) = \mathbf{y}] \quad (25)$$

whenever $\mathbf{x}_a \neq \mathbf{x}_b$ (and equals 1 when $\mathbf{x}_a = \mathbf{x}_b$).

Finally, as $p \rightarrow \infty$, the exponent $p/(p-1)$ in the budget composition rule in Eqs. (17)(18) tends to 1, and hence

$$\sum_{\ell=1}^N \epsilon_{\ell}^{\frac{p}{p-1}} \leq \epsilon^{\frac{p}{p-1}} \implies \sum_{\ell=1}^N \epsilon_{\ell} \leq \epsilon, \quad (26)$$

which is exactly the familiar sequential composition condition. Thus, ℓ_p -norm mDP recovers multi-attribute LDP in the $p \rightarrow \infty$ limit on binary domains (equivalently, under the Hamming metric).

5 Multi-Dimensional Interpolation

Having established one-dimensional interpolation and the corresponding privacy composition property in Section 4, we now turn to extending our framework to multi-dimensional domains. Directly applying log-convex interpolation in higher dimensions can violate (ϵ, d_p) -mDP due to the geometric properties of ℓ_p -norms. Based on **Theorem 1**, we adopt a coordinate-wise approach: we interpolate along each dimension and then combine the results using a carefully designed composition rule to ensure global privacy guarantees. For clarity, we present the anchor perturbation optimization (Step ②) before introducing the interpolation function (Step ③), as the optimization depends on the specific interpolation structure.

5.1 Step ① - Domain Partitioning

According to **Theorem 1**, ℓ_p -norm mDP can be enforced by bounding privacy leakage separately along each coordinate. To support this dimension-wise composition, we partition the secret domain \mathcal{X} into M non-overlapping N -orthotopes $\mathcal{C}_1, \dots, \mathcal{C}_M$, axis-aligned hyperrectangles that generalize rectangles to N dimensions. This coordinate-aligned structure ensures that neighboring anchors differ in only one dimension, enabling efficient log-convex interpolation while preserving (ϵ, d_p) -mDP.

More precisely, for each N -orthotope \mathcal{C}_m , we let $\hat{\mathbf{x}}_{i_m} = [\hat{x}_{i_m,1}, \dots, \hat{x}_{i_m,N}]$ denote its base (minimum) corner, and let $\Delta = [\Delta_1, \dots, \Delta_N]$ represent the side lengths along each dimension. The full set of 2^N corner points of \mathcal{C}_m is given by: $\hat{\mathcal{X}}_m = \{\hat{\mathbf{x}}_{i_m} + \gamma \odot \Delta \mid \gamma \in \{0, 1\}^N\}$, where γ is a binary indicator vector and \odot denotes element-wise multiplication. Each corner point thus has coordinate $\hat{x}_{i_m,\ell} + \gamma_\ell \Delta_\ell$ along dimension ℓ . We refer to $\hat{\mathcal{X}}_m$ as the *anchor set* of \mathcal{C}_m , and define the full anchor set as $\hat{\mathcal{X}} = \bigcup_m \hat{\mathcal{X}}_m$, which serves as the support for interpolation and optimization.

Definition 4 (Axis-Aligned Anchor Neighbors). *Let $\hat{\mathbf{x}}_i, \hat{\mathbf{x}}_j \in \hat{\mathcal{X}}_m$ be two anchor points within the same N -orthotope \mathcal{C}_m . We say that $\hat{\mathbf{x}}_i$ and $\hat{\mathbf{x}}_j$ are ℓ -axis neighbors (or simply ℓ -neighbors) if they differ only along the ℓ th coordinate; that is, $\hat{x}_{i,\ell} \neq \hat{x}_{j,\ell}$ and $\hat{x}_{i,\ell'} = \hat{x}_{j,\ell'} \neq \ell$ for all $\ell' \neq \ell$.*

5.2 Step ③ - Perturbation Interpolation

With the domain partitioned into N -orthotopes (Step ①), we interpolate perturbation distributions for non-anchor records using their corner anchors. For a record inside a cell, we first construct an *unnormalized* multi-dimensional log-convex interpolant f_{int} by applying log-convex interpolation *separately* along each coordinate and composing the results multiplicatively (**Definition 5**). Because these interpolated values might not sum to one over \mathcal{Y} , we then obtain a valid probability distribution by *normalizing* them, yielding the *normalized* multi-dimensional log-convex interpolation \bar{f}_{int} (**Definition 6**). The *Lipschitz continuity* of the interpolated (log-)values is established by **Theorem 2**, and the (ϵ, d_p) -mDP guarantee for the normalized mechanism follows from **Proposition 3**.

Definition 5 (Unnormalized Multi-Dimensional Log-Convex Interpolation f_{int}). *Let $\hat{\mathcal{X}}_m$ denote the set of 2^N anchor points at the corners of an N -dimensional orthotope \mathcal{C}_m , and let $\mathbf{Z}_{\hat{\mathcal{X}}_m}$ represent their corresponding perturbation distributions. For any point $\mathbf{x}_a \in \mathcal{C}_m$ and output $\mathbf{y}_k \in \mathcal{Y}$, the interpolated value is defined as:*

$$\ln f_{\text{int}}(\mathbf{x}_a, \mathbf{y}_k, \mathbf{Z}_{\hat{\mathcal{X}}_m}) = \sum_{\gamma \in \{0,1\}^N} w(\gamma) \ln z(\mathbf{y}_k \mid \hat{\mathbf{x}}_{i_m} + \gamma \odot \Delta), \quad (27)$$

or equivalently:

$$f_{\text{int}}(\mathbf{x}_a, \mathbf{y}_k, \mathbf{Z}_{\hat{\mathcal{X}}_m}) = \prod_{\gamma \in \{0,1\}^N} z(\mathbf{y}_k \mid \hat{\mathbf{x}}_{i_m} + \gamma \odot \Delta)^{w(\gamma)}. \quad (28)$$

Here, the weight function $w(\gamma)$, defined as

$$w(\gamma) = \prod_{\ell=1}^N \left[(1 - \gamma_\ell) \lambda_{\hat{\mathbf{x}}_{i_m}, \mathbf{x}_a}^\ell + \gamma_\ell \left(1 - \lambda_{\hat{\mathbf{x}}_{i_m}, \mathbf{x}_a}^\ell \right) \right], \quad (29)$$

represents how each anchor point's distribution contributes to the interpolated distribution at the non-anchor point \mathbf{x}_a , with the weights reflecting the relative position of the point within its cell.

Theorem 2 (Correctness of Log-Convex Interpolation f_{int}). *Given that (ϵ_ℓ, d_1) -Lipschitz bound holds between each pair of ℓ -neighbors in $\hat{\mathcal{X}}$ and $\{\epsilon_\ell\}_{\ell=1}^N$ satisfy the privacy budget composition condition formalized in Eq. (17)(18), the use of the interpolation function f_{int} (defined by Eq. (27)) guarantees that any two interpolated values within the entire secret data domain \mathcal{X} satisfy (ϵ, d_p) -Lipschitz bound.*

Proof Sketch. We begin by proving that if two records $\mathbf{x}_a, \mathbf{x}_b \in \mathcal{X}$ differ only in a single coordinate ℓ , then their interpolated perturbation probabilities under f_{int} satisfy (ϵ_ℓ, d_1) -mDP along that dimension. Then by applying the dimension-wise composition theorem (**Theorem 1**), we establish that the composed mechanism satisfies (ϵ, d_p) -mDP globally. The full proof is provided in **Appendix B.4**. \square

While the unnormalized log-convex interpolant preserves coordinate-wise Lipschitz continuity, its outputs do not necessarily lie on the probability simplex. To obtain a valid perturbation mechanism, we normalize these values (**Definition 6**), which restores a proper probability distribution at the cost of increasing the effective Lipschitz bound by at most a factor of 2 (**Proposition 3**).

Definition 6 (Normalized Multi-Dimensional Log-Convex Interpolation \bar{f}_{int}). *Given a point \mathbf{x}_a within cell \mathcal{C}_m and a perturbation candidate $\mathbf{y}_k \in \mathcal{Y}$, the normalized interpolated probability is defined as:*

$$\bar{f}_{\text{int}}(\mathbf{x}_a, \mathbf{y}_k, \mathbf{Z}_{\hat{\mathcal{X}}_m}) = \frac{f_{\text{int}}(\mathbf{x}_a, \mathbf{y}_k, \mathbf{Z}_{\hat{\mathcal{X}}_m})}{\sum_{\mathbf{y}_j \in \mathcal{Y}} f_{\text{int}}(\mathbf{x}_a, \mathbf{y}_j, \mathbf{Z}_{\hat{\mathcal{X}}_m})}, \quad (30)$$

where the denominator normalizes the interpolated scores over all possible outputs, ensuring that the resulting distribution is valid: $\sum_{\mathbf{y}_k \in \mathcal{Y}} \bar{f}_{\text{int}}(\mathbf{x}_a, \mathbf{y}_k, \mathbf{Z}_{\hat{\mathcal{X}}_m}) = 1$.

Proposition 3. *Given that any pair of real records $\mathbf{x}_a \in \mathcal{X}_m$ and $\mathbf{x}_b \in \mathcal{X}_{m'}$ with their perturbation probabilities interpolated by*

$$z(\mathbf{y}_k \mid \mathbf{x}_a) = \bar{f}_{\text{int}}(\mathbf{x}_a, \mathbf{y}_k, \mathbf{Z}_{\hat{\mathcal{X}}_m}) \quad (31)$$

$$z(\mathbf{y}_k \mid \mathbf{x}_b) = \bar{f}_{\text{int}}(\mathbf{x}_b, \mathbf{y}_k, \mathbf{Z}_{\hat{\mathcal{X}}_{m'}}) \quad (32)$$

then their perturbation probabilities satisfy $(2\epsilon, d_p)$ -mDP.

Proof Sketch. The unnormalized interpolant f_{int} already satisfies pointwise (ϵ, d_p) -mDP, i.e., $\frac{f_{\text{int}}(\mathbf{x}_a, \mathbf{y}_k, \mathbf{Z}_{\hat{\mathcal{X}}_m})}{f_{\text{int}}(\mathbf{x}_b, \mathbf{y}_k, \mathbf{Z}_{\hat{\mathcal{X}}_m})} \leq e^{\epsilon d_p(\mathbf{x}_a, \mathbf{x}_b)}$.

Summing over \mathbf{y}_j shows that the partition function $Z(\mathbf{x}) = \sum_{\mathbf{y}_j \in \mathcal{Y}} f_{\text{int}}(\mathbf{x}_a, \mathbf{y}_j, \mathbf{Z}_{\hat{\mathcal{X}}_m})$ obeys the same multiplicative bounds. The normalized mechanism is $z(\mathbf{y}_k \mid \mathbf{x}_a) = \frac{f_{\text{int}}(\mathbf{x}_a, \mathbf{y}_k)}{Z(\mathbf{x}_a)}$. Thus, the ratio of normalized probabilities is the product of the per-class ratio and the inverse normalizer ratio, giving $\frac{z(\mathbf{y}_k \mid \mathbf{x}_a)}{z(\mathbf{y}_k \mid \mathbf{x}_b)} \leq e^{2\epsilon d_p(\mathbf{x}_a, \mathbf{x}_b)}$. Hence, the normalized mechanism is $(2\epsilon, d_p)$ -mDP. The detailed proof can be found in **Appendix B.5**. \square

5.3 Step ② - Anchor Perturbation Optimization (APO)

The goal of APO is to jointly optimize (1) the per-dimension privacy budgets $\{\epsilon_\ell\}_{\ell=1}^N$ under a global privacy budget composition constraint (formalized in Eq. (17)(18) in **Theorem 1**), and (2) the perturbation distributions of each pair of ℓ -neighbor in the anchor set $\hat{\mathcal{X}}$ satisfy (ϵ_ℓ, d_1) -mDP constraints along each dimension ℓ , so as to minimize the expected utility loss over the secret domain. Here, we define the expected utility loss of the secret data within each N -orthotope \mathcal{C}_m by

$$\mathcal{L}(\mathbf{Z}_{\hat{\mathcal{X}}_m}) = \sum_{\mathbf{y}_k \in \mathcal{Y}} \int_{\mathcal{C}_m} \bar{f}_{\text{int}}(\mathbf{x}, \mathbf{y}_k, \mathbf{Z}_{\hat{\mathcal{X}}_m}) p(\mathbf{x}) \mathcal{L}(\mathbf{x}, \mathbf{y}_k) d\mathbf{x}. \quad (33)$$

Definition 7 (Anchor Perturbation Optimization (APO)). *The APO problem jointly optimizes the anchor perturbation distributions and the per-dimension privacy budgets to minimize the total expected utility loss $\sum_{m=1}^M \mathcal{L}(\mathbf{Z}_{\hat{\mathcal{X}}_m})$, subject to privacy and probability constraints. Formally:*

$$\min \quad \sum_{m=1}^M \mathcal{L}(\mathbf{Z}_{\hat{\mathcal{X}}_m}) \quad (34)$$

$$\text{s.t.} \quad \sum_{\ell=1}^N \epsilon_\ell^{\frac{p}{p-1}} \leq \left(\frac{\epsilon}{2}\right)^{\frac{p}{p-1}}, \quad \text{when } p > 1, \quad (35)$$

$$\max_{\ell} \epsilon_\ell \leq \frac{\epsilon}{2}, \quad \text{when } p = 1 \quad (36)$$

$$z(\mathbf{y}_k \mid \hat{\mathbf{x}}_i) - e^{\epsilon_\ell \Delta_\ell} z(\mathbf{y}_k \mid \hat{\mathbf{x}}_j) \leq 0, \quad (37)$$

$$\text{for each pair } \ell\text{-neighbor } \hat{\mathbf{x}}_i, \hat{\mathbf{x}}_j \in \hat{\mathcal{X}}, \forall \ell \quad (37)$$

$$\sum_{\mathbf{y}_k \in \mathcal{Y}} z(\mathbf{y}_k \mid \hat{\mathbf{x}}_i) = 1, \quad \forall \hat{\mathbf{x}}_i \in \hat{\mathcal{X}}, \quad (38)$$

$$z(\mathbf{y}_k \mid \hat{\mathbf{x}}_i) \geq 0, \quad \forall \hat{\mathbf{x}}_i \in \hat{\mathcal{X}}, \quad \forall \mathbf{y}_k \in \mathcal{Y}. \quad (39)$$

Here, Eq. (35) enforces the privacy budget composition constraint, Eq. (37) imposes (ϵ_ℓ, d_1) -mDP constraints between each pair of ℓ -neighbor anchors, and Eqs. (38)–(39) define the normalization and non-negativity constraints.

The APO formulation introduces a nontrivial coupling between two sets of decision variables: the per-dimension privacy budgets $\{\epsilon_\ell\}_{\ell=1}^N$ and the perturbation matrix $\mathbf{Z}_{\hat{\mathcal{X}}} = \{z(\mathbf{y}_k \mid \hat{\mathbf{x}}_i)\}_{(\hat{\mathbf{x}}_i, \mathbf{y}_k) \in \hat{\mathcal{X}} \times \mathcal{Y}}$. Since the feasible space of

Table 1: Statistics of Road Network Datasets and Grid Partitioning

City	Bounding Box (SW – NE)	#Nodes	#Edges	Grid Size	Cell Size
Rome, Italy	(41.66, 12.24) – (42.10, 12.81)	43,160	89,739	15 × 20	3.18km × 3.18km
NYC, USA	(40.50, 73.70) – (40.91, 74.25)	55,353	139,638	10 × 20	4.58km × 4.58km
London, UK	(51.29, -0.51) – (51.69, 0.28)	12,820	299,524	10 × 20	4.52km × 4.52km

$\mathbf{Z}_{\hat{\mathcal{X}}}$ is constrained by the choice of $\{\varepsilon_\ell\}$, this coupling complicates joint optimization. In our experiments (Section 6), we focus on a 2D ℓ_2 -norm setting, where the set of feasible privacy budget allocations $\{(\varepsilon_1, \varepsilon_2)\}$ must satisfy the constraint $\varepsilon_1^2 + \varepsilon_2^2 \leq \varepsilon^2/4$. This defines a quarter-circle region in the first quadrant. To search for the optimal allocation, we discretize this curve by sampling values of ε_1 , compute the corresponding $\varepsilon_2 = \sqrt{\varepsilon^2/4 - \varepsilon_1^2}$, and evaluate the resulting utility loss. This grid search remains tractable in low dimensions. For higher-dimensional settings, we discuss potential scalable extensions based on decomposition techniques in Appendix E.2.

Another practical obstacle in solving the APO problem is the form of the expected-loss objective $\mathcal{L}(\mathbf{Z}_X) = \sum_m \mathcal{L}(\mathbf{Z}_{\hat{\mathcal{X}}_m})$, where for any fixed cell C_m the integrand $\tilde{f}_{\text{int}}(\mathbf{x}_a, \mathbf{y}_k, \mathbf{Z}_{\hat{\mathcal{X}}_m})$ is a *ratio of products of exponentials*; hence the resulting integral in Eq. (33) is analytically intractable and costly to evaluate numerically. Therefore, we replace this exact probability by a weighted geometric mean of the anchor probabilities and thereby convert the cell-level loss into a linear form.

Proposition 4 (Linear Surrogate for Utility Loss). *Let $\mathbf{x} = \hat{\mathbf{x}}_{i_m} + \lambda \odot \Delta \in C_m$ be a non-anchor point, where $\lambda = [\lambda_{\hat{\mathbf{x}}_{i_m}, \mathbf{x}}^1, \dots, \lambda_{\hat{\mathbf{x}}_{i_m}, \mathbf{x}}^N] \in [0, 1]^N$ are the convex interpolation weights. Approximating the perturbation probability in the objective function via weighted geometric interpolation yields:*

$$\begin{aligned} & \Pr[\mathcal{M}(\mathbf{x}; \mathbf{Z}_{\hat{\mathcal{X}}_m}) = \mathbf{y}_k] \quad (40) \\ & \approx \sum_{\gamma \in \{0,1\}^N} \left(\prod_{\ell=1}^N ((1-\gamma_\ell)\lambda_{\hat{\mathbf{x}}_{i_m}, \mathbf{x}}^\ell + \gamma_\ell(1-\lambda_{\hat{\mathbf{x}}_{i_m}, \mathbf{x}}^\ell)) \right) \\ & \quad \times z(\mathbf{y}_k | \hat{\mathbf{x}}_{i_m} + \gamma \odot \Delta). \quad (41) \end{aligned}$$

Under this approximation, the expected utility loss over cell C_m admits a linear surrogate: $\tilde{\mathcal{L}}(\mathbf{Z}_{\hat{\mathcal{X}}_m}) = \langle \tilde{\mathbf{C}}_{\hat{\mathcal{X}}_m}, \mathbf{Z}_{\hat{\mathcal{X}}_m} \rangle$, where $\tilde{\mathbf{C}}_{\hat{\mathcal{X}}_m} = \{\tilde{c}(\hat{\mathbf{x}}_i, \mathbf{y}_k)\}_{(\hat{\mathbf{x}}_i, \mathbf{y}_k) \in \hat{\mathcal{X}}_m \times \mathcal{Y}}$ is a constant coefficient matrix that depends only on the prior distribution $p(\mathbf{x})$ and the pointwise utility loss $\mathcal{L}(\mathbf{x}, \mathbf{y}_k)$. Here, $\langle A, B \rangle$ denotes the standard Frobenius inner product between two matrices of the same shape: $\langle A, B \rangle = \sum_{i,k} A_{i,k} \cdot B_{i,k}$. A closed-form derivation of $\tilde{\mathbf{C}}_{\hat{\mathcal{X}}_m}$ is provided in Appendix B.6.

Definition 8 (Approximate Anchor Perturbation Optimization (Approx-APO)). *Approx-APO retains all linear (ε_ℓ, d_p) -mDP and probability constraints from the original APO formulation, but replaces the expected utility loss objec-*

tive $\sum_{m=1}^M \mathcal{L}(\mathbf{Z}_{\hat{\mathcal{X}}_m})$ with its linear surrogate:

$$\sum_{m=1}^M \tilde{\mathcal{L}}(\mathbf{Z}_{\hat{\mathcal{X}}_m}) = \sum_{m=1}^M \langle \tilde{\mathbf{C}}_{\hat{\mathcal{X}}_m}, \mathbf{Z}_{\hat{\mathcal{X}}_m} \rangle, \quad (42)$$

as defined in Proposition 4.

Approx-APO can be solved efficiently using standard linear programming solvers [2], making it scalable to larger domains. However, since the surrogate objective is an approximation of the original expected utility loss, the resulting solution may not be optimal for the original APO. To assess its quality, we derive a universal lower bound on the optimal utility loss of the full APO formulation (see Appendix C). This bound serves as a benchmark for evaluating how closely the Approx-APO solution approaches the true optimum.

6 Case Study: Location Privacy in Navigation and Spatial Crowdsourcing

This section presents a case study of mDP in the context of location privacy protection. Such problems commonly arise when users must approach a target location to obtain a service or complete a task. Representative examples include (i) navigation services [31], where users query for routes while concealing their true location, and (ii) spatial crowdsourcing [33], where participants contribute geo-tagged data under privacy constraints.

To investigate this setting, we evaluate the proposed *Anchor-Interpolated Privacy Optimization (AIPO)* algorithm on real-world road-network datasets and compare it against representative baselines. The evaluation covers three dimensions: (i) *privacy* (Section 6.2), measured by violations of the (ε, d_p) -mDP constraints; (ii) *utility loss* (Section 6.3), quantified by expected service loss under different distance metrics; and (iii) *computational efficiency* (Section 6.4), assessed via runtime performance. The results show that AIPO enforces strict privacy with zero observed mDP violations, consistently reduces utility loss relative to existing methods, and achieves lower runtime compared to other optimization-based approaches. We begin by describing the experimental setup in Section 6.1, including details on the *datasets*, *computational resources*, and *baseline methods*.

Rome road map									
Method		$\epsilon = 0.2$	$\epsilon = 0.4$	$\epsilon = 0.6$	$\epsilon = 0.8$	$\epsilon = 1.0$	$\epsilon = 1.2$	$\epsilon = 1.4$	$\epsilon = 1.6$
Pre-defined	EM	0.00±0.00	0.00±0.00	0.00±0.00	0.00±0.00	0.00±0.00	0.00±0.00	0.00±0.00	0.00±0.00
Noise	Laplace	0.00±0.00	0.00±0.00	0.00±0.00	0.00±0.00	0.00±0.00	0.00±0.00	0.00±0.00	0.00±0.00
Distribution	TEM	0.00±0.00	0.00±0.00	0.00±0.00	0.00±0.00	0.00±0.00	0.00±0.00	0.00±0.00	0.00±0.00
Hybrid	RMP	0.00±0.00	0.00±0.00	0.00±0.00	0.00±0.00	0.00±0.00	0.00±0.00	0.00±0.00	0.00±0.00
Method	COPT	1.17±0.72	3.14±2.04	1.12±0.54	0.99±0.39	0.90±0.32	0.82±0.27	0.76±0.23	0.70±0.20
LP		1.76±0.14	1.55±0.13	1.32±0.11	1.06±0.10	1.21±0.05	1.11±0.04	0.95±0.03	0.88±0.03
AIPO-R		7.24±0.51	6.91±0.38	4.80±0.30	3.84±0.17	2.70±0.04	0.00±0.00	0.00±0.00	0.00±0.00
AIPO [†]		0.00±0.00	0.00±0.00	0.00±0.00	0.00±0.00	0.00±0.00	0.00±0.00	0.00±0.00	0.00±0.00
London road map									
Method		$\epsilon = 0.2$	$\epsilon = 0.4$	$\epsilon = 0.6$	$\epsilon = 0.8$	$\epsilon = 1.0$	$\epsilon = 1.2$	$\epsilon = 1.4$	$\epsilon = 1.6$
Pre-defined	EM	0.00±0.00	0.00±0.00	0.00±0.00	0.00±0.00	0.00±0.00	0.00±0.00	0.00±0.00	0.00±0.00
Noise	Laplace	0.00±0.00	0.00±0.00	0.00±0.00	0.00±0.00	0.00±0.00	0.00±0.00	0.00±0.00	0.00±0.00
Distribution	TEM	0.00±0.00	0.00±0.00	0.00±0.00	0.00±0.00	0.00±0.00	0.00±0.00	0.00±0.00	0.00±0.00
Hybrid	RMP	0.00±0.00	0.00±0.00	0.00±0.00	0.00±0.00	0.00±0.00	0.00±0.00	0.00±0.00	0.00±0.00
Method	COPT	0.72±0.69	2.43±1.10	0.64±0.29	0.63±0.26	0.59±0.24	0.55±0.21	0.51±0.19	0.48±0.17
LP		1.35±0.10	1.35±0.09	1.10±0.06	0.82±0.05	0.72±0.04	0.58±0.03	0.65±0.04	1.86±0.17
AIPO-R		7.82±0.25	9.26±0.32	5.77±0.30	4.21±0.14	1.75±0.02	1.40±0.05	1.08±0.06	0.89±0.08
AIPO [†]		0.00±0.00	0.00±0.00	0.00±0.00	0.00±0.00	0.00±0.00	0.00±0.00	0.00±0.00	0.00±0.00
New York City road map									
Method		$\epsilon = 0.2$	$\epsilon = 0.4$	$\epsilon = 0.6$	$\epsilon = 0.8$	$\epsilon = 1.0$	$\epsilon = 1.2$	$\epsilon = 1.4$	$\epsilon = 1.6$
Pre-defined	EM	0.00±0.00	0.00±0.00	0.00±0.00	0.00±0.00	0.00±0.00	0.00±0.00	0.00±0.00	0.00±0.00
Noise	Laplace	0.00±0.00	0.00±0.00	0.00±0.00	0.00±0.00	0.00±0.00	0.00±0.00	0.00±0.00	0.00±0.00
Distribution	TEM	0.00±0.00	0.00±0.00	0.00±0.00	0.00±0.00	0.00±0.00	0.00±0.00	0.00±0.00	0.00±0.00
Hybrid	RMP	0.00±0.00	0.00±0.00	0.00±0.00	0.00±0.00	0.00±0.00	0.00±0.00	0.00±0.00	0.00±0.00
Method	COPT	0.97±0.48	4.10±0.84	0.74±0.39	0.72±0.41	0.68±0.41	0.65±0.40	0.61±0.38	0.57±0.37
LP		1.28±0.08	1.27±0.07	1.00±0.05	1.12±0.08	0.88±0.05	0.77±0.06	0.64±0.05	1.76±0.12
AIPO-R		10.99±0.52	6.84±0.36	6.01±0.37	4.22±0.29	2.07±0.11	1.35±0.06	1.06±0.07	0.90±0.08
AIPO [†]		0.00±0.00	0.00±0.00	0.00±0.00	0.00±0.00	0.00±0.00	0.00±0.00	0.00±0.00	0.00±0.00

Table 2: mDP violation ratio (Mean±1.96×standard deviation).

6.1 Experiment Settings

Datasets. We conducted experiments on road network datasets from three major cities: *Rome, Italy, New York City (NYC), USA*, and *London, UK*. Each dataset comprises nodes representing intersections, junctions, and other key points in the urban road infrastructure, with edges corresponding to actual road segments. The data were obtained from OpenStreetMap [1]. To support our interpolation-based method, we discretize each city’s geographic area into a uniform grid map. Table 1 provides a summary of geographic boundaries, node and edge counts, grid configurations, and cell sizes for each dataset.

Distance metric. Unless otherwise stated, all main results are reported under the Euclidean distance d_2 (i.e., the ℓ_2 norm) when evaluating (ϵ, d_p) -mDP and utility. For completeness, we also include a full set of results under the Manhattan distance d_1 (i.e., the ℓ_1 norm) in **Appendix D.4**: utility loss (Table 8), privacy compliance (Table 9), and runtime (Table 10). These ℓ_1 results corroborate the conclusions drawn from the ℓ_2 setting.

Experiments Compute Resources. Our experiments were conducted on a workstation equipped with an Intel Core i9-13900F processor (24 cores, 2.00–5.60 GHz), 32 GB of DDR5

memory (4800 MHz), and an NVIDIA GeForce RTX 4090 GPU with 24 GB of GDDR6X VRAM. Linear programs were solved using the MATLAB Optimization Toolbox function `linearprog` [2].

Representative baselines. We list several representative baselines that achieve ϵ -mDP:

- (1) *Pre-defined Noise Distribution Methods*, including *Exponential Mechanism (EM)* [11], *Planar Laplace Mechanism (Laplace)* [3], and *Truncated Exponential Mechanism (TEM)* [8].
- (2) *Linear programming (LP)* [6], which minimizes expected utility under mDP constraints via a LP on a *discretized* domain; this approximation can misestimate pairwise distances and weaken mDP enforcement in fine-grained settings.
- (3) *Hybrid Methods*, including *ConstOPTMech (COPT)* [23], which combines LP with EM to balance utility and scalability under mDP, and *Bayesian Remapping (RMP)* [10], which is a post-processing technique that enhances utility without compromising mDP.
- (4) *AIPO-Relaxed (AIPO-R)*. AIPO-R is a relaxed variant of the proposed method that directly enforces the (ϵ, d_p) -

Rome road map								
Method		$\epsilon = 0.2$	$\epsilon = 0.4$	$\epsilon = 0.6$	$\epsilon = 0.8$	$\epsilon = 1.0$	$\epsilon = 1.2$	$\epsilon = 1.4$
Pre-defined	EM	8.71 \pm 0.78	8.70 \pm 1.13	8.65 \pm 1.28	8.62 \pm 1.38	8.58 \pm 1.45	8.56 \pm 1.51	8.54 \pm 1.55
Noise	Laplace	8.71 \pm 0.71	8.48 \pm 1.00	8.46 \pm 1.40	8.45 \pm 1.69	8.44 \pm 1.90	8.43 \pm 2.05	8.42 \pm 2.16
Distribution	TEM	8.85 \pm 2.71	8.95 \pm 3.19	8.66 \pm 2.44	8.64 \pm 1.83	8.66 \pm 1.11	8.66 \pm 0.69	8.66 \pm 0.27
Hybrid	RMP	5.94 \pm 0.25	4.96 \pm 0.45	4.28 \pm 0.36	3.85 \pm 0.26	3.58 \pm 0.21	3.40 \pm 0.19	3.28 \pm 0.18
Method	COPT	7.99 \pm 1.53	7.95 \pm 1.04	8.33 \pm 1.50	8.29 \pm 1.57	8.27 \pm 1.59	8.25 \pm 1.61	8.24 \pm 1.60
LP		4.25 \pm 0.41	2.97 \pm 0.11	2.56 \pm 0.03	2.45 \pm 0.07	2.43 \pm 0.03	2.42 \pm 0.02	2.42 \pm 0.01
AIPO-R		5.19 \pm 0.23	3.97 \pm 0.21	3.34 \pm 0.17	3.01 \pm 0.12	2.81 \pm 0.07	2.66 \pm 0.03	2.56 \pm 0.05
LB		1.82 \pm 0.01	1.73 \pm 0.01	1.73 \pm 0.00	1.73 \pm 0.01	1.73 \pm 0.00	1.73 \pm 0.01	1.73 \pm 0.00
AIPO [†]		5.68\pm0.34	4.65\pm0.45	4.02\pm0.22	3.63\pm0.08	3.38\pm0.37	3.14\pm0.25	2.99\pm0.11
London road map								
Method		$\epsilon = 0.2$	$\epsilon = 0.4$	$\epsilon = 0.6$	$\epsilon = 0.8$	$\epsilon = 1.0$	$\epsilon = 1.2$	$\epsilon = 1.4$
Pre-defined	EM	7.69 \pm 0.74	7.44 \pm 1.30	7.30 \pm 1.58	7.20 \pm 1.73	7.14 \pm 1.82	7.09 \pm 1.88	7.05 \pm 1.93
Noise	Laplace	8.65 \pm 0.93	8.63 \pm 0.92	8.60 \pm 0.91	8.56 \pm 0.90	8.51 \pm 0.88	8.42 \pm 0.83	8.29 \pm 0.71
Distribution	TEM	8.01 \pm 2.22	7.72 \pm 2.27	7.87 \pm 1.94	7.96 \pm 1.11	7.98 \pm 0.62	7.99 \pm 0.35	7.99 \pm 0.12
Hybrid	RMP	5.86 \pm 0.21	5.07 \pm 0.39	4.49 \pm 0.41	4.09 \pm 0.37	3.83 \pm 0.32	3.65 \pm 0.29	3.53 \pm 0.26
Method	COPT	8.06 \pm 2.24	8.06 \pm 2.22	8.06 \pm 2.18	8.07 \pm 2.15	8.07 \pm 2.10	8.07 \pm 2.04	8.11 \pm 1.19
LP		4.19 \pm 0.24	2.92 \pm 0.13	2.56 \pm 0.14	2.47 \pm 0.11	2.45 \pm 0.07	2.44 \pm 0.09	2.44 \pm 0.05
AIPO-R		4.97 \pm 0.21	3.94 \pm 0.13	3.22 \pm 0.08	2.83 \pm 0.03	2.59 \pm 0.01	2.43 \pm 0.04	2.31 \pm 0.03
LB		1.51 \pm 0.05	1.44 \pm 0.02	1.44 \pm 0.03	1.44 \pm 0.01	1.44 \pm 0.00	1.44 \pm 0.01	1.44 \pm 0.00
AIPO [†]		5.42\pm0.76	4.50\pm0.26	3.90\pm0.17	3.43\pm0.17	3.11\pm0.11	2.88\pm0.09	2.71\pm0.21
New York City road map								
Method		$\epsilon = 0.2$	$\epsilon = 0.4$	$\epsilon = 0.6$	$\epsilon = 0.8$	$\epsilon = 1.0$	$\epsilon = 1.2$	$\epsilon = 1.4$
Pre-defined	EM	13.96 \pm 1.59	13.95 \pm 2.38	13.88 \pm 2.78	13.80 \pm 3.06	13.73 \pm 3.27	13.69 \pm 3.44	13.65 \pm 3.57
Noise	Laplace	13.75 \pm 1.95	13.62 \pm 2.52	13.48 \pm 2.58	13.41 \pm 2.63	13.37 \pm 2.72	13.36 \pm 2.82	13.35 \pm 2.92
Distribution	TEM	13.62 \pm 3.79	13.53 \pm 4.02	13.77 \pm 3.00	13.98 \pm 1.96	13.95 \pm 1.11	13.92 \pm 0.64	13.83 \pm 0.23
Hybrid	RMP	7.69 \pm 0.37	5.58 \pm 0.37	4.55 \pm 0.24	4.00 \pm 0.24	3.69 \pm 0.28	3.50 \pm 0.31	3.38 \pm 0.32
Method	COPT	8.19 \pm 1.63	13.39 \pm 2.91	13.72 \pm 3.30	13.64 \pm 3.55	13.62 \pm 3.64	13.61 \pm 3.72	13.63 \pm 3.75
LP		4.80 \pm 0.12	3.14 \pm 0.07	2.67 \pm 0.11	2.56 \pm 0.21	2.53 \pm 0.09	2.52 \pm 0.04	2.52 \pm 0.07
AIPO-R		6.10 \pm 0.21	4.24 \pm 0.05	3.42 \pm 0.08	2.97 \pm 0.12	2.73 \pm 0.03	2.59 \pm 0.01	2.49 \pm 0.01
LB		2.18 \pm 0.11	2.04 \pm 0.02	2.03 \pm 0.01	2.03 \pm 0.01	2.03 \pm 0.00	2.03 \pm 0.00	2.03 \pm 0.00
AIPO [†]		7.14\pm0.32	5.26\pm0.21	4.32\pm0.11	3.73\pm0.09	3.36\pm0.12	3.10\pm0.17	2.91\pm0.36

Table 3: Utility loss across different perturbation methods (Mean \pm 1.96 \times standard deviation; see Table 11 in the appendix for the full version).

mDP constraint using pairwise distances between anchors, without decomposing the privacy budget across dimensions.

6.2 Privacy Evaluation

To evaluate the empirical compliance of each mechanism with (ϵ, d_p) -mDP, we introduce the *perturbation probability ratio (PPR)* as a diagnostic metric. We randomly sample 1,000 locations from the input domain, denoted by \mathcal{S} , and for each pair $\mathbf{x}, \mathbf{x}' \in \mathcal{S}$ and output \mathbf{y}_k , compute

$$\text{PPR}(\mathbf{x}, \mathbf{x}', \mathbf{y}_k) = \frac{|\ln z(\mathbf{y}_k | \mathbf{x}) - \ln z(\mathbf{y}_k | \mathbf{x}')|}{d_p(\mathbf{x}, \mathbf{x}')}. \quad (43)$$

A violation of the (ϵ, d_p) -mDP constraint is recorded whenever $\text{PPR}(\mathbf{x}, \mathbf{x}', \mathbf{y}_k) > \epsilon$ for any output \mathbf{y}_k .

Table 2 reports empirical violation ratios under privacy budgets $\epsilon \in \{0.2, 0.4, \dots, 1.6\} \text{ km}^{-1}$. AIPO attains 0% violations across all datasets and budgets, corroborating the correctness of its dimension-wise composition and log-convex interpolation. In contrast, LP and COPT exhibit nonzero violation

ratios because they enforce constraints over discretized representatives, thereby *approximating* pairwise distances; such approximations can overestimate true continuous distances and relax the effective mDP constraints, missing privacy leakage at finer granularity. Pre-defined Noise Distribution mechanisms (e.g., Laplace, EM, TEM) do not incur violations but achieve this via heavier randomization, as reflected in their utility (detailed in Section 6.3).

Complementing the aggregate ratios, the distributional analysis in Section D.1 (Fig. 8–Fig. 10) shows that AIPO’s PPR values concentrate well below ϵ with tight tails, whereas LP-based and hybrid methods yield broader spreads with noticeable mass near (and occasionally beyond) the threshold; these patterns are consistent in Rome, London, and NYC.

The relaxed variant, AIPO-R, exhibits higher violation ratios. Unlike AIPO, it enforces mDP only between anchor points and does not guarantee compliance in interpolated regions; consequently, violations arise in areas between anchors, especially under sparse anchoring or in higher-dimensional settings. A formal discussion is provided in Appendix E.1.

Rome road map								
Method	$\epsilon = 0.2$	$\epsilon = 0.4$	$\epsilon = 0.6$	$\epsilon = 0.8$	$\epsilon = 1.0$	$\epsilon = 1.2$	$\epsilon = 1.4$	$\epsilon = 1.6$
COPT	147.4±18.2	138.7±10.3	140.4±9.2	135.8±6.2	137.2±6.6	136.7±8.2	136.2±4.2	137.6±5.0
LP	210.8±296.7	122.1±19.3	345.5±323.4	342.1±242.8	399.0±158.7	318.1±138.7	428.2±223.9	366.3±249.4
AIPO [†]	29.3±10.9	20.0±5.8	28.6±5.6	64.7±159.9	10.0±2.4	8.3±2.6	5.1±0.9	8.0±19.3
London road map								
Method	$\epsilon = 0.2$	$\epsilon = 0.4$	$\epsilon = 0.6$	$\epsilon = 0.8$	$\epsilon = 1.0$	$\epsilon = 1.2$	$\epsilon = 1.4$	$\epsilon = 1.6$
COPT	285.1±115.0	274.6±110.9	272.9±114.4	272.2±113.2	271.5±118.1	269.7±117.8	266.4±109.7	269.4±103.2
LP	159.3±48.7	106.9±32.2	125.7±100.3	99.9±41.3	111.8±57.6	104.7±51.3	101.5±34.3	180.7±208.6
AIPO [†]	78.2±13.9	77.0±22.4	78.5±24.2	77.4±13.8	80.7±16.1	75.0±26.4	62.3±8.7	63.9±10.9
New York City road map								
Method	$\epsilon = 0.2$	$\epsilon = 0.4$	$\epsilon = 0.6$	$\epsilon = 0.8$	$\epsilon = 1.0$	$\epsilon = 1.2$	$\epsilon = 1.4$	$\epsilon = 1.6$
COPT	157.3±12.3	159.4±16.2	154.6±14.5	153.1±15.6	155.2±5.1	151.3±11.9	152.5±12.6	153.5±9.6
LP	303.8±140.8	324.1±218.8	263.0±141.9	418.6±202.1	265.6±178.5	284.8±203.5	393.7±304.8	403.2±174.9
AIPO [†]	75.1±25.9	56.3±12.9	39.9±14.9	29.3±7.5	24.3±7.7	21.3±3.8	27.6±44.7	17.3±3.9

Table 4: Computation time of different perturbation methods (Mean±1.96×standard deviation).

6.3 Utility Loss Comparison

Given a true vehicle position \mathbf{x}_i and a task destination \mathbf{x}_{task} , the loss incurred by releasing the perturbed location \mathbf{y}_k is defined as the absolute difference between the corresponding shortest-path lengths, $|\text{path}(\mathbf{x}_i, \mathbf{x}_{\text{task}}) - \text{path}(\mathbf{y}_k, \mathbf{x}_{\text{task}})|$. Aggregating over the prior distribution $p(\mathbf{x}_{\text{task}})$ of task locations Q yields the expected utility loss:

$$\mathcal{L}(\mathbf{x}_i, \mathbf{y}_k) = \sum_{\mathbf{x}_{\text{task}} \in Q} p(\mathbf{x}_{\text{task}}) |\text{path}(\mathbf{x}_i, \mathbf{x}_{\text{task}}) - \text{path}(\mathbf{y}_k, \mathbf{x}_{\text{task}})|. \quad (44)$$

To compute $\text{path}(\cdot, \cdot)$, we apply Dijkstra's algorithm [5] to determine the shortest-path distance between the origin and destination nodes.

Table 3 reports the utility loss of our interpolation mechanism AIPO versus baseline perturbation methods on three road-network datasets:

AIPO vs. pre-defined Noise Distribution Methods (EM, TEM, Laplace). Across all three datasets, AIPO consistently outperforms pre-defined noise distribution methods in terms of utility. *On average, AIPO reduces utility loss by 59.03%, 60.94%, and 60.65% compared to EM, Laplace, and TEM, respectively.* EM and TEM define perturbation probabilities using (truncated) exponential scoring functions, while Laplace adds noise sampled independently from a fixed distribution. These methods rely on global or isotropic perturbation rules that ignore the underlying geometry and the direction-dependent sensitivity of task-specific utility. Consequently, they tend to over-perturb in dense regions and under-protect in sparse ones. In contrast, AIPO optimizes perturbation distributions at a sparse set of anchor points and interpolates them across the domain via log-convex combinations, yielding smooth transitions aligned with the metric structure.

AIPO vs. Hybrid Methods (COPT and RMP). *Across the three datasets, AIPO achieves an average of 59.16% lower utility loss compared to COPT.* The limited scalability of

COPT stems from its rigid LP formulation, which becomes impractical in high-resolution domains. In contrast, AIPO employs an anchor-based framework with log-convex interpolation, enabling flexible adaptation to fine-grained input spaces. By explicitly optimizing perturbation probabilities at a sparse set of anchor points, AIPO preserves the mDP guarantee while achieving improved utility.

AIPO also outperforms RMP, achieving 10.36% lower utility loss on average across the evaluated datasets. While RMP improves pre-defined noise mechanisms by reshaping posterior distributions to approximate mDP, its effectiveness is fundamentally limited by the quality of the initial noise distribution, which often falls short of global optimality. In contrast, AIPO formulates and solves an optimization problem directly under mDP constraints, without relying on any pre-defined perturbation mechanism, leading to a lower utility loss.

AIPO vs. LP. The LP method achieves lower utility loss compared to AIPO, since LP directly optimizes the perturbation distributions to minimize expected loss under distance-based constraints. However, this comes at the expense of privacy: the LP method only enforces the mDP constraints on a discrete grid of locations, without guaranteeing that the constraints hold for all possible input pairs in the continuous domain. As a result, while LP appears effective in terms of utility, it may produce perturbation probabilities that violate the mDP guarantee in off-grid regions, which has been demonstrated in Table 2.

AIPO vs. Lower Bound (LB). For theoretical reference, we also compare AIPO with a universal lower bound (LB) from Proposition 5 (Appendix C), which lower-bounds the minimum utility loss attainable by *any* mechanism satisfying (ϵ, d_p) -mDP. Empirically, AIPO lies within $1.36\times$ – $3.13\times$ of this bound across datasets and budgets, with larger gaps at tighter privacy (e.g., $\epsilon = 0.4$) due to stricter constraints; the ratio narrows as ϵ increases.

AIPO vs. AIPO-R. Empirically, AIPO achieves higher util-

ity loss compared to AIPO-R as AIPO-R relaxes the mDP constraint. In return, AIPO offers stronger theoretical guarantees, ensuring full compliance with (ϵ, d_p) -mDP across the continuous space.

Ablation Study: Utility loss with and without privacy budget optimization. Additionally, we compare *AIPO* with an equal-split variant (*AIPO-E*) that assigns identical per-dimension budgets (e.g., $\epsilon_1 = \epsilon_2 = \epsilon/\sqrt{2}$ under ℓ_2). Across Rome, London, and NYC, *AIPO* consistently achieves lower utility loss, with gains enlarging at higher ϵ (up to 7.8% on NYC at $\epsilon = 1.6$), indicating that learned asymmetric budgets better match directional sensitivity and improve privacy–utility trade-offs. The detailed experimental results can be found in Table 7 and Fig. 11–13 in Appendix D.2.

6.4 Computation Efficiency

Table 4 compares runtimes for the optimization-based methods (AIPO, LP) and the hybrid method COPT, each leveraging LP at some stage to construct perturbation mechanisms. AIPO attains a favorable utility–efficiency trade-off: it solves LPs only at a sparse set of anchors, and then uses log-convex interpolation to cover the continuous domain without a dense, full-scale program. This anchor-based design reduces both the number of decision variables and the effective constraint set, yielding stable performance across cities. Consistent with this, the grid-granularity study in Appendix D.3 (Fig. 14) shows that while finer grids monotonically reduce utility loss, runtime grows super-linearly, with gains saturating around 8 horizontal cells for Rome/London and 10 for NYC.

By contrast, the LP baseline incurs substantially higher cost in fine-grained settings because it solves a large program with mDP constraints over (nearly) all pairs of grid cells: the constraint count grows quadratically with grid size, and barrier/simplex iterations amplify this growth, making LP increasingly prohibitive as resolution increases.

7 Related Works

The earliest and most extensively studied applications of mDP focus on *location privacy over grid maps*. Foundational works such as Andrés et al. [3] and Bordenabe et al. [6] introduced geo-indistinguishability and linear programming (LP)-based mechanisms to enforce spatial privacy while preserving utility. These approaches rely on *pre-defined noise distributions* or *grid-based optimization* over discretized spatial domains. Subsequent works improve utility or scalability by incorporating personalized or group-based noise [25, 38], truncated noise distributions [35], and adaptations to federated or blockchain settings [21]. Hybrid mechanisms such as Bayesian remapping [10] and utility-aware post-processing [27] refine pre-defined perturbations to improve performance. Yu et al. [37] exemplify a hybrid design that combines mDP with an al-

ternative privacy metric, "expected inference error", using context-aware noise adaptation.

A parallel line of research applies mDP to *high-dimensional embeddings* in domains such as natural language processing and multimedia. In these settings, input records reside in continuous semantic vector spaces. Fernandes et al. [17] and Feyisetan et al. [19] added Laplace noise directly to text embeddings or used nearest-neighbor remapping. Carvalho et al. [8] proposed a truncated exponential mechanism constrained to semantically similar candidates. For non-text data, Han et al. [22] and Chen et al. [13] adapted Laplace-based perturbations to voice and facial embeddings. These approaches often fall under *pre-defined* or *hybrid* categories, tailored for continuous or structured vector domains.

Recent work has shifted toward *optimization-based mDP mechanisms* designed for *fine-grained or continuous domains*, where more precise control over privacy–utility trade-offs is critical. Imola et al. [23] introduced ConstOPT, which combines LP with the exponential mechanism to improve scalability and utility. Qiu et al. [29, 30] proposed decomposition-based perturbation frameworks, including partitioning and Benders decomposition. Other studies explore reinforcement learning [26] and bilevel optimization [36] to enforce mDP under task-specific utility objectives such as mobility prediction. These results demonstrate the versatility of *customized optimization* strategies for enforcing mDP in high-resolution domains. Additionally, trajectory privacy methods such as sequential perturbation [34] showcase the broader applicability of mDP frameworks in complex spatiotemporal contexts.

Taken together, Table 12 in Appendix illustrates a clear evolution in the mDP literature, from pre-defined, coarse-grained perturbation mechanisms to increasingly sophisticated, optimization-based frameworks designed for continuous and fine-grained domains.

8 Conclusion

We propose an interpolation-based framework for optimizing (ϵ, d_p) -mDP in continuous domains. By learning perturbation distributions at anchor points and applying dimension-wise log-convex interpolation, our method achieves both *strict privacy guarantees* (zero mDP violations) and *low utility loss*, supported by rigorous theoretical analysis and empirical evaluation on real-world datasets. This approach enables practical and theoretically grounded privacy mechanisms for fine-grained spatial and continuous data. While our method is highly effective in low-dimensional settings, its scalability is challenged in high-dimensional domains due to the exponential growth in anchor points, increased interpolation complexity, and fragmented privacy budget allocation. These limitations, common across mDP mechanisms under ℓ_p -norms, motivate future work on bilevel programming, optimization decomposition, or adaptive partitioning. A detailed discussion is provided in Appendix E.3.

Ethical Considerations

We reviewed the venue’s ethics guidance, submission instructions, and ethics-document requirements. The study was conducted responsibly, and our planned next steps adhere to those principles.

Stakeholders. The primary stakeholders of this work include: (i) the research team and the broader community of researchers working on mDP; (ii) practitioners and platform operators who may deploy mDP mechanisms in navigation, mobility analytics, spatial crowdsourcing, or related services, and the end-users of such systems; (iii) data subjects whose locations or other sensitive attributes might be protected by such mechanisms in future deployments; (iv) data and infrastructure providers such as OpenStreetMap contributors; and (v) society at large, including companies and institutions that rely on privacy-preserving data analytics, as well as marginalized or highly surveilled groups who may face disproportionate harms if location privacy is weak. For the identified stakeholders, the research process has negligible direct impact beyond advancing mDP methodology, whereas publication and deployment primarily affect practitioners, data subjects, and society by shaping how privacy mechanisms are chosen and used in practice.

Impacts of the research process and publication. Regarding the *research process*, our evaluation relies solely on publicly available OpenStreetMap road-network graphs and synthetic perturbations. We do not collect, process, or attempt to infer personal or identifiable user-level information, and we do not interact with live systems. As a result, we believe that tangible harms (e.g., financial loss, exposure to disturbing content) and rights-based harms (e.g., violations of informed consent or expectations of privacy) to individuals during the research process are minimal.

Regarding the *publication and potential deployment* of our results, the intended impact is positive: our interpolation-based optimization framework aims to make ℓ_p -mDP mechanisms for continuous and fine-grained domains more scalable, analyzable, and usable, thereby strengthening protections for sensitive data. This can benefit researchers (clearer theory and reproducible baselines), practitioners (deployable and auditable mechanisms with guidance on composition and parameter selection), and data subjects (stronger protection for location and similar data in downstream applications). At the same time, there is a dual-use risk: our framework could be misused to justify overly weak privacy configurations, such as very large ϵ or poorly chosen metrics, that technically satisfy formal definitions while providing limited real-world protection, particularly for vulnerable populations. There is also a risk that deployers might over-interpret our results outside the assumptions we state (e.g., different threat models), leading to a mismatch between perceived and actual privacy.

Mitigations and residual risks. To mitigate these risks, we (i) clearly document the assumptions and limitations of our approach, including its sensitivity to ϵ , metric choice, and modeling assumptions; (ii) explicitly warn against using extreme parameter settings or metrics that do not reflect meaningful notions of distance or harm for the affected population; (iii) recommend that practitioners adopt conservative privacy budgets and carefully evaluate deployments in light of relevant ethical, legal, and fairness considerations, especially in high-risk or high-stakes domains; and (iv) restrict our artifacts to code and derived or synthetic data that support defensive, privacy-preserving mechanisms, without releasing additional sensitive raw data. Despite these steps, some residual risk remains that third parties may deploy mechanisms irresponsibly or ignore our guidance; this residual risk cannot be fully eliminated.

Decision to conduct and publish the research. In deciding to conduct this research, we judged, under the lens of Beneficence and Respect for Persons, that simulation-based analysis on public infrastructure-level data, with no new collection or linkage of individual records, posed low risk relative to the potential benefit of improving privacy protection tools. Justice and Respect for Law and Public Interest are reflected in our use of publicly available, properly licensed datasets and in our aim to strengthen protections for users, including those at higher risk of surveillance or discrimination. In deciding to publish, we considered whether withholding the methods would better protect stakeholders; however, we concluded that making the techniques public, together with explicit discussion of their assumptions, limitations, potential dual use, and recommended safeguards, provides a net ethical benefit. Publication enables community scrutiny, supports more robust and transparent privacy mechanisms, and offers practitioners concrete guidance on responsible deployment.

Open Science

We provide a detailed MATLAB implementation of the proposed AIPO framework to ensure full reproducibility of all experimental results reported in the paper. The same artifact is available at the link: <https://doi.org/10.5281/zenodo.17851733>. Table 5 shows the script files and estimated running time of each figure and table.

(1) Code and Scripts. The following MATLAB scripts reproduce the key tables and figures in the paper. All experiments were run on a machine with MATLAB R2024b and the Optimization Toolbox and Statistics and Machine Learning Toolbox enabled.

- ▷ `main_2norm.m`: Reproduces main results under the ℓ_2 utility metric, including Tables 2–4 and Fig. 8–10.
Estimated runtime: 37.0 hours

Table 5: Summary of reproducible tables and figures from the provided artifact.

Reproduced Tables and Figures	Script File	Estimated Run Time
Tables 2–4 (Main), Figures 8–10 (Appendix)	main_2norm.m	37.0 hours
Tables 8–10 (Appendix)	main_1norm.m	36.0 hours
Figure 14 (Appendix)	main_granularity.m	15.0 hours
Table 7 (Appendix), Figures 11–13 (Appendix)	main_ablation_privacybudget.m	7.5 hours

- ▷ `main_1norm.m`: Reproduces experiments under the ℓ_1 utility metric, including Tables 8–10.
Estimated runtime: 36.0 hours
- ▷ `main_granularity.m`: Evaluates the effect of grid granularity (Fig. 14).
Estimated runtime: 15.0 hours
- ▷ `main_ablation_privacybudget.m`: Investigates the impact of privacy budget allocation strategies, reproducing Table 7 and Fig. 11–13.
Estimated runtime: 7.5 hours

(2) Instructions. To reproduce the results:

1. Set the working directory in MATLAB to the root folder containing the provided scripts.
2. Run the desired script (e.g., `main_2norm.m`) to generate the corresponding tables and figures.
3. Output files (e.g., utility loss, mDP violation ratio, and runtime of different methods) will be saved in the following directories:

- ▷ `./results/1norm/`: Output of `main_1norm.m`, including utility loss, mDP violation ratio, PPR, and runtime of all compared methods across the three datasets.
- ▷ `./results/2norm/`: Output of `main_2norm.m`, including utility loss, mDP violation ratio, PPR, and runtime of all compared methods across the three datasets.
- ▷ `./results/granularity/`: Output of `main_granularity.m`, including utility loss, runtime, and the number of anchors used in AIPO.
- ▷ `./results/ablation_budget/`: Output of `main_ablation_privacybudget.m`, including the utility loss of AIPO with and without privacy budget optimization.

References

- [1] 2020. openstreetmap. <https://www.openstreetmap.org/>. Accessed: 2020-04-07.
- [2] 2024. linprog: Solve linear programming problems. <https://www.mathworks.com/help/optim/ug/linprog.html>. Accessed in January 2024.
- [3] Miguel E. Andrés, Nicolás E. Bordenabe, Konstantinos Chatzikokolakis, and Catuscia Palamidessi. 2013. Geo-indistinguishability: differential privacy for location-based systems. In *Proceedings of the 2013 ACM SIGSAC Conference on Computer & Communications Security* (Berlin, Germany) (CCS '13). Association for Computing Machinery, New York, NY, USA, 901–914. [doi:10.1145/2508859.2516735](https://doi.org/10.1145/2508859.2516735)
- [4] Héber H. Arcolezi, Sébastien Gambs, Jean-François Couchot, and Catuscia Palamidessi. 2023. On the Risks of Collecting Multidimensional Data Under Local Differential Privacy. *Proc. VLDB Endow.* 16, 5 (Jan. 2023), 1126–1139. [doi:10.14778/3579075.3579086](https://doi.org/10.14778/3579075.3579086)
- [5] Harsh Bhasin. 2015. *Algorithms: Design and Analysis*. Oxford Univ Press.
- [6] N. E. Bordenabe, K. Chatzikokolakis, and C. Palamidessi. 2014. Optimal Geo-Indistinguishable Mechanisms for Location Privacy. In *Proc. of ACM CCS*. 251–262.
- [7] Stephen Boyd and Lieven Vandenberghe. 2004. *Convex Optimization*. Cambridge University Press, New York, NY, USA.
- [8] Ricardo Silva Carvalho, Theodore Vasiloudis, and Oluwaseyi Feyisetan. 2021. TEM: High Utility Metric Differential Privacy on Text. *ArXiv* abs/2107.07928 (2021). <https://api.semanticscholar.org/CorpusID:236034456>
- [9] Konstantinos Chatzikokolakis, Miguel E. Andrés, Nicolás Emilio Bordenabe, and Catuscia Palamidessi. 2013. Broadening the Scope of Differential Privacy Using Metrics. In *Proc. of Privacy Enhancing Technologies*, Emiliano De Cristofaro and Matthew Wright (Eds.). Springer Berlin Heidelberg, Berlin, Heidelberg, 82–102.
- [10] Kostas Chatzikokolakis, Ehab Elsalamouny, and Catuscia Palamidessi. 2017. Efficient Utility Improvement for Location Privacy. *Proceedings on Privacy Enhancing Technologies* 2017 (10 2017). [doi:10.1515/popets-2017-0051](https://doi.org/10.1515/popets-2017-0051)
- [11] Konstantinos Chatzikokolakis, Catuscia Palamidessi, and Marco Stronati. 2015. Constructing elastic

distinguishability metrics for location privacy. *Privacy Enhancing Technologies (PoPETs) 2015* (2015), 156–170. <http://www.degruyter.com/view/j/popets.2015.2015.issue-2/popets-2015-0023/popets-2015-0023.xml>

[12] Konstantinos Chatzikokolakis, Catuscia Palamidessi, and Marco Stronati. 2015. Constructing elastic distinguishability metrics for location privacy. *Proc. on Privacy Enhancing Technologies 2015*, 2 (2015), 156–170.

[13] Jia-Wei Chen, Li-Ju Chen, Chia-Mu Yu, and Chun-Shien Lu. 2021. Perceptual Indistinguishability-Net (PI-Net): Facial Image Obfuscation with Manipulable Semantics . In *2021 IEEE/CVF Conference on Computer Vision and Pattern Recognition (CVPR)*. IEEE Computer Society, Los Alamitos, CA, USA, 6474–6483. [doi:10.1109/CVPR46437.2021.00641](https://doi.org/10.1109/CVPR46437.2021.00641)

[14] Prathamesh Dharangutte, Jie Gao, Ruobin Gong, and Fang-Yi Yu. 2023. Integer subspace differential privacy. In *Proceedings of the Thirty-Seventh AAAI Conference on Artificial Intelligence and Thirty-Fifth Conference on Innovative Applications of Artificial Intelligence and Thirteenth Symposium on Educational Advances in Artificial Intelligence (AAAI'23/IAAI'23/EAAI'23)*. AAAI Press, Article 826, 9 pages. [doi:10.1609/aaai.v37i6.25895](https://doi.org/10.1609/aaai.v37i6.25895)

[15] John C. Duchi, Michael I. Jordan, and Martin J. Wainwright. 2013. Local Privacy and Statistical Minimax Rates. In *2013 IEEE 54th Annual Symposium on Foundations of Computer Science*. 429–438. [doi:10.1109/FOCS.2013.53](https://doi.org/10.1109/FOCS.2013.53)

[16] Liyue Fan. 2019. Practical Image Obfuscation with Provable Privacy. In *2019 IEEE International Conference on Multimedia and Expo (ICME)*. 784–789. [doi:10.1109/ICME.2019.00140](https://doi.org/10.1109/ICME.2019.00140)

[17] Natasha Fernandes, Mark Dras, and Annabelle McIver. 2018. Author Obfuscation Using Generalised Differential Privacy. *ArXiv* abs/1805.08866 (2018). <https://api.semanticscholar.org/CorpusID:43942677>

[18] Oluwaseyi Feyisetan, Borja Balle, Thomas Drake, and Tom Diethe. 2020. Privacy- and Utility-Preserving Textual Analysis via Calibrated Multivariate Perturbations. In *Proceedings of the 13th International Conference on Web Search and Data Mining* (Houston, TX, USA) (WSDM '20). Association for Computing Machinery, New York, NY, USA, 178–186. [doi:10.1145/3336191.3371856](https://doi.org/10.1145/3336191.3371856)

[19] O. Feyisetan, T. Diethe, and T. Drake. 2019. Leveraging Hierarchical Representations for Preserving Privacy and Utility in Text. In *2019 IEEE International Conference on Data Mining (ICDM)*. IEEE Computer Society, Los Alamitos, CA, USA, 210–219. [doi:10.1109/ICDM.2019.00031](https://doi.org/10.1109/ICDM.2019.00031)

[20] Oluwaseyi Feyisetan and Shiva Kasiviswanathan. 2021. Private Release of Text Embedding Vectors. In *Proceedings of the First Workshop on Trustworthy Natural Language Processing*, Yada Pruksachatkun, Anil Ramakrishna, Kai-Wei Chang, Satyapriya Krishna, Jwala Dhamala, Tanaya Guha, and Xiang Ren (Eds.). Association for Computational Linguistics, Online, 15–27. [doi:10.18653/v1/2021.trustnlp-1.3](https://doi.org/10.18653/v1/2021.trustnlp-1.3)

[21] Filippo Galli, Sayan Biswas, Kangsoo Jung, Tommaso Cucinotta, and Catuscia Palamidessi. 2022. Group privacy for personalized federated learning. In *Workshop on Federated Learning: Recent Advances and New Challenges (in Conjunction with NeurIPS 2022)*. <https://openreview.net/forum?id=R45g30SnwsR>

[22] Yaowei Han, Sheng Li, Yang Cao, Qiang Ma, and Masatoshi Yoshikawa. 2020. Voice-Indistinguishability: Protecting Voiceprint In Privacy-Preserving Speech Data Release . In *2020 IEEE International Conference on Multimedia and Expo (ICME)*. IEEE Computer Society, Los Alamitos, CA, USA, 1–6. [doi:10.1109/ICME46284.2020.9102875](https://doi.org/10.1109/ICME46284.2020.9102875)

[23] Jacob Imola, Shiva Kasiviswanathan, Stephen White, Abhinav Aggarwal, and Nathanael Teissier. 2022. Balancing utility and scalability in metric differential privacy. In *Proc. of UAI 2022*.

[24] Fragkiskos Koufogiannis, Shuo Han, and George J. Pappas. 2015. Optimality of the Laplace Mechanism in Differential Privacy. *arXiv:1504.00065 [cs.CR]* <https://arxiv.org/abs/1504.00065>

[25] Baihe Ma, Xu Wang, Wei Ni, and Ren Ping Liu. 2022. Personalized Location Privacy With Road Network-Indistinguishability. *IEEE Transactions on Intelligent Transportation Systems* 23, 11 (2022), 20860–20872. [doi:10.1109/TITS.2022.3179501](https://doi.org/10.1109/TITS.2022.3179501)

[26] Minghui Min, Haopeng Zhu, Jiahao Ding, Shiyin Li, Liang Xiao, Miao Pan, and Zhu Han. 2024. Personalized 3D Location Privacy Protection With Differential and Distortion Geo-Perturbation. *IEEE Trans. Dependable Secur. Comput.* 21, 4 (July - August 2024), 3629–3643. <https://doi.org/10.1109/TDSC.2023.3335374>

[27] Simon Oya, Carmela Troncoso, and Fernando Pérez-González. 2017. Is Geo-Indistinguishability What You Are Looking For?. In *Proc. of the 2017 on Workshop on Privacy in the Electronic Society* (Dallas, Texas, USA) (WPES '17). Association for Computing Machinery,

New York, NY, USA, 137–140. [doi:10.1145/3139550.3139555](https://doi.org/10.1145/3139550.3139555)

- [28] P. Pappachan, C. Qiu, A. Squicciarini, and V. Manjunath. 2023. User Customizable and Robust Geo-Indistinguishability for Location Privacy. In *Proc. of International Conference on Extending Database Technology (EDBT)*.
- [29] Chenxi Qiu. 2024. Enhancing Scalability of Metric Differential Privacy via Secret Dataset Partitioning and Benders Decomposition. In *Proc. of 33rd International Joint Conference on Artificial Intelligence (IJCAI)*.
- [30] Chenxi Qiu, Ruiyao Liu, Primal Pappachan, Anna Squicciarini, and Xinpeng Xie. 2025. Time-Efficient Locally Relevant Geo-Location Privacy Protection. In *Proc. on Privacy Enhancing Technologies*.
- [31] C. Qiu, A. C. Squicciarini, C. Pang, N. Wang, and B. Wu. 2022. Location Privacy Protection in Vehicle-Based Spatial Crowdsourcing via Geo-Indistinguishability. *IEEE Transactions on Mobile Computing* (2022), 1–1. [doi:10.1109/TMC.2020.3037911](https://doi.org/10.1109/TMC.2020.3037911)
- [32] Daniel W. Stroock. 2010. *Probability Theory: An Analytic View* (2nd ed.). Cambridge University Press.
- [33] L. Wang, D. Yang, X. Han, T. Wang, D. Zhang, and X. Ma. 2017. Location Privacy-Preserving Task Allocation for Mobile Crowdsensing with Differential Geo-Obfuscation. In *Proc. of ACM WWW*. 627–636.
- [34] Yonghui Xiao and Li Xiong. 2015. Protecting Locations with Differential Privacy under Temporal Correlations (CCS '15). Association for Computing Machinery, New York, NY, USA, 1298–1309. [doi:10.1145/2810103.2813640](https://doi.org/10.1145/2810103.2813640)
- [35] Changxin et al. Yang. 2021. Blockchain-based indoor location paging and answering service with truncated-geo-indistinguishability. *IET Blockchain* (2021).
- [36] Dan Yu, Xiufang Shi, Li Chai, Wen-An Zhang, and Jiming Chen. 2023. Balancing Localization Accuracy and Location Privacy in Mobile Cooperative Localization. *IEEE Transactions on Signal Processing PP* (01 2023), 1–14. [doi:10.1109/TSP.2023.3292505](https://doi.org/10.1109/TSP.2023.3292505)
- [37] L. Yu, L. Liu, and C. Pu. 2017. Dynamic Differential Location Privacy with Personalized Error Bounds. In *Proc. of IEEE NDSS*.
- [38] Pengfei Zhang, Xiang Cheng, Sen Su, and Ning Wang. 2023. Task Allocation Under Geo-Indistinguishability via Group-Based Noise Addition. *IEEE Transactions on Big Data* 9, 3 (2023), 860–877. [doi:10.1109/TBDA.2022.3215467](https://doi.org/10.1109/TBDA.2022.3215467)

A Math Notations

Table 6: Summary of Mathematical Notation

Symbol	Description
Sets and Domains	
\mathcal{X}	Continuous secret data domain
$\hat{\mathcal{X}}$	Set of anchor records (corners of all N -orthotopes)
\mathcal{Y}	Perturbed (output) data domain
\mathcal{C}_m	The m -th N -orthotope (hyperrectangle) partition of \mathcal{X}
$\hat{\mathcal{X}}_m$	Anchor set for partition \mathcal{C}_m
\mathcal{Q}	Set of task locations for utility evaluation
Variables and Vectors	
$\mathbf{x}_i, \mathbf{x}_j$	Secret input records
\mathbf{y}_k	Perturbed output records
$\hat{\mathbf{x}}_i$	Anchor record indexed by i
$\gamma \in \{0, 1\}^N$	Binary vector to enumerate cube corners
ϵ_ℓ	Privacy budget allocated to dimension ℓ
Δ_ℓ	Length of cube edge along dimension ℓ
Functions and Distributions	
$d_p(\mathbf{x}, \mathbf{x}')$	ℓ_p -norm distance between two records
$p(\mathbf{x})$	Prior distribution over secret data domain \mathcal{X}
\mathcal{M}	Randomized perturbation mechanism
$z(\mathbf{y}_k \mid \mathbf{x})$	Probability of reporting \mathbf{y}_k given input \mathbf{x}
$\mathcal{L}(\mathbf{x}, \mathbf{y}_k)$	Task-specific utility loss between \mathbf{x} and \mathbf{y}_k
$\mathcal{L}(\mathbf{Z})$	Expected utility loss under perturbation matrix \mathbf{Z}
Optimization and Mechanisms	
AIPO	Anchor-based Interpolation for enforcing ℓ_p -mDP
AIPO-R	Relaxed variant of AIPO (enforces mDP only at anchor pairs)
APO	Anchor Perturbation Optimization (jointly optimizes anchors and budget)
Approx-APO	Linear approximation of APO with bounded optimality gap
\mathbf{Z}	Perturbation matrix $\{z(\mathbf{y}_k \mid \mathbf{x}_i)\}$
Constants and Parameters	
ϵ	Global privacy budget for ℓ_p -mDP
N	Dimensionality of the secret domain
M	Number of N -orthotope partitions

B Omitted Proofs

B.1 Proof of Proposition 1: Intra-Interval Validity

Proposition 1 (Intra-interval validity). *Let \mathbf{x}_i and $\mathbf{x}_{i'}$ be two records that differ only in their ℓ th coordinate, with $x_{i,\ell} < x_{i',\ell}$, and suppose their corresponding log-perturbation probabilities $\ln z(\mathbf{y}_k \mid \mathbf{x}_i)$ and $\ln z(\mathbf{y}_k \mid \mathbf{x}_{i'})$ satisfy the (ϵ, d_1) -Lipschitz*

bound. Then, for any $\mathbf{x}_a, \mathbf{x}_b \in \mathcal{X}$ such that $x_{a,\ell}, x_{b,\ell} \in [x_{i,\ell}, x_{i',\ell}]$ and all other coordinates are identical to those of \mathbf{x}_i , if the interpolated values $\hat{z}(\mathbf{y}_k \mid \mathbf{x}_a)$ and $\hat{z}(\mathbf{y}_k \mid \mathbf{x}_b)$ are calculated by

$$\hat{z}(\mathbf{y}_k \mid \mathbf{x}_a) \xrightarrow{\text{logcvx}} (z(\mathbf{y}_k \mid \mathbf{x}_i), z(\mathbf{y}_k \mid \mathbf{x}_{i'})), \quad (45)$$

$$\hat{z}(\mathbf{y}_k \mid \mathbf{x}_b) \xrightarrow{\text{logcvx}} (z(\mathbf{y}_k \mid \mathbf{x}_i), z(\mathbf{y}_k \mid \mathbf{x}_{i'})), \quad (46)$$

then $\ln \hat{z}(\mathbf{y}_k \mid \mathbf{x}_a)$ and $\ln \hat{z}(\mathbf{y}_k \mid \mathbf{x}_b)$ also satisfy the (ϵ, d_1) -Lipschitz bound between \mathbf{x}_a and \mathbf{x}_b . This property is illustrated in Fig. 4(a).

Proof. The ℓ th coordinates of \mathbf{x}_a and \mathbf{x}_b can be expressed as convex combinations of \mathbf{x}_i and $\mathbf{x}_{i'}$, i.e.,

$$x_{a,\ell} = \lambda_{\mathbf{x}_i, \mathbf{x}_a}^\ell x_{i,\ell} + (1 - \lambda_{\mathbf{x}_i, \mathbf{x}_a}^\ell)(x_{i,\ell} + \Delta), \quad (47)$$

$$x_{b,\ell} = \lambda_{\mathbf{x}_i, \mathbf{x}_b}^\ell x_{i,\ell} + (1 - \lambda_{\mathbf{x}_i, \mathbf{x}_b}^\ell)(x_{i,\ell} + \Delta). \quad (48)$$

Then, their ℓ_1 distance is:

$$d_1(\mathbf{x}_a, \mathbf{x}_b) = |x_{a,\ell} - x_{b,\ell}| = |\lambda_{\mathbf{x}_i, \mathbf{x}_a}^\ell - \lambda_{\mathbf{x}_i, \mathbf{x}_b}^\ell| \cdot \Delta. \quad (49)$$

From the log-convexity assumption:

$$\begin{aligned} & \ln z(\mathbf{y}_k \mid \mathbf{x}_a) \\ &= \lambda_{\mathbf{x}_i, \mathbf{x}_a}^\ell \ln z(\mathbf{y}_k \mid \mathbf{x}_i) + (1 - \lambda_{\mathbf{x}_i, \mathbf{x}_a}^\ell) \ln z(\mathbf{y}_k \mid \mathbf{x}_{i'}) \\ & \quad \ln z(\mathbf{y}_k \mid \mathbf{x}_b) \\ &= \lambda_{\mathbf{x}_i, \mathbf{x}_b}^\ell \ln z(\mathbf{y}_k \mid \mathbf{x}_i) + (1 - \lambda_{\mathbf{x}_i, \mathbf{x}_b}^\ell) \ln z(\mathbf{y}_k \mid \mathbf{x}_{i'}) \end{aligned} \quad (50)$$

Subtracting the two expressions:

$$\begin{aligned} & \ln z(\mathbf{y}_k \mid \mathbf{x}_a) - \ln z(\mathbf{y}_k \mid \mathbf{x}_b) \\ &= (\lambda_{\mathbf{x}_i, \mathbf{x}_a}^\ell - \lambda_{\mathbf{x}_i, \mathbf{x}_b}^\ell)(\ln z(\mathbf{y}_k \mid \mathbf{x}_i) - \ln z(\mathbf{y}_k \mid \mathbf{x}_{i'})) \\ &= \frac{d_1(\mathbf{x}_a, \mathbf{x}_b)}{\Delta} \cdot (\ln z(\mathbf{y}_k \mid \mathbf{x}_i) - \ln z(\mathbf{y}_k \mid \mathbf{x}_{i'})). \end{aligned} \quad (52)$$

Since $z(\cdot \mid \mathbf{x}_i)$ and $z(\cdot \mid \mathbf{x}_{i'})$ satisfy (ϵ_ℓ, d_1) -mDP:

$$|\ln z(\mathbf{y}_k \mid \mathbf{x}_i) - \ln z(\mathbf{y}_k \mid \mathbf{x}_{i'})| \leq \epsilon_\ell \cdot \Delta, \quad (53)$$

from which we obtain:

$$|\ln z(\mathbf{y}_k \mid \mathbf{x}_a) - \ln z(\mathbf{y}_k \mid \mathbf{x}_b)| \leq \epsilon_\ell \cdot d_1(\mathbf{x}_a, \mathbf{x}_b). \quad (54)$$

Hence, the perturbation distributions satisfy (ϵ_ℓ, d_1) -Lipschitz bound between \mathbf{x}_a and \mathbf{x}_b . The proof is complete. \square

B.2 Proof of Proposition 2: Across-Interval Validity

Proposition 2 (Across-interval Validity). *Let $\mathbf{x}_i, \mathbf{x}_{i'}, \mathbf{x}_j, \mathbf{x}_{j'}$ be four records that differ only in their ℓ th coordinate, with $x_{i,\ell} < x_{i',\ell} \leq x_{j,\ell} < x_{j',\ell}$. Suppose that each pair of log-perturbation probabilities $\ln z(\mathbf{y}_k \mid \mathbf{x}_i)$, $\ln z(\mathbf{y}_k \mid \mathbf{x}_{i'})$, $\ln z(\mathbf{y}_k \mid \mathbf{x}_j)$, and $\ln z(\mathbf{y}_k \mid \mathbf{x}_{j'})$ satisfy (ϵ, d_1) -Lipschitz bound.*

Let \mathbf{x}_a and \mathbf{x}_b be two additional records that differ from the above four points only in the ℓ th coordinate, with $x_{a,\ell} \in [x_{i,\ell}, x_{i',\ell}]$ and $x_{b,\ell} \in [x_{j,\ell}, x_{j',\ell}]$. If the corresponding interpolated values $\hat{z}(\mathbf{y}_k | \mathbf{x}_a)$ and $\hat{z}(\mathbf{y}_k | \mathbf{x}_b)$ are defined via log-convex interpolation as:

$$\hat{z}(\mathbf{y}_k | \mathbf{x}_a) \stackrel{\text{logcvx}}{\sim} (z(\mathbf{y}_k | \mathbf{x}_i), z(\mathbf{y}_k | \mathbf{x}_{i'})) \quad (55)$$

$$\hat{z}(\mathbf{y}_k | \mathbf{x}_b) \stackrel{\text{logcvx}}{\sim} (z(\mathbf{y}_k | \mathbf{x}_j), z(\mathbf{y}_k | \mathbf{x}_{j'})), \quad (56)$$

then the pair $(\hat{z}(\mathbf{y}_k | \mathbf{x}_a), \hat{z}(\mathbf{y}_k | \mathbf{x}_b))$ satisfies (ε, d_1) -Lipschitz bound between \mathbf{x}_a and \mathbf{x}_b . This property is illustrated in Fig. 4(b).

Proof. Since both $z(\mathbf{y}_k | \mathbf{x}_a)$ and $z(\mathbf{y}_k | \mathbf{x}_b)$ satisfy the logarithmic convexity condition in Eq. (12)

$$\ln z(\mathbf{y}_k | \mathbf{x}_a) \quad (57)$$

$$= \lambda_{\mathbf{x}_i, \mathbf{x}_a}^\ell \ln z(\mathbf{y}_k | \mathbf{x}_i) + (1 - \lambda_{\mathbf{x}_i, \mathbf{x}_a}^\ell) \ln z(\mathbf{y}_k | \mathbf{x}_{i'}). \quad (58)$$

$$\ln z(\mathbf{y}_k | \mathbf{x}_b) \quad (59)$$

$$= \lambda_{\mathbf{x}_j, \mathbf{x}_b}^\ell \ln z(\mathbf{y}_k | \mathbf{x}_j) + (1 - \lambda_{\mathbf{x}_j, \mathbf{x}_b}^\ell) \ln z(\mathbf{y}_k | \mathbf{x}_{j'}). \quad (60)$$

We decompose the log-ratio between $z(\mathbf{y}_k | \mathbf{x}_a)$ and $z(\mathbf{y}_k | \mathbf{x}_b)$ into three additive segments:

$$\ln z(\mathbf{y}_k | \mathbf{x}_a) - \ln z(\mathbf{y}_k | \mathbf{x}_b) \quad (61)$$

$$= \ln z(\mathbf{y}_k | \mathbf{x}_a) - \underbrace{\ln z(\mathbf{y}_k | \mathbf{x}_{i'})}_{=0} + \underbrace{\ln z(\mathbf{y}_k | \mathbf{x}_{i'})}_{=0} \quad (62)$$

$$= \underbrace{\ln z(\mathbf{y}_k | \mathbf{x}_a) - \ln z(\mathbf{y}_k | \mathbf{x}_{i'})}_{\text{Component}_1} \quad (63)$$

$$+ \underbrace{\ln z(\mathbf{y}_k | \mathbf{x}_{i'}) - \ln z(\mathbf{y}_k | \mathbf{x}_j)}_{\text{Component}_2} \quad (64)$$

$$+ \underbrace{\ln z(\mathbf{y}_k | \mathbf{x}_j) - \ln z(\mathbf{y}_k | \mathbf{x}_b)}_{\text{Component}_3} \quad (65)$$

Using the fact that all involved distributions satisfy (ε_ℓ, d_1) -Lipschitz bound, we apply distance-based upper bounds:

$$|\text{Component}_1| = |\ln z(\mathbf{y}_k | \mathbf{x}_a) - \ln z(\mathbf{y}_k | \mathbf{x}_{i'})| \quad (66)$$

$$\leq \varepsilon_\ell \cdot |x_{i',\ell} - x_{a,\ell}|, \quad (67)$$

$$|\text{Component}_2| = |\ln z(\mathbf{y}_k | \mathbf{x}_{i'}) - \ln z(\mathbf{y}_k | \mathbf{x}_j)| \quad (68)$$

$$\leq \varepsilon_\ell \cdot |x_{j,\ell} - x_{i',\ell}|, \quad (69)$$

$$|\text{Component}_3| = |\ln z(\mathbf{y}_k | \mathbf{x}_j) - \ln z(\mathbf{y}_k | \mathbf{x}_b)| \quad (70)$$

$$\leq \varepsilon_\ell \cdot |x_{b,\ell} - x_{j,\ell}|. \quad (71)$$

Summing these bounds:

$$|\ln z(\mathbf{y}_k | \mathbf{x}_a) - \ln z(\mathbf{y}_k | \mathbf{x}_b)| \quad (72)$$

$$\leq \varepsilon_\ell \cdot (|x_{i',\ell} - x_{a,\ell}| + |x_{j,\ell} - x_{i',\ell}| + |x_{b,\ell} - x_{j,\ell}|) \quad (73)$$

$$= \varepsilon_\ell \cdot |x_{b,\ell} - x_{a,\ell}| \quad (74)$$

$$= \varepsilon_\ell \cdot d_1(\mathbf{x}_a, \mathbf{x}_b).$$

Thus, $z(\mathbf{y}_k | \mathbf{x}_a)$ and $z(\mathbf{y}_k | \mathbf{x}_b)$ satisfy (ε_ℓ, d_1) -Lipschitz bound, as required. The proof is completed. \square

B.3 Proof of Theorem 1: Dimension-wise Composition for Lipschitz Bound Condition

Theorem 1 (Dimension-wise Composition for Lipschitz Bound Condition). Let $f : \mathcal{X} \rightarrow \mathbb{R}$ be a mechanism that interpolates values in an N -dimensional space. Suppose that for each $\ell \in \{1, \dots, N\}$, f satisfies (ε_ℓ, d_1) -Lipschitz bound when the input records differ only in the ℓ th coordinate. If the parameters $\varepsilon_1, \dots, \varepsilon_N$ satisfy the following budget composition condition:

$$\sum_{\ell=1}^N \varepsilon_\ell^{\frac{p}{p-1}} \leq \varepsilon^{\frac{p}{p-1}}, \quad \text{for } p > 1, \quad (75)$$

$$\text{and} \quad \max_\ell \varepsilon_\ell \leq \varepsilon, \quad \text{for } p = 1, \quad (76)$$

then f is (ε, d_p) -Lipschitz continuous.

Proof. For any pair $\mathbf{x}_a, \mathbf{x}_b \in \mathcal{X}$, we write the coordinate difference as $\Delta = \mathbf{x}' - \mathbf{x}$ with components $\Delta_\ell = x'_\ell - x_\ell$ for $\ell \in \{1, \dots, N\}$, and let \mathbf{e}_ℓ denote the ℓ th standard basis vector. Consider the axis-aligned path that changes one coordinate at a time:

$$\mathbf{x}^{(0)} := \mathbf{x}, \quad \mathbf{x}^{(\ell)} := \mathbf{x}^{(\ell-1)} + \Delta_\ell \mathbf{e}_\ell \quad \text{for } \ell = 1, \dots, N, \quad (77)$$

i.e., at the ℓ th step only coordinate ℓ changes while all other coordinates are held fixed at their current values.

Given that the mechanism satisfies the (ε_ℓ, d_1) -Lipschitz bound along each coordinate, for each ℓ and for any $\mathbf{y}_k \in \mathcal{Y}$,

$$|\ln z(\mathbf{y}_k | \mathbf{x}^{(\ell)}) - \ln z(\mathbf{y}_k | \mathbf{x}^{(\ell-1)})| \leq \varepsilon_\ell |\Delta_\ell|. \quad (78)$$

Iterating (78) along the N steps and telescoping yields

$$\begin{aligned} & |\ln z(\mathbf{y}_k | \mathbf{x}') - \ln z(\mathbf{y}_k | \mathbf{x})| \\ & \leq \sum_{\ell=1}^N \left| \ln z(\mathbf{y}_k | \mathbf{x}^{(\ell)}) - \ln z(\mathbf{y}_k | \mathbf{x}^{(\ell-1)}) \right| \\ & \leq \sum_{\ell=1}^N \varepsilon_\ell |\Delta_\ell|. \end{aligned} \quad (79)$$

Given $p \in [1, \infty]$, we let q be its Hölder dual $(1/p + 1/q = 1)$. Define the vectors $\varepsilon = (\varepsilon_1, \dots, \varepsilon_N)$ and $\Delta = (\Delta_1, \dots, \Delta_N)$. By Hölder's inequality,

$$\sum_{\ell=1}^N \varepsilon_\ell |\Delta_\ell| \leq \|\varepsilon\|_q \|\Delta\|_p. \quad (80)$$

Note that according to Eq. (17), and $q = \frac{p}{p-1}$

$$\sum_{\ell=1}^N \varepsilon_\ell^{\frac{p}{p-1}} \leq \varepsilon^{\frac{p}{p-1}} \Rightarrow \sum_{\ell=1}^N \varepsilon_\ell^q \leq \varepsilon^q \quad (81)$$

$$\Rightarrow \|\varepsilon\|_q \leq \varepsilon, \quad (82)$$

and by definition $d_p(\mathbf{x}_a, \mathbf{x}_b) := \|\mathbf{x}_b - \mathbf{x}_a\|_p = \|\Delta\|_p$. Therefore, we can obtain that

$$|\ln z(\mathbf{y}_k|\mathbf{x}') - \ln z(\mathbf{y}_k|\mathbf{x})| \quad (83)$$

$$\leq \sum_{\ell=1}^N \varepsilon_\ell |\Delta_\ell| \quad (\text{according to Eq. (79)}) \quad (84)$$

$$\leq \|\varepsilon\|_q \|\Delta\|_p \quad (\text{according to Eq. (80)}) \quad (85)$$

$$\leq \varepsilon d_p(\mathbf{x}_a, \mathbf{x}_b) \quad (86)$$

which is precisely the (ε, d_p) -Lipschitz bound between \mathbf{x} and \mathbf{x}' .

Remarks on edge cases. For $p = 1$ (so $q = \infty$), the bound reduces to $\sum_\ell \varepsilon_\ell |\Delta_\ell| \leq \|\varepsilon\|_\infty \|\Delta\|_1$. For $p = \infty$ (so $q = 1$), it becomes $\sum_\ell \varepsilon_\ell |\Delta_\ell| \leq \|\varepsilon\|_1 \|\Delta\|_\infty$. Both cases are encompassed by (80) and thus by the argument above.

This establishes that coordinating the per-dimension budgets $\{\varepsilon_\ell\}_{\ell=1}^N$ via $\|\varepsilon\|_q \leq \varepsilon$ yields a mechanism that satisfies the global (ε, d_p) -Lipschitz bound on \mathcal{X} . \square

B.4 Proof of Theorem 2: Correctness of Interpolation Function

Theorem 2 (Correctness of Log-Convex Interpolation f_{int}). *Given that (ε_ℓ, d_1) -Lipschitz bound holds between each pair of ℓ -neighbors in $\hat{\mathcal{X}}$ and $\{\varepsilon_\ell\}_{\ell=1}^N$ satisfy the privacy budget composition condition formalized in Eq. (17)(18), the use of the interpolation function f_{int} (defined by Eq. (30)) guarantees that any two interpolated values within the entire secret data domain \mathcal{X} satisfy (ε, d_p) -Lipschitz bound.*

Before proving Theorem 2, we introduce the following *Dimension-Wise Lipschitz bound*, which provides a sufficient condition for ensuring (ε, d_p) -mDP.

Definition 9 (Dimension-Wise Lipschitz bound (DW-Lipschitz bound)). *Given coordinate-specific privacy budgets $\varepsilon = \{\varepsilon_1, \dots, \varepsilon_N\}$, a mechanism f satisfies (ε, d_p) -DW-Lipschitz bound if for any two records $\mathbf{x}_a \in \mathcal{X}_m, \mathbf{x}_b \in \mathcal{X}_{m'}$ and perturbed value $\mathbf{y}_k \in \mathcal{Y}$, it holds that*

$$\frac{f(\mathbf{x}_a, \mathbf{y}_k, \mathbf{Z}_{\hat{\mathcal{X}}_m})}{f(\mathbf{x}_b, \mathbf{y}_k, \mathbf{Z}_{\hat{\mathcal{X}}_{m'}})} \leq e^{\sum_{\ell=1}^N \varepsilon_\ell |x_{a,\ell} - x_{b,\ell}|}. \quad (87)$$

Satisfying the DW-Lipschitz bound ensures that the overall privacy leakage between any two records is controlled by their ℓ_p -norm distance. We formalize this connection in the following **Lemma 1**.

Lemma 1. *Suppose that an interpolation mechanism f satisfies (ε, d_p) -DW-Lipschitz bound, where $\varepsilon = (\varepsilon_1, \dots, \varepsilon_N)$ are coordinate-specific privacy parameters. Then, if the*

dimension-wise composition condition holds:

$$\sum_{\ell=1}^N \varepsilon_\ell^{\frac{p}{p-1}} \leq \varepsilon^{\frac{p}{p-1}} \quad \text{for } p > 1, \quad (88)$$

$$\max_\ell \varepsilon_\ell \leq \varepsilon \quad \text{for } p = 1, \quad (89)$$

the mechanism \mathcal{M} satisfies (ε, d_p) -Lipschitz bound.

Proof of Lemma 1. Applying Hölder's inequality, we have

$$\sum_{\ell=1}^N \varepsilon_\ell |x_{a,\ell} - x_{b,\ell}| \quad (90)$$

$$\leq \left(\sum_{\ell=1}^N \varepsilon_\ell^{\frac{p}{p-1}} \right)^{\frac{p-1}{p}} \left(\sum_{\ell=1}^N |x_{a,\ell} - x_{b,\ell}|^p \right)^{\frac{1}{p}} \quad (91)$$

$$= \varepsilon d_p(\mathbf{x}_a, \mathbf{x}_b). \quad (92)$$

Thus, $\forall \mathbf{y}_k$

$$\frac{f(\mathbf{x}_a, \mathbf{y}_k, \mathbf{Z}_{\hat{\mathcal{X}}_m})}{f(\mathbf{x}_b, \mathbf{y}_k, \mathbf{Z}_{\hat{\mathcal{X}}_{m'}})} \leq e^{\sum_{\ell=1}^N \varepsilon_\ell |x_{a,\ell} - x_{b,\ell}|} \quad (93)$$

$$\Rightarrow \frac{f(\mathbf{x}_a, \mathbf{y}_k, \mathbf{Z}_{\hat{\mathcal{X}}_m})}{f(\mathbf{x}_b, \mathbf{y}_k, \mathbf{Z}_{\hat{\mathcal{X}}_{m'}})} \leq e^{\varepsilon d_p(\mathbf{x}_a, \mathbf{x}_b)}, \quad (94)$$

which establishes that f satisfies (ε, d_p) -Lipschitz bound. \square

Next, we introduce **Lemma 2–Lemma 4** as a preparation of the proof for **Theorem 2**.

Lemma 2 (Chain Rule for (ε, d_p) -DW-Lipschitz bound). *Let $\hat{\mathcal{X}}$ denote the set of anchor records obtained from the N -orthotope partitioning of the secret domain. If an interpolation mechanism f ensures that every pair of ℓ -neighbor anchors satisfies (ε, d_p) -DW-Lipschitz bound, then f also guarantees that any pair of anchors $\hat{\mathbf{x}}_i, \hat{\mathbf{x}}_j \in \hat{\mathcal{X}}$ satisfies (ε, d_p) -DW-Lipschitz bound.*

Proof of Lemma 2. For any two anchors $\hat{\mathbf{x}}_i, \hat{\mathbf{x}}_j \in \hat{\mathcal{X}}$, we construct a path \mathcal{P} by sequentially changing each coordinate from $\hat{\mathbf{x}}_i$ to $\hat{\mathbf{x}}_j$. Specifically, for each dimension $\ell \in \{1, \dots, N\}$:

- ▷ Move along the ℓ -th coordinate in steps of size Δ , where each step transitions between ℓ -neighbor anchors (i.e., points differing only in dimension ℓ by exactly Δ),
- ▷ The number of steps along dimension ℓ is $n_\ell = \frac{|\hat{x}_{i,\ell} - \hat{x}_{j,\ell}|}{\Delta}$.

Thus, the total path consists of $\sum_{\ell=1}^N n_\ell$ hops, each between ℓ -neighbor anchors. By assumption, f satisfies (ε, d_p) -DW-Lipschitz bound between every pair of ℓ -neighbor anchors, so at each hop along dimension ℓ , the privacy loss is at most $\varepsilon_\ell \Delta$. Therefore, the cumulative privacy leakage over the path is bounded by $\sum_{\ell=1}^N n_\ell \varepsilon_\ell \Delta = \sum_{\ell=1}^N \varepsilon_\ell |\hat{x}_{i,\ell} - \hat{x}_{j,\ell}| = (\varepsilon, d_p)$ -DW-Lipschitz bound. \square

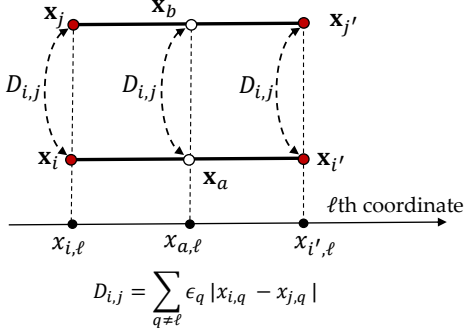


Figure 5: Proof of Lemma 3.

Lemma 3. As shown in Fig. 5, let $\mathbf{x}_a, \mathbf{x}_b, \mathbf{x}_i, \mathbf{x}_{i'}, \mathbf{x}_j$, and $\mathbf{x}_{j'}$ be six points in \mathbb{R}^N such that:

- ▷ \mathbf{x}_a shares the same coordinates with \mathbf{x}_i and $\mathbf{x}_{i'}$ at all dimensions except ℓ ;
- ▷ \mathbf{x}_b shares the same coordinates with \mathbf{x}_j and $\mathbf{x}_{j'}$ at all dimensions except ℓ ;
- ▷ at dimension ℓ , $x_{a,\ell} = x_{b,\ell}$, and $x_{i,\ell} = x_{j,\ell}$, $x_{i',\ell} = x_{j',\ell}$.

Suppose further that: both pairs $(\mathbf{x}_i, \mathbf{x}_j)$ and $(\mathbf{x}_{i'}, \mathbf{x}_{j'})$ satisfy (ϵ, d_p) -DW-Lipschitz bound; and the perturbation distributions satisfy log-convex interpolation:

$$z(\mathbf{y}_k | \mathbf{x}_a) \xrightarrow{\text{logcvx}} (z(\mathbf{y}_k | \mathbf{x}_i), z(\mathbf{y}_k | \mathbf{x}_{i'})) \quad (95)$$

$$z(\mathbf{y}_k | \mathbf{x}_b) \xrightarrow{\text{logcvx}} (z(\mathbf{y}_k | \mathbf{x}_j), z(\mathbf{y}_k | \mathbf{x}_{j'})). \quad (96)$$

Then, the pair $(\mathbf{x}_a, \mathbf{x}_b)$ satisfies (ϵ, d_p) -DW-Lipschitz bound, and hence (ϵ, d_p) -Lipschitz bound.

Proof of Lemma 3. Let $\lambda \in [0, 1]$ the convex interpolation coefficient determined by the relative position of \mathbf{x}_a between \mathbf{x}_i and $\mathbf{x}_{i'}$ along dimension ℓ , and similarly for \mathbf{x}_b between \mathbf{x}_j and $\mathbf{x}_{j'}$. Specifically, λ is chosen such that

$$x_{a,\ell} = \lambda x_{i,\ell} + (1 - \lambda) x_{i',\ell}, \quad x_{b,\ell} = \lambda x_{j,\ell} + (1 - \lambda) x_{j',\ell}, \quad (97)$$

The perturbation distributions at \mathbf{x}_a and \mathbf{x}_b are constructed via log-convex interpolation:

$$\ln z(\mathbf{y}_k | \mathbf{x}_a) = \lambda \ln z(\mathbf{y}_k | \mathbf{x}_i) + (1 - \lambda) \ln z(\mathbf{y}_k | \mathbf{x}_{i'}), \quad (98)$$

$$\ln z(\mathbf{y}_k | \mathbf{x}_b) = \lambda \ln z(\mathbf{y}_k | \mathbf{x}_j) + (1 - \lambda) \ln z(\mathbf{y}_k | \mathbf{x}_{j'}). \quad (99)$$

Applying the triangle inequality, we have

$$|\ln z(\mathbf{y}_k | \mathbf{x}_a) - \ln z(\mathbf{y}_k | \mathbf{x}_b)| \quad (100)$$

$$= |\lambda (\ln z(\mathbf{y}_k | \mathbf{x}_i) - \ln z(\mathbf{y}_k | \mathbf{x}_j))| \quad (101)$$

$$+ (1 - \lambda) |\ln z(\mathbf{y}_k | \mathbf{x}_{i'}) - \ln z(\mathbf{y}_k | \mathbf{x}_{j'})| \quad (102)$$

$$\leq \lambda |\ln z(\mathbf{y}_k | \mathbf{x}_i) - \ln z(\mathbf{y}_k | \mathbf{x}_j)| \quad (103)$$

$$+ (1 - \lambda) |\ln z(\mathbf{y}_k | \mathbf{x}_{i'}) - \ln z(\mathbf{y}_k | \mathbf{x}_{j'})|. \quad (104)$$

By the assumption that $(\mathbf{x}_i, \mathbf{x}_j)$ and $(\mathbf{x}_{i'}, \mathbf{x}_{j'})$ satisfy DW-Lipschitz bound, we have

$$|\ln z(\mathbf{y}_k | \mathbf{x}_i) - \ln z(\mathbf{y}_k | \mathbf{x}_j)| \leq \sum_{q=1}^N \epsilon_q |x_{i,q} - x_{j,q}|, \quad (105)$$

$$|\ln z(\mathbf{y}_k | \mathbf{x}_{i'}) - \ln z(\mathbf{y}_k | \mathbf{x}_{j'})| \leq \sum_{q=1}^N \epsilon_q |x_{i',q} - x_{j',q}|. \quad (106)$$

By construction: we have $q \neq \ell$, $x_{i,q} = x_{i',q}$ and $x_{j,q} = x_{j',q}$, and hence $x_{i,q} - x_{j,q} = x_{i',q} - x_{j',q}$ for all $q \neq \ell$. Also, we have $x_{i,\ell} = x_{j,\ell}$, $x_{i',\ell} = x_{j',\ell}$. Therefore:

$$x_{i,\ell} - x_{j,\ell} = 0, \quad x_{i',\ell} - x_{j',\ell} = 0. \quad (107)$$

and for $q \neq \ell$:

$$x_{i,q} - x_{j,q} = x_{i',q} - x_{j',q}. \quad (108)$$

Thus, the privacy bounds simplify to:

$$|\ln z(\mathbf{y}_k | \mathbf{x}_i) - \ln z(\mathbf{y}_k | \mathbf{x}_j)| \leq \sum_{q \neq \ell} \epsilon_q |x_{i,q} - x_{j,q}|, \quad (109)$$

$$|\ln z(\mathbf{y}_k | \mathbf{x}_{i'}) - \ln z(\mathbf{y}_k | \mathbf{x}_{j'})| \leq \sum_{q \neq \ell} \epsilon_q |x_{i',q} - x_{j',q}|, \quad (110)$$

where for $q \neq \ell$, the differences match.

Substituting back into the triangle inequality in Eq. (100)–(103), we get

$$|\ln z(\mathbf{y}_k | \mathbf{x}_a) - \ln z(\mathbf{y}_k | \mathbf{x}_b)| \leq \sum_{q \neq \ell} \epsilon_q |x_{i,q} - x_{j,q}|, \quad (111)$$

where the right-hand side depends only on differences at dimensions $q \neq \ell$.

Since \mathbf{x}_a and \mathbf{x}_b share the same value at dimension ℓ and differ only at other coordinates, the above bound implies that $(\mathbf{x}_a, \mathbf{x}_b)$ satisfy (ϵ, d_p) -DW-Lipschitz bound, and hence (ϵ, d_p) -Lipschitz bound. \square

Lemma 4. Let $\mathbf{x}_i, \mathbf{x}_{i'} \in \mathcal{X}_m$ be any two points within an N -orthotope that differ only in the ℓ th coordinate, and let $\mathbf{x}_a \in \mathcal{X}_m$ be any point such that $x_{i,\ell} \leq x_{a,\ell} \leq x_{i',\ell}$ and \mathbf{x}_a also differs from \mathbf{x}_i and $\mathbf{x}_{i'}$ only in the ℓ th coordinate. Then, the interpolation function defined in Definition 6 satisfies the following log-convexity condition:

$$z(\mathbf{y}_k | \mathbf{x}_a) \xrightarrow{\text{logcvx}} (z(\mathbf{y}_k | \mathbf{x}_i), z(\mathbf{y}_k | \mathbf{x}_{i'})). \quad (112)$$

Proof of Lemma 4. Let $\hat{\mathbf{x}}_{i_m}$ be the base corner of the N -orthotope \mathcal{X}_m , and let Δ denote the side length vector. Recall from Definition 6 that the log-interpolated probability at \mathbf{x}_a is:

$$\ln z(\mathbf{y}_k | \mathbf{x}_a) \quad (113)$$

$$= \sum_{q \in \{0, 1\}^N} \prod_{q=1}^N \left((1 - \gamma_q) \lambda_{\hat{\mathbf{x}}_{i_m}, \mathbf{x}_a}^q + \gamma_q (1 - \lambda_{\hat{\mathbf{x}}_{i_m}, \mathbf{x}_a}^q) \right) \times \ln z(\mathbf{y}_k | \hat{\mathbf{x}}_{i_m} + \gamma \odot \Delta). \quad (114)$$

To verify log-convexity, we compute:

$$\ln z(\mathbf{y}_k \mid \mathbf{x}_a) - \lambda_{\hat{\mathbf{x}}_{i_m}, \mathbf{x}_a}^\ell \ln z(\mathbf{y}_k \mid \mathbf{x}_i) \quad (115)$$

$$- (1 - \lambda_{\hat{\mathbf{x}}_{i_m}, \mathbf{x}_a}^\ell) \ln z(\mathbf{y}_k \mid \mathbf{x}_{i'}) \quad (116)$$

$$= \sum_{\gamma \in \{0,1\}^N} \prod_{q=1}^N ((1 - \gamma_q) \lambda_{\hat{\mathbf{x}}_{i_m}, \mathbf{x}_a}^q + \gamma_q (1 - \lambda_{\hat{\mathbf{x}}_{i_m}, \mathbf{x}_a}^q)) \quad (117)$$

$$- \lambda_{\hat{\mathbf{x}}_{i_m}, \mathbf{x}_a}^\ell \sum_{\gamma \in \{0,1\}^N} \prod_{q \neq \ell} ((1 - \gamma_q) \lambda_{\hat{\mathbf{x}}_{i_m}, \mathbf{x}_a}^q + \gamma_q (1 - \lambda_{\hat{\mathbf{x}}_{i_m}, \mathbf{x}_a}^q))$$

$$\times \underbrace{((1 - \gamma_\ell) \lambda_{\hat{\mathbf{x}}_{i_m}, \mathbf{x}_i}^\ell + \gamma_\ell (1 - \lambda_{\hat{\mathbf{x}}_{i_m}, \mathbf{x}_i}^\ell))}_{\text{It equals to } (1 - \gamma_\ell) \text{ since } \lambda_{\hat{\mathbf{x}}_{i_m}, \mathbf{x}_i}^\ell = 1} \quad (118)$$

$$- (1 - \lambda_{\hat{\mathbf{x}}_{i_m}, \mathbf{x}_a}^\ell) \sum_{\gamma \in \{0,1\}^N} \prod_{q \neq \ell} ((1 - \gamma_q) \lambda_{\hat{\mathbf{x}}_{i_m}, \mathbf{x}_a}^q + \gamma_q (1 - \lambda_{\hat{\mathbf{x}}_{i_m}, \mathbf{x}_a}^q))$$

$$\times \underbrace{((1 - \gamma_\ell) \lambda_{\hat{\mathbf{x}}_{i_m}, \mathbf{x}_{i'}}^\ell + \gamma_\ell (1 - \lambda_{\hat{\mathbf{x}}_{i_m}, \mathbf{x}_{i'}}^\ell))}_{\text{It equals to } \gamma_\ell \text{ since } \lambda_{\hat{\mathbf{x}}_{i_m}, \mathbf{x}_{i'}}^\ell = 0} \quad (119)$$

$$\times \ln(z(\mathbf{y}_k \mid \hat{\mathbf{x}}_{i_m} + \gamma \odot \Delta)) \quad (120)$$

$$= \sum_{\gamma \in \{0,1\}^N} \prod_{q=1}^N ((1 - \gamma_q) \lambda_{\hat{\mathbf{x}}_{i_m}, \mathbf{x}_a}^q + \gamma_q (1 - \lambda_{\hat{\mathbf{x}}_{i_m}, \mathbf{x}_a}^q)) \quad (121)$$

$$\times \ln(z(\mathbf{y}_k \mid \hat{\mathbf{x}}_{i_m} + \gamma \odot \Delta)) \quad (121)$$

$$- \sum_{\gamma \in \{0,1\}^N} \prod_{q \neq \ell} ((1 - \gamma_q) \lambda_{\hat{\mathbf{x}}_{i_m}, \mathbf{x}_a}^q + \gamma_q (1 - \lambda_{\hat{\mathbf{x}}_{i_m}, \mathbf{x}_a}^q))$$

$$\times \lambda_{\hat{\mathbf{x}}_{i_m}, \mathbf{x}_a}^\ell (1 - \gamma_\ell) \times \ln(z(\mathbf{y}_k \mid \hat{\mathbf{x}}_{i_m} + \gamma \odot \Delta)) \quad (122)$$

$$- \sum_{\gamma \in \{0,1\}^N} \prod_{q \neq \ell} ((1 - \gamma_q) \lambda_{\hat{\mathbf{x}}_{i_m}, \mathbf{x}_a}^q + \gamma_q (1 - \lambda_{\hat{\mathbf{x}}_{i_m}, \mathbf{x}_a}^q))$$

$$\times (1 - \lambda_{\hat{\mathbf{x}}_{i_m}, \mathbf{x}_a}^\ell) \gamma_\ell \times \ln(z(\mathbf{y}_k \mid \hat{\mathbf{x}}_{i_m} + \gamma \odot \Delta)) \quad (123)$$

$$= 0, \quad (124)$$

meaning that $z(\mathbf{y}_k \mid \mathbf{x}_a) \stackrel{\text{logcvx}}{\sim} (z(\mathbf{y}_k \mid \mathbf{x}_i), z(\mathbf{y}_k \mid \mathbf{x}_{i'}))$. This concludes the proof. \square

Next, we provide the detailed proof of **Theorem 2**:

Proof of Theorem 2. Without loss of generality, assume that \mathbf{x}_a and \mathbf{x}_b differ only in dimension 1, with $x_{a,1} < x_{b,1}$. Let $\mathbf{x}_a \in \mathcal{C}_i$ and $\mathbf{x}_b \in \mathcal{C}_j$, where the ranges of \mathcal{C}_i and \mathcal{C}_j along dimension ℓ are $[\hat{x}_{i,\ell}, \hat{x}_{i',\ell}]$ and $[\hat{x}_{j,\ell}, \hat{x}_{j',\ell}]$, respectively.

We construct two trees rooted at \mathbf{x}_a and \mathbf{x}_b as follows:

Intuitively, the two trees systematically decompose the difference between \mathbf{x}_a and \mathbf{x}_b along one dimension at a time. At each level ℓ , nodes extend along the ℓ -th coordinate toward their cell boundaries, progressively aligning the records with anchor points. This recursive structure allows us to apply a dimension-wise induction, ultimately connecting the original records to anchor records through a sequence of intermediate steps that satisfy local Lipschitz bound.

▷ **Initialization (Level 0):** Set \mathbf{x}_a and \mathbf{x}_b as the roots.

▷ **Level 1 Construction:** Extend both \mathbf{x}_a and \mathbf{x}_b along dimension 1 toward the boundaries of their respective cells, producing four points $\mathbf{x}_c, \mathbf{x}_d, \mathbf{x}_e, \mathbf{x}_f$, where:

$$x_{c,1} = \hat{x}_{i,1}, \quad x_{d,1} = \hat{x}_{i',1}, \quad x_{e,1} = \hat{x}_{j,1}, \quad x_{f,1} = \hat{x}_{j',1}. \quad (125)$$

Add $\mathbf{x}_c, \mathbf{x}_d$ as children of \mathbf{x}_a , and $\mathbf{x}_e, \mathbf{x}_f$ as children of \mathbf{x}_b (see Fig. 6).

▷ **Level ℓ Construction** ($\ell = 2, \dots, N$): For each node \mathbf{x}_v at level $\ell - 1$, extend along dimension ℓ toward the cell boundaries, producing children $\mathbf{x}_{v'}$ and $\mathbf{x}_{v''}$, where $x_{v',\ell} = \hat{x}_{i,\ell}$ and $x_{v'',\ell} = \hat{x}_{i',\ell}$. All other coordinates are inherited from \mathbf{x}_v .

By construction, every node at level ℓ lies on the boundary along the first ℓ dimensions.

We now prove the theorem via **induction** on the tree levels:

▷ **Base case (Level N):** Each leaf node lies on the boundaries in all N dimensions, thus is an anchor record. Since every pair of ℓ -neighbor anchors satisfies (ϵ, d_p) -DW-Lipschitz bound by assumption, any pair of leaves satisfies (ϵ, d_p) -DW-Lipschitz bound (according to **Lemma 2**).

▷ **Inductive step:** Suppose at level ℓ ($2 \leq \ell \leq N$), any pair of nodes satisfies (ϵ, d_p) -DW-Lipschitz bound. We show that at level $\ell - 1$, their parents also satisfy (ϵ, d_p) -DW-Lipschitz bound.

Consider two parent nodes \mathbf{x}_v and \mathbf{x}_u at level $\ell - 1$ with children $\{\mathbf{x}_{v'}, \mathbf{x}_{v''}\}$ and $\{\mathbf{x}_{u'}, \mathbf{x}_{u''}\}$, respectively. As shown in Fig. 7:

- \mathbf{x}_v shares all coordinates with $\mathbf{x}_{v'}$ and $\mathbf{x}_{v''}$ except along dimension ℓ .
- \mathbf{x}_u shares all coordinates with $\mathbf{x}_{u'}$ and $\mathbf{x}_{u''}$ except along dimension ℓ .
- Moreover, $x_{v,\ell} = x_{u,\ell} = x_{a,\ell}$, $x_{v',\ell} = x_{u',\ell} = \hat{x}_{i,\ell}$, and $x_{v'',\ell} = x_{u'',\ell} = \hat{x}_{i',\ell}$.

Then, by applying **Lemma 4**, we can obtain

$$z(\mathbf{y}_k \mid \mathbf{x}_v) \stackrel{\text{logcvx}}{\sim} (z(\mathbf{y}_k \mid \mathbf{x}_{v'}), z(\mathbf{y}_k \mid \mathbf{x}_{v''})) \quad (126)$$

$$z(\mathbf{y}_k \mid \mathbf{x}_u) \stackrel{\text{logcvx}}{\sim} (z(\mathbf{y}_k \mid \mathbf{x}_{u'}), z(\mathbf{y}_k \mid \mathbf{x}_{u''})). \quad (127)$$

and then by **Lemma 3**, we can obtain the parent nodes \mathbf{x}_v and \mathbf{x}_u satisfy (ϵ, d_p) -DW-Lipschitz bound.

▷ **Conclusion (Level 0):** At level 1, by induction, we have deduced that the four nodes $\mathbf{x}_c, \mathbf{x}_d, \mathbf{x}_e, \mathbf{x}_f$ satisfy (ϵ, d_p) -DW-Lipschitz bound. Finally, by applying **Proposition 2** (or **Proposition 1** if \mathbf{x}_a and \mathbf{x}_b lie in the same N -orthotope), we conclude that the original pair $(\mathbf{x}_a, \mathbf{x}_b)$ satisfies (ϵ, d_p) -DW-Lipschitz bound, and hence ϵ, d_p -mDP (according to **Lemma 1**).

This completes the proof. \square

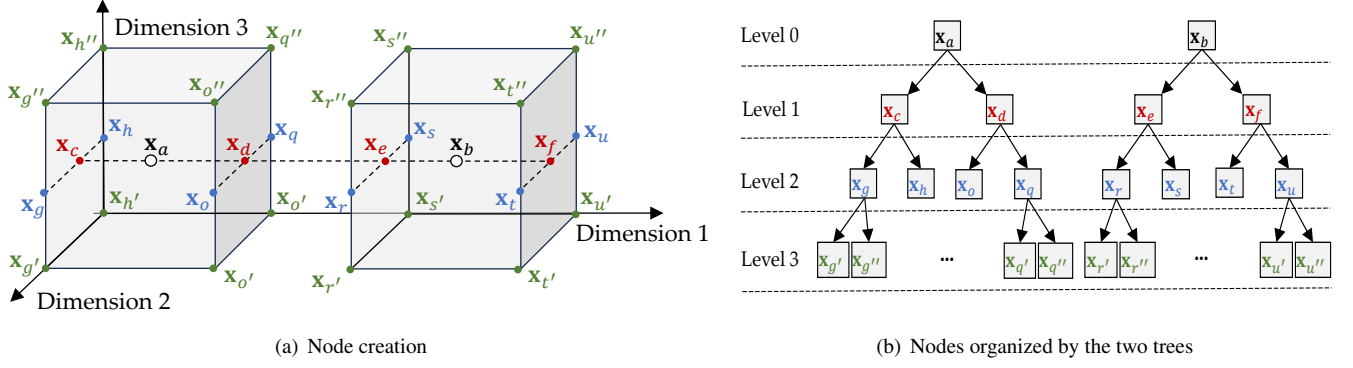


Figure 6: Illustration of node creation in Proof of Theorem 2 (Nodes are recursively extended along dimensions 1, 2, and 3 toward cell boundaries, reaching anchor points at the leaves).

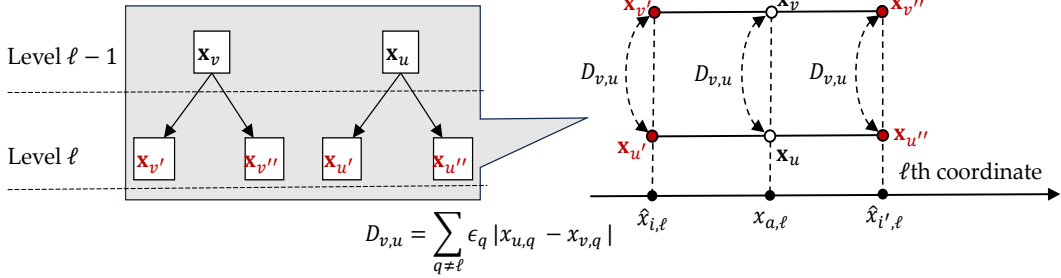


Figure 7: Illustration of Property P-B.

B.5 Proof of Proposition 3

Proposition 3. *Given that any pair of real records $\mathbf{x}_a \in \mathcal{X}_m$ and $\mathbf{x}_b \in \mathcal{X}_{m'}$ with their perturbation probabilities interpolated by*

$$z(\mathbf{y}_k | \mathbf{x}_a) = \bar{f}_{\text{int}}(\mathbf{x}_a, \mathbf{y}_k, \mathbf{Z}_{\hat{\mathcal{X}}_m}) \quad (128)$$

$$z(\mathbf{y}_k | \mathbf{x}_b) = \bar{f}_{\text{int}}(\mathbf{x}_b, \mathbf{y}_k, \mathbf{Z}_{\hat{\mathcal{X}}_{m'}}) \quad (129)$$

then their perturbation probabilities satisfy $(2\epsilon, d_p)$ -mDP.

Proof. We assume that the unnormalized interpolation function f_{int} satisfies (ϵ, d_p) -Lipschitz bound, i.e.,

$$e^{-\epsilon d_p(\mathbf{x}_a, \mathbf{x}_b)} \leq \frac{f_{\text{int}}(\mathbf{x}_a, \mathbf{y}_k, \mathbf{Z}_{\hat{\mathcal{X}}_m})}{f_{\text{int}}(\mathbf{x}_b, \mathbf{y}_k, \mathbf{Z}_{\hat{\mathcal{X}}_{m'}})} \leq e^{\epsilon d_p(\mathbf{x}_a, \mathbf{x}_b)}. \quad (130)$$

By summing both the numerator and denominator over all $\mathbf{y}_j \in \mathcal{Y}$, the same multiplicative bounds hold for the partition function:

$$e^{-\epsilon d_p(\mathbf{x}_a, \mathbf{x}_b)} \leq \frac{\sum_{\mathbf{y}_j \in \mathcal{Y}} f_{\text{int}}(\mathbf{x}_a, \mathbf{y}_j, \mathbf{Z}_{\hat{\mathcal{X}}_m})}{\sum_{\mathbf{y}_j \in \mathcal{Y}} f_{\text{int}}(\mathbf{x}_b, \mathbf{y}_j, \mathbf{Z}_{\hat{\mathcal{X}}_{m'}})} \leq e^{\epsilon d_p(\mathbf{x}_a, \mathbf{x}_b)}. \quad (131)$$

Recall that the normalized output distribution is defined as:

$$z(\mathbf{y}_k | \mathbf{x}) = \bar{f}_{\text{int}}(\mathbf{x}, \mathbf{y}_k, \mathbf{Z}_{\hat{\mathcal{X}}_m}) = \frac{f_{\text{int}}(\mathbf{x}, \mathbf{y}_k, \mathbf{Z}_{\hat{\mathcal{X}}_m})}{\sum_{\mathbf{y}_j \in \mathcal{Y}} f_{\text{int}}(\mathbf{x}, \mathbf{y}_j, \mathbf{Z}_{\hat{\mathcal{X}}_m})}.$$

Then, the ratio of normalized probabilities becomes:

$$\begin{aligned} \frac{z(\mathbf{y}_k | \mathbf{x}_a)}{z(\mathbf{y}_k | \mathbf{x}_b)} &= \frac{\bar{f}_{\text{int}}(\mathbf{x}_a, \mathbf{y}_k, \mathbf{Z}_{\hat{\mathcal{X}}_m})}{\bar{f}_{\text{int}}(\mathbf{x}_b, \mathbf{y}_k, \mathbf{Z}_{\hat{\mathcal{X}}_{m'}})} \\ &= \frac{f_{\text{int}}(\mathbf{x}_a, \mathbf{y}_k, \mathbf{Z}_{\hat{\mathcal{X}}_m})}{f_{\text{int}}(\mathbf{x}_b, \mathbf{y}_k, \mathbf{Z}_{\hat{\mathcal{X}}_{m'}})} \cdot \frac{\sum_{\mathbf{y}_j \in \mathcal{Y}} f_{\text{int}}(\mathbf{x}_b, \mathbf{y}_j, \mathbf{Z}_{\hat{\mathcal{X}}_{m'}})}{\sum_{\mathbf{y}_j \in \mathcal{Y}} f_{\text{int}}(\mathbf{x}_a, \mathbf{y}_j, \mathbf{Z}_{\hat{\mathcal{X}}_m})}. \end{aligned} \quad (132)$$

Applying inequalities (130) and (131) to each term, we obtain:

$$e^{-2\epsilon d_p(\mathbf{x}_a, \mathbf{x}_b)} \leq \frac{z(\mathbf{y}_k | \mathbf{x}_a)}{z(\mathbf{y}_k | \mathbf{x}_b)} \leq e^{2\epsilon d_p(\mathbf{x}_a, \mathbf{x}_b)}, \quad (133)$$

which concludes the proof that the normalized distribution satisfies $(2\epsilon, d_p)$ -metric differential privacy. \square

B.6 Proof of Proposition 4: Linear Surrogate For Utility Loss

Proposition 4 (Linear surrogate for utility loss). *For any point $\mathbf{x} = \hat{\mathbf{x}}_{i_m} + \lambda_a \odot \Delta \in \mathcal{C}_m$, with the convex coefficients $\lambda = [\lambda_{\hat{\mathbf{x}}_{i_m}, \mathbf{x}}^1, \dots, \lambda_{\hat{\mathbf{x}}_{i_m}, \mathbf{x}}^N] \in [0, 1]^N$, approximate the perturba-*

tion probability by

$$\Pr[\mathcal{M}(\mathbf{x}; \mathbf{Z}_{\hat{\mathcal{X}}_m}) = \mathbf{y}_k] \quad (134)$$

$$\approx \sum_{\gamma \in \{0,1\}^N} \prod_{\ell=1}^N ((1-\gamma_\ell) \lambda_{\hat{\mathbf{x}}_{i_m}, \mathbf{x}}^\ell + \gamma_\ell (1 - \lambda_{\hat{\mathbf{x}}_{i_m}, \mathbf{x}}^\ell)) \quad (135)$$

$$\times z(\mathbf{y}_k \mid \hat{\mathbf{x}}_{i_m} + \gamma \odot \Delta) \quad (136)$$

the cell loss $\mathcal{L}(\mathbf{Z}_{\hat{\mathcal{X}}_m})$ admits the linear surrogate $\tilde{\mathcal{L}}(\mathbf{Z}_{\hat{\mathcal{X}}_m}) = \langle \tilde{\mathbf{C}}_{\hat{\mathcal{X}}_m}, \mathbf{Z}_{\hat{\mathcal{X}}_m} \rangle$, where $\tilde{\mathbf{C}}_{\hat{\mathcal{X}}_m} = \{\tilde{c}(\hat{\mathbf{x}}_i, \mathbf{y}_k)\}_{(\hat{\mathbf{x}}_i, \mathbf{y}_k) \in \hat{\mathcal{X}}_m \times \mathcal{Y}}$ is a constant coefficient matrix depending only on the prior $p(\mathbf{x})$ and the utility loss $\mathcal{L}(\mathbf{x}, \mathbf{y}_k)$. For each $\hat{\mathbf{x}}_j = \hat{\mathbf{x}}_{i_m} + \gamma \odot \Delta \in \hat{\mathcal{X}}_m$

$$\tilde{c}(\hat{\mathbf{x}}_j, \mathbf{y}_k) \quad (137)$$

$$= \int_{\mathcal{C}_m} \prod_{\ell=1}^N ((1-\gamma_\ell) \lambda_{\hat{\mathbf{x}}_{i_m}, \mathbf{x}}^\ell + \gamma_\ell (1 - \lambda_{\hat{\mathbf{x}}_{i_m}, \mathbf{x}}^\ell)) p(\mathbf{x}) \mathcal{L}(\mathbf{x}, \mathbf{y}_k) d\mathbf{x}.$$

If \mathcal{X} is discretized,

$$\begin{aligned} & \tilde{c}(\hat{\mathbf{x}}_j, \mathbf{y}_k) \quad (138) \\ &= \sum_{\mathbf{x} \in \mathcal{X}_m} \prod_{\ell=1}^N ((1-\gamma_\ell) \lambda_{\hat{\mathbf{x}}_{i_m}, \mathbf{x}}^\ell + \gamma_\ell (1 - \lambda_{\hat{\mathbf{x}}_{i_m}, \mathbf{x}}^\ell)) p(\mathbf{x}) \mathcal{L}(\mathbf{x}, \mathbf{y}_k). \end{aligned}$$

Proof. Let $\mathbf{x} = \hat{\mathbf{x}}_{i_m} + \lambda \odot \Delta$ where $\lambda = [\lambda_{\hat{\mathbf{x}}_{i_m}, \mathbf{x}}^1, \dots, \lambda_{\hat{\mathbf{x}}_{i_m}, \mathbf{x}}^N] \in [0, 1]^N$. By definition of the approximated mechanism, we have:

$$\begin{aligned} & \tilde{\mathcal{L}}(\mathbf{Z}_{\hat{\mathcal{X}}_m}) \\ &= \sum_{\mathbf{y}_k \in \mathcal{Y}} \int_{\mathcal{C}_m} \Pr[\mathcal{M}(\mathbf{x}, \mathbf{Z}_{\hat{\mathcal{X}}_m}) = \mathbf{y}_k] p(\mathbf{x}) \mathcal{L}(\mathbf{x}, \mathbf{y}_k) d\mathbf{x} \\ &\approx \sum_{\mathbf{y}_k \in \mathcal{Y}} \int_{\mathcal{C}_m} \left[\sum_{\gamma \in \{0,1\}^N} ((1-\gamma_\ell) \lambda_{\hat{\mathbf{x}}_{i_m}, \mathbf{x}}^\ell + \gamma_\ell (1 - \lambda_{\hat{\mathbf{x}}_{i_m}, \mathbf{x}}^\ell)) z(\mathbf{y}_k \mid \hat{\mathbf{x}}_{i_m} + \gamma \odot \Delta) \right] p(\mathbf{x}) \mathcal{L}(\mathbf{x}, \mathbf{y}_k) d\mathbf{x} \\ &= \sum_{\mathbf{y}_k \in \mathcal{Y}} \sum_{\gamma \in \{0,1\}^N} z(\mathbf{y}_k \mid \hat{\mathbf{x}}_{i_m} + \gamma \odot \Delta) \\ &\quad \times \int_{\mathcal{C}_m} ((1-\gamma_\ell) \lambda_{\hat{\mathbf{x}}_{i_m}, \mathbf{x}}^\ell + \gamma_\ell (1 - \lambda_{\hat{\mathbf{x}}_{i_m}, \mathbf{x}}^\ell)) p(\mathbf{x}) \mathcal{L}(\mathbf{x}, \mathbf{y}_k) d\mathbf{x} \\ &= \sum_{(\hat{\mathbf{x}}_j, \mathbf{y}_k) \in \hat{\mathcal{X}}_m \times \mathcal{Y}} \tilde{c}(\hat{\mathbf{x}}_j, \mathbf{y}_k) z(\mathbf{y}_k \mid \hat{\mathbf{x}}_j), \quad (139) \end{aligned}$$

where $\hat{\mathbf{x}}_j = \hat{\mathbf{x}}_{i_m} + \gamma \odot \Delta$ and the coefficient

$$\tilde{c}(\hat{\mathbf{x}}_j, \mathbf{y}_k) \quad (140)$$

$$= \int_{\mathcal{C}_m} \prod_{\ell=1}^N ((1-\gamma_\ell) \lambda_{\hat{\mathbf{x}}_{i_m}, \mathbf{x}}^\ell + \gamma_\ell (1 - \lambda_{\hat{\mathbf{x}}_{i_m}, \mathbf{x}}^\ell)) \quad (141) \\ \times p(\mathbf{x}) \mathcal{L}(\mathbf{x}, \mathbf{y}_k) d\mathbf{x} \quad (142)$$

is a constant with respect to \mathbf{Z} .

If \mathcal{X} is discretized, then the integral becomes a summation:

$$\tilde{c}(\hat{\mathbf{x}}_j, \mathbf{y}_k) = \sum_{\mathbf{x} \in \mathcal{X}_m} \prod_{\ell=1}^N ((1-\gamma_\ell) \lambda_{\hat{\mathbf{x}}_{i_m}, \mathbf{x}}^\ell + \gamma_\ell (1 - \lambda_{\hat{\mathbf{x}}_{i_m}, \mathbf{x}}^\ell)) p(\mathbf{x}) \mathcal{L}(\mathbf{x}, \mathbf{y}_k). \quad (143)$$

In both cases, the resulting loss $\tilde{\mathcal{L}}(\mathbf{Z}_{\hat{\mathcal{X}}_m})$ is a linear function of the perturbation matrix $\mathbf{Z}_{\hat{\mathcal{X}}_m}$. \square

C Optimal Gap Analysis

To evaluate how closely our solution can approach the true optimum, we derive a universal lower bound on the utility loss, labeled as "**LB**" in the following experiment part.

For any two cells \mathcal{C}_m and $\mathcal{C}_{m'}$, we first define the following inter-cell distance:

$$\hat{d}_p(\mathcal{C}_m, \mathcal{C}_{m'}) := \max_{\mathbf{x} \in \mathcal{C}_m, \mathbf{x}' \in \mathcal{C}_{m'}} d_p(\mathbf{x}, \mathbf{x}'). \quad (144)$$

Since $d_p(\mathbf{x}, \mathbf{x}') \leq \hat{d}_p(\mathcal{C}_m, \mathcal{C}_{m'})$ for all $\mathbf{x} \in \mathcal{C}_m, \mathbf{x}' \in \mathcal{C}_{m'}$, replacing d_p with \hat{d}_p yields a relaxation of the original mDP constraints. We define the aggregated decision variables:

$$z(\mathbf{y}_k \mid \mathcal{C}_m) := \int_{\mathcal{C}_m} \Pr[\mathcal{M}(\mathbf{x}) = \mathbf{y}_k] d\mathbf{x}, \quad (145)$$

and impose the relaxed mDP constraints:

$$z(\mathbf{y}_k \mid \mathcal{C}_m) - e^{\epsilon \hat{d}_p(\mathcal{C}_m, \mathcal{C}_{m'})} z(\mathbf{y}_k \mid \mathcal{C}_{m'}) \leq 0, \quad \forall \mathcal{C}_m, \mathcal{C}_{m'}. \quad (146)$$

and normalization constraint:

$$\sum_{\mathbf{y}_k \in \mathcal{Y}} z(\mathbf{y}_k \mid \mathcal{C}_m) = \int_{\mathcal{C}_m} d\mathbf{x} = \prod_{\ell=1}^N \Delta_\ell. \quad (147)$$

Finally, define the minimal utility loss over each cell:

$$\bar{\mathcal{L}}_m(\mathbf{y}_k) := \min_{\mathbf{x} \in \mathcal{C}_m} p(\mathbf{x}) \mathcal{L}(\mathbf{x}, \mathbf{y}_k). \quad (148)$$

We now formulate the relaxed problem APO_{lb} that minimizes a lower bound of the cell-aggregated utility loss:

$$\min \quad \hat{\mathcal{L}}(\mathbf{Z}) := \sum_{m=1}^M \sum_{\mathbf{y}_k \in \mathcal{Y}} \bar{\mathcal{L}}_m(\mathbf{y}_k) \cdot z(\mathbf{y}_k \mid \mathcal{C}_m), \quad (149)$$

$$\text{s.t.} \quad z(\mathbf{y}_k \mid \mathcal{C}_m) - e^{\epsilon \hat{d}_p(\mathcal{C}_m, \mathcal{C}_{m'})} z(\mathbf{y}_k \mid \mathcal{C}_{m'}) \leq 0, \quad \forall \mathcal{C}_m, \mathcal{C}_{m'}$$

$$\sum_{\mathbf{y}_k \in \mathcal{Y}} z(\mathbf{y}_k \mid \mathcal{C}_m) = \prod_{\ell=1}^N \Delta_\ell, \quad \forall \mathcal{C}_m \quad (151)$$

and denote its optimal value by $\hat{\mathcal{L}}^*$.

Proposition 5 (Universal Lower Bound). *Let $\mathcal{M} : \mathcal{X} \rightarrow \mathcal{Y}$ be any mechanism satisfying (ϵ, d_p) -mDP. Let*

$$\mathcal{L}(\mathcal{M}) := \int_{\mathcal{X}} \sum_{\mathbf{y}_k \in \mathcal{Y}} p(\mathbf{x}) \mathcal{L}(\mathbf{x}, \mathbf{y}_k) \Pr[\mathcal{M}(\mathbf{x}) = \mathbf{y}_k] d\mathbf{x} \quad (152)$$

denote its expected utility loss. Then,

$$\mathcal{L}(\mathcal{M}) \geq \hat{\mathcal{L}}^*. \quad (153)$$

Proof of Proposition 5. Fix any data perturbation mechanism \mathcal{M} that satisfies (ϵ, d_p) -mDP. For a fixed output symbol \mathbf{y}_k let

$$f(\mathbf{x}) := \Pr(\mathcal{M}(\mathbf{x}) = \mathbf{y}_k), \quad \mathbf{x} \in \mathcal{X}. \quad (154)$$

For any two cells $\mathcal{C}_m, \mathcal{C}_{m'}$ and for every $\mathbf{x} \in \mathcal{C}_m, \mathbf{x}' \in \mathcal{C}_{m'}$ the mDP guarantee gives

$$\frac{f(\mathbf{x})}{f(\mathbf{x}')} \leq e^{\epsilon d_p(\mathbf{x}_a, \mathbf{x}_b)} \leq e^{\epsilon \hat{d}_p(\mathcal{C}_m, \mathcal{C}_{m'})}, \quad (155)$$

$$\hat{d}_p(\mathcal{C}_m, \mathcal{C}_{m'}) = \max_{\mathbf{u} \in \mathcal{C}_m, \mathbf{v} \in \mathcal{C}_{m'}} d_p(\mathbf{u}, \mathbf{v}). \quad (156)$$

Set $M_m := \sup_{\mathbf{x} \in \mathcal{C}_m} f(\mathbf{x}), m_{m'} := \inf_{\mathbf{x}' \in \mathcal{C}_{m'}} f(\mathbf{x}')$. By Eq. (155) we have

$$M_m \leq e^{\epsilon \hat{d}_p(\mathcal{C}_m, \mathcal{C}_{m'})} m_{m'}. \quad (157)$$

Since every grid cell has the same volume $V := \mu(\mathcal{C}_m) = \prod_{\ell=1}^N \Delta_\ell$,

$$z(\mathbf{y}_k \mid \mathcal{C}_m) := \int_{\mathcal{C}_m} f(\mathbf{x}) d\mathbf{x} \leq V M_m, z(\mathbf{y}_k \mid \mathcal{C}_{m'}) \geq V m_{m'}. \quad (158)$$

Combining with Eq. (157) yields

$$z(\mathbf{y}_k \mid \mathcal{C}_m) \leq e^{\epsilon \hat{d}_p(\mathcal{C}_m, \mathcal{C}_{m'})} z(\mathbf{y}_k \mid \mathcal{C}_{m'}), \quad (159)$$

i.e. the vector $\{z(\mathbf{y}_k \mid \mathcal{C}_m)\}$ satisfies the relaxed mDP constraints (146). Normalisation also holds because $\sum_{\mathbf{y}_k} f(\mathbf{x}) = 1$ for every \mathbf{x} . Hence, **the aggregated variables induced by \mathcal{M} form a feasible solution of APO_{lb}** .

Now, we can derive the expected loss of \mathcal{M} as

$$\mathcal{L}(\mathcal{M}) \quad (160)$$

$$= \sum_{\mathbf{y}_k \in \mathcal{Y}} \int_{\mathcal{X}} p(\mathbf{x}) \mathcal{L}(\mathbf{x}, \mathbf{y}_k) f(\mathbf{x}) d\mathbf{x} \quad (161)$$

$$= \sum_{m=1}^M \sum_{\mathbf{y}_k \in \mathcal{Y}} \int_{\mathcal{C}_m} p(\mathbf{x}) \mathcal{L}(\mathbf{x}, \mathbf{y}_k) f(\mathbf{x}) d\mathbf{x} \quad (162)$$

$$\geq \sum_{m=1}^M \sum_{\mathbf{y}_k \in \mathcal{Y}} \underbrace{\min_{\mathbf{x} \in \mathcal{C}_m} p(\mathbf{x}) \mathcal{L}(\mathbf{x}, \mathbf{y}_k)}_{= \hat{\mathcal{L}}_m(\mathbf{y}_k)} z(\mathbf{y}_k \mid \mathcal{C}_m) \quad (163)$$

$$= \hat{\mathcal{L}}(\mathbf{Z}). \quad (164)$$

Because \mathbf{Z} is feasible for APO_{lb} , $\hat{\mathcal{L}}(\mathbf{Z}) \geq \hat{\mathcal{L}}^*$. Therefore $\mathcal{L}(\mathcal{M}) \geq \hat{\mathcal{L}}^*$, establishing that $\hat{\mathcal{L}}^*$ is a universal lower bound on the utility loss of any (ϵ, d_p) -mDP mechanism. \square

D Additional Experimental Results

This section presents additional experimental results to support our main findings in Section 6.

In this section, we present supplementary experiments to further validate our framework. Section D.1 provides a detailed distributional analysis of the *perturbation probability*

ratio (PPR), as a supplementary results for Table 2. Section D.3 investigates the performance of the interpolation-based method under varying grid granularities, highlighting the trade-off between accuracy and efficiency. Section D.2 conducts an ablation study that compares utility loss with and without privacy budget optimization, illustrating the benefits of joint optimization. Section D.4 evaluates the framework when spatial proximity is measured by the ℓ_1 -norm instead of the ℓ_2 -norm, demonstrating the generality of our approach across different distance metrics.

D.1 Privacy Evaluation: Perturbation Probability Ratio Distributional Analysis

Fig. 8–10 (corresponding to Rome, London, and New York City) illustrate the distributional behavior of the perturbation probability ratio (PPR) under different mechanisms.

Recall that PPR measures the log-probability difference between two inputs normalized by their ℓ_p distance (Eq. (43)), and violations occur when this ratio exceeds the privacy budget ϵ . Across all three datasets, AIPO exhibits a sharp concentration of PPR values strictly below the threshold, confirming zero mDP violations in practice. In contrast, LP-based optimization yields wider distributions with noticeable mass near or beyond the ϵ boundary, reflecting the effect of discretization and distance approximation errors. Hybrid methods such as COPT and RMP partially mitigate these issues, but their distributions remain more dispersed than AIPO. pre-defined mechanisms (Laplace, EM, TEM) also avoid explicit violations, yet their distributions are much flatter, indicating weaker privacy-utility trade-offs due to excessive randomization. Overall, the distributional analysis highlights the superiority of AIPO: not only does it enforce strict compliance with (ϵ, d_p) -mDP, but it also produces sharply bounded PPR profiles that are consistent across cities of varying scale and density.

D.2 Ablation Study: Utility Loss With And Without Privacy Budget Optimization

Table 7 compares *AIPO* with its equal-budget counterpart *AIPO-E*, which uniformly allocates the privacy budget across dimensions (e.g., $\epsilon_1 = \epsilon_2 = \epsilon/\sqrt{2}$ under ℓ_2). Across Rome, London, and NYC, *AIPO* consistently achieves lower utility loss than *AIPO-E*, and the margin widens as the overall privacy level ϵ increases. This trend is expected: at small ϵ , noise is necessarily large and budget reallocation has limited effect, whereas at larger ϵ the mechanism has more freedom to shape direction-dependent noise, and optimizing (ϵ_1, ϵ_2) yields tangible gains. The improvement stems from *AIPO*'s asymmetric allocation adapting to directional utility sensitivity and map anisotropy (e.g., corridor-like connectivity or dominant travel directions). Concretely, on the NYC dataset, *AIPO* attains up to 7.8% lower utility loss than *AIPO-E* at $\epsilon = 1.6$, highlighting the value of optimizing privacy allocation. Similar, though

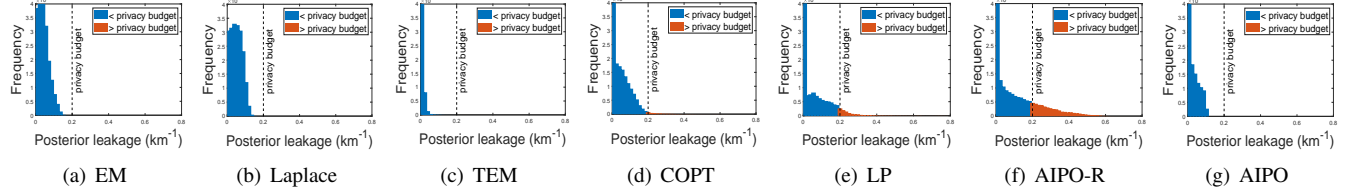


Figure 8: Example of posterior leakage distribution (Rome).

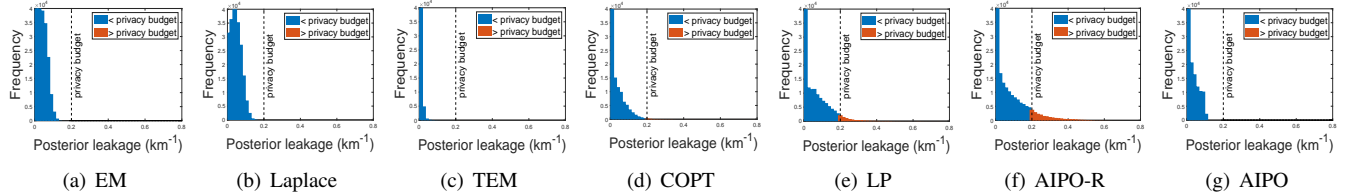


Figure 9: Example of posterior leakage distribution (London).

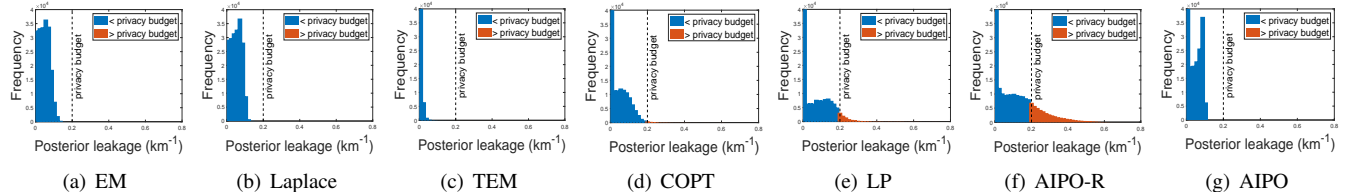


Figure 10: Example of posterior leakage distribution (New York City).

slightly smaller, gains are observed in Rome and London, consistent with their less anisotropic street layouts. These results validate that dimension-wise budget composition (Theorem 1) is not merely theoretically sufficient for (ϵ, d_p) -mDP but also practically important for enhancing utility.

Budget-sweep methodology and insights. To quantify how allocation affects utility, we fix the total budget ϵ and vary the first-dimension share ϵ_1 along the feasible arc $\epsilon_1^p + \epsilon_2^p = \epsilon^p$ (with $p = 2$ in our main experiments), discretizing ϵ_1 over a uniform grid and setting $\epsilon_2 = (\epsilon^p - \epsilon_1^p)^{1/p}$. For each candidate (ϵ_1, ϵ_2) we solve AIPO and record the utility loss; the best value for a given ϵ is the minimum over this sweep. Fig. 11–13 plot utility as a function of ϵ_1 : the curves are characteristically U-shaped with minima *away* from the equal-split point, indicating that equal allocation is suboptimal in all three cities. Moreover, the optimal ϵ_1 shifts with ϵ , reflecting that the most effective directional protection depends jointly on the privacy level and the dataset’s geometric/traffic structure. Together with Table 7, these observations underscore that learning the per-dimension budgets is a key lever for improving utility while preserving (ϵ, d_p) -mDP.

D.3 Performance of the Interpolation-Based Method under Varying Grid Granularity

Fig. 14(a)–(c) evaluates AIPO across grid resolutions by varying the number of discretized cells. As resolution increases, utility loss decreases monotonically because denser anchor placement better captures local geometry (e.g., turn penalties and anisotropy along road segments), thereby reducing interpolation error. This gain, however, comes with higher computational cost: the number of decision variables grows as $O(|\mathcal{X}| \cdot |\mathcal{Y}|)$ and the number of mDP constraints grows with anchor neighborhood pairs (super-linearly in practice due to barrier/simplex iterations), leading to longer runtimes and higher memory usage. We also note that privacy is *insensitive* to grid granularity for AIPO: the PPR distributions remain tightly concentrated below ϵ at all resolutions (cf. Section D.1), since mDP is enforced via dimension-wise composition on anchors and preserved by log-convex interpolation. Importantly, diminishing returns emerge beyond a dataset-specific threshold—utility gains saturate once horizontal cells exceed ~ 8 for Rome and London and ~ 10 for New York City—while runtime continues to rise super-linearly. In light of this trade-off, we default to 10 horizontal cells for all three datasets, which is near the knee of the curve: it retains most of the achievable utility improvement while keeping the opti-

Rome road map								
Method	$\epsilon = 0.2$	$\epsilon = 0.4$	$\epsilon = 0.6$	$\epsilon = 0.8$	$\epsilon = 1.0$	$\epsilon = 1.2$	$\epsilon = 1.4$	$\epsilon = 1.6$
AIPO[†]	6.01 \pm 0.26	4.96 \pm 0.56	4.28 \pm 0.67	3.77 \pm 0.67	3.52 \pm 0.83	3.22 \pm 4.01	3.14 \pm 0.92	3.01 \pm 0.93
AIPO-E	6.24 \pm 0.02	5.02 \pm 0.26	4.37 \pm 0.48	3.86 \pm 0.59	3.58 \pm 0.66	3.37 \pm 0.70	3.21 \pm 0.73	3.09 \pm 0.74
London road map								
Method	$\epsilon = 0.2$	$\epsilon = 0.4$	$\epsilon = 0.6$	$\epsilon = 0.8$	$\epsilon = 1.0$	$\epsilon = 1.2$	$\epsilon = 1.4$	$\epsilon = 1.6$
AIPO[†]	5.42 \pm 0.03	4.34 \pm 0.07	3.66 \pm 0.12	3.20 \pm 0.14	2.90 \pm 0.16	2.66 \pm 0.14	2.50 \pm 0.14	2.37 \pm 0.17
AIPO-E	5.46 \pm 0.03	4.42 \pm 0.08	3.85 \pm 0.13	3.44 \pm 0.15	3.14 \pm 0.16	2.91 \pm 0.16	2.73 \pm 0.16	2.58 \pm 0.16
New York City road map								
Method	$\epsilon = 0.2$	$\epsilon = 0.4$	$\epsilon = 0.6$	$\epsilon = 0.8$	$\epsilon = 1.0$	$\epsilon = 1.2$	$\epsilon = 1.4$	$\epsilon = 1.6$
AIPO[†]	7.15 \pm 0.14	5.16 \pm 0.14	4.14 \pm 0.21	3.54 \pm 0.22	3.13 \pm 0.22	2.86 \pm 0.23	2.66 \pm 0.24	2.51 \pm 0.22
AIPO-E	7.19 \pm 0.13	5.33 \pm 0.14	4.39 \pm 0.22	3.80 \pm 0.23	3.40 \pm 0.24	3.05 \pm 0.64	2.90 \pm 0.25	2.74 \pm 0.25

Table 7: AIPO with and without privacy budget optimization (Mean \pm 1.96 \times standard deviation).

mization tractable. Practically, coarser grids (e.g., 8 horizontal cells) already offer near-optimal utility for Rome/London, whereas NYC’s denser and more heterogeneous street topology benefits from the finer 10-cell configuration.

D.4 Performance Evaluation when Distance is Measured by ℓ_1 -Norm

Table 8 compares the expected utility loss across all mechanisms when proximity is measured by d_1 . Consistent with the ℓ_2 case (Table 3), our interpolation-based method (AIPO) achieves uniformly low utility loss on Rome, London, and NYC, tracking the best-performing methods while preserving formal guarantees. As expected, LP often attains the lowest loss because it directly optimizes over (discretized) input–output pairs; however, this advantage comes at the cost of *not* ensuring (ϵ, d_1) -mDP on the underlying continuous domain. pre-defined mechanisms (Laplace, EM, TEM) remain privacy-safe but exhibit larger losses due to heavier randomization, and hybrid approaches (e.g., COPT) typically lie between LP and the pre-defined baselines. Notably, the gap between AIPO and LP narrows as ϵ increases, reflecting that AIPO’s log-convex interpolation and anchor optimization can better exploit higher privacy budgets even under the Manhattan geometry of road networks (e.g., axis-aligned anisotropy and corridor effects).

Table 9 reports the empirical violation ratios for (ϵ, d_1) -mDP. AIPO preserves perfect privacy with *zero* violations across all datasets and privacy budgets, validating the dimension-wise composition and the correctness of the interpolation mechanism under d_1 . In contrast, LP and hybrid variants (e.g., COPT) exhibit persistent violations, especially at smaller ϵ where discretization-induced distance overestimation most strongly relaxes the effective constraints. These findings mirror the PPR distributional patterns observed in Section D.1: AIPO concentrates well below ϵ with tight tails, while LP/hybrids show broader spreads and nontrivial mass near or beyond the threshold.

Table 10 compares runtimes under d_1 . AIPO demonstrates

strong scalability, reducing computation time by approximately 30%–70% on average relative to LP and COPT. The efficiency gain stems from constraining only axis-neighbor anchor pairs along each dimension and then interpolating, which yields far fewer effective constraints than the (near) cubic growth in pairwise constraints characteristic of LP/COPT. Practically, this translates into lower memory use and faster solver convergence as grid resolution increases, while retaining strict (ϵ, d_1) -mDP. Taken together, the ℓ_1 results corroborate our main conclusions: AIPO delivers rigorous privacy, competitive (often near-LP) utility, and substantially improved efficiency under an alternative and widely used metric for spatial domains.

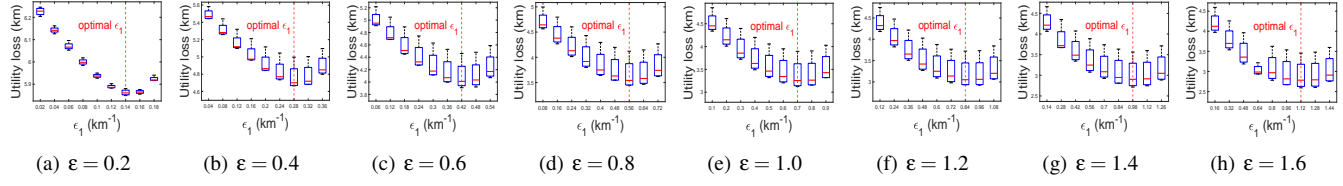


Figure 11: Utility loss vs. privacy budget assigned to dimension 1 (Rome).

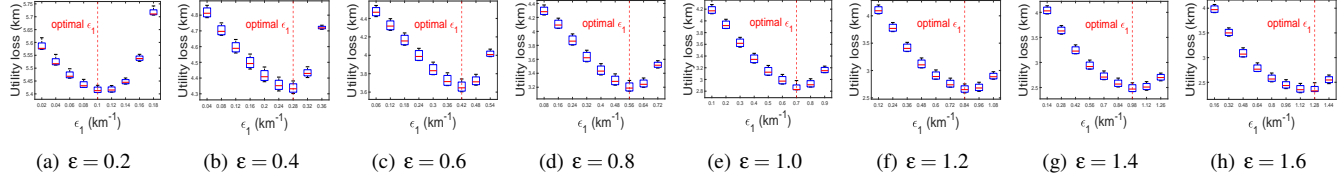


Figure 12: Utility loss vs. privacy budget assigned to dimension 1 (London).

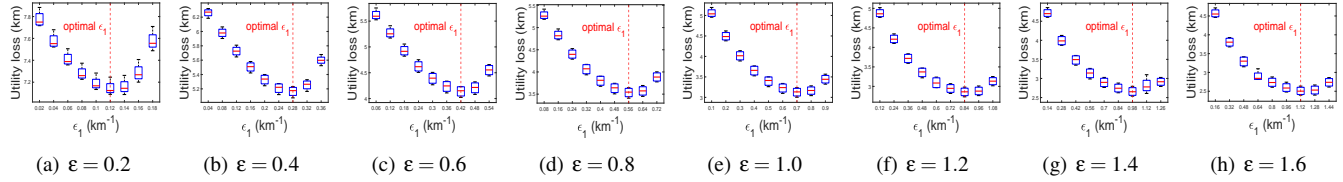


Figure 13: Utility loss vs. privacy budget assigned to dimension 1 (New York City).

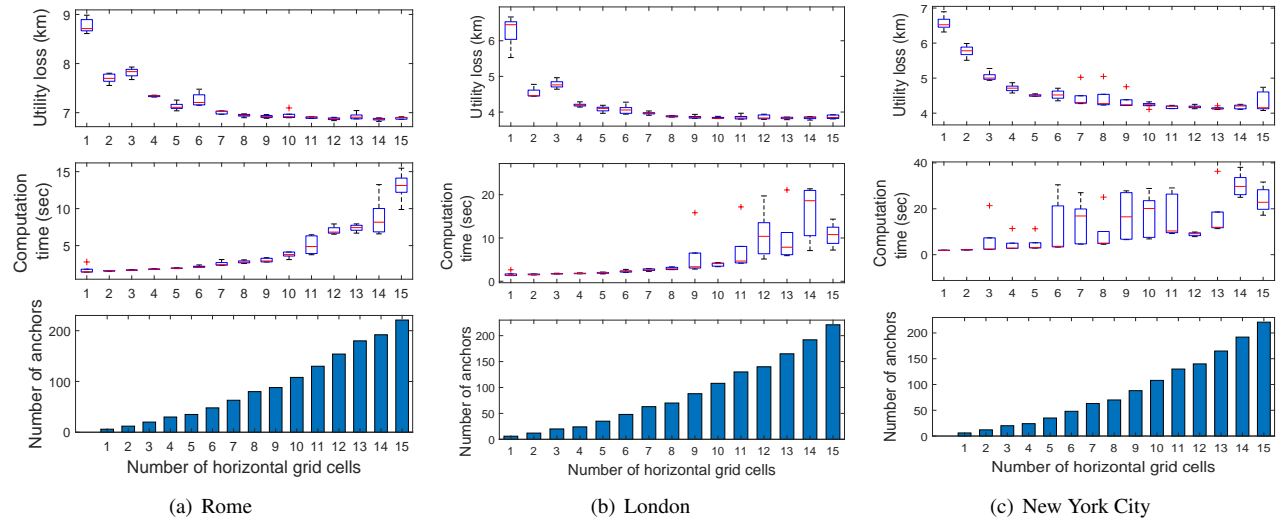


Figure 14: Performance of AIPO with varying Grid Granularity.

Rome road map									
Method		$\epsilon = 0.2$	$\epsilon = 0.4$	$\epsilon = 0.6$	$\epsilon = 0.8$	$\epsilon = 1.0$	$\epsilon = 1.2$	$\epsilon = 1.4$	$\epsilon = 1.6$
Pre-defined	EM	6.57±0.55	5.15±0.72	4.32±0.79	3.82±0.81	3.50±0.82	3.28±0.81	3.13±0.80	3.01±0.78
Distribution	Laplace	6.57±0.55	5.15±0.72	4.32±0.79	3.82±0.81	3.50±0.82	3.28±0.81	3.13±0.80	3.01±0.78
Hybrid	TEM	8.51±0.65	8.66±0.67	8.72±0.68	8.74±0.69	8.75±0.69	8.75±0.69	8.75±0.69	8.76±0.69
Hybrid	RMP	5.83±0.12	4.80±0.37	4.07±0.50	3.60±0.52	3.28±0.51	3.06±0.48	2.90±0.45	2.79±0.43
method	COPT	7.27±0.88	4.59±0.90	3.53±0.85	3.27±0.84	3.13±0.82	3.04±0.80	2.98±0.79	2.93±0.75
LP		3.56±0.06	2.44±0.14	2.07±0.17	1.96±0.18	1.93±0.18	1.96±0.08	1.92±0.18	1.92±0.18
AIPO-R		2.96±0.04	2.26±0.16	2.09±0.15	2.03±0.17	1.96±0.15	4.12±7.59	1.89±0.14	1.88±0.15
LB		2.31±0.15	1.94±0.18	1.92±0.18	1.92±0.18	1.92±0.18	1.92±0.18	1.92±0.18	1.92±0.18
AIPO [†]		4.95±0.09	3.74±0.32	3.11±0.41	2.76±0.49	2.52±0.50	2.38±0.54	2.29±0.55	2.23±0.59
Pre-defined	vs EM	-24.7% ↓	-27.3% ↓	-28.1% ↓	-27.8% ↓	-28.1% ↓	-27.4% ↓	-26.7% ↓	-26.1% ↓
Noise	vs Laplace	-24.7% ↓	-27.3% ↓	-28.1% ↓	-27.8% ↓	-28.1% ↓	-27.4% ↓	-26.7% ↓	-26.1% ↓
Distribution	vs TEM	-41.9% ↓	-56.8% ↓	-64.4% ↓	-68.4% ↓	-71.2% ↓	-72.8% ↓	-73.8% ↓	-74.6% ↓
Hybrid	vs RMP	-15.2% ↓	-22.1% ↓	-23.6% ↓	-23.4% ↓	-23.3% ↓	-22.1% ↓	-21.1% ↓	-20.1% ↓
Method	vs COPT	-31.9% ↓	-18.5% ↓	-12.0% ↓	-15.7% ↓	-19.5% ↓	-21.6% ↓	-23.1% ↓	-24.0% ↓
vs LP		39.0% ↑	53.6% ↑	50.4% ↑	40.8% ↑	30.4% ↑	21.7% ↑	19.4% ↑	16.0% ↑
London road map									
Method		$\epsilon = 0.2$	$\epsilon = 0.4$	$\epsilon = 0.6$	$\epsilon = 0.8$	$\epsilon = 1.0$	$\epsilon = 1.2$	$\epsilon = 1.4$	$\epsilon = 1.6$
Pre-defined	EM	6.37±0.41	4.90±0.05	4.13±0.38	3.72±0.57	3.47±0.68	3.32±0.74	3.22±0.78	3.15±0.81
Noise	Laplace	6.37±0.41	4.90±0.05	4.13±0.38	3.72±0.57	3.47±0.68	3.32±0.74	3.22±0.78	3.15±0.81
Distribution	TEM	8.36±0.93	8.49±0.95	8.52±0.96	8.53±0.96	8.53±0.96	8.53±0.96	8.53±0.96	8.53±0.96
Hybrid	RMP	5.51±0.23	4.45±0.31	3.81±0.37	3.43±0.43	3.20±0.46	3.06±0.46	2.96±0.46	2.89±0.46
Method	COPT	6.38±0.13	3.93±0.66	3.49±0.68	3.33±0.74	3.25±0.76	3.19±0.76	3.16±0.76	3.13±0.77
LP		3.32±0.02	2.40±0.07	2.13±0.09	2.04±0.10	2.01±0.11	2.00±0.11	2.00±0.11	2.00±0.11
AIPO-R		3.06±0.04	2.41±0.06	2.30±0.14	2.17±0.20	2.15±0.21	2.13±0.21	2.13±0.20	2.16±0.19
LB		2.30±0.07	2.02±0.11	2.00±0.11	2.00±0.11	2.00±0.11	2.00±0.11	2.00±0.11	2.00±0.11
AIPO [†]		4.59±0.02	3.46±0.07	2.87±0.12	2.54±0.16	2.38±0.20	2.27±0.21	2.19±0.21	2.15±0.22
Pre-defined	vs EM	-28.0% ↓	-29.3% ↓	-30.6% ↓	-31.5% ↓	-31.5% ↓	-31.6% ↓	-31.9% ↓	-31.8% ↓
Noise	vs Laplace	-28.0% ↓	-29.3% ↓	-30.6% ↓	-31.5% ↓	-31.5% ↓	-31.6% ↓	-31.9% ↓	-31.8% ↓
Distribution	vs TEM	-45.2% ↓	-59.2% ↓	-66.3% ↓	-70.2% ↓	-72.1% ↓	-73.4% ↓	-74.3% ↓	-74.8% ↓
Hybrid	vs RMP	-16.8% ↓	-22.2% ↓	-24.7% ↓	-25.9% ↓	-25.8% ↓	-25.8% ↓	-26.0% ↓	-25.6% ↓
Method	vs COPT	-28.1% ↓	-11.9% ↓	-17.9% ↓	-23.6% ↓	-26.8% ↓	-28.9% ↓	-30.6% ↓	-31.4% ↓
vs LP		38.0% ↑	44.5% ↑	35.0% ↑	24.7% ↑	18.1% ↑	13.3% ↑	9.6% ↑	7.5% ↑
New York City road map									
Method		$\epsilon = 0.2$	$\epsilon = 0.4$	$\epsilon = 0.6$	$\epsilon = 0.8$	$\epsilon = 1.0$	$\epsilon = 1.2$	$\epsilon = 1.4$	$\epsilon = 1.6$
Pre-defined	EM	8.21±0.46	5.65±0.41	4.39±0.37	3.70±0.31	3.30±0.27	3.05±0.24	2.89±0.22	2.78±0.21
Noise	Laplace	8.21±0.46	5.65±0.41	4.39±0.37	3.70±0.31	3.30±0.27	3.05±0.24	2.89±0.22	2.78±0.21
Distribution	TEM	13.17±1.48	13.56±1.55	13.64±1.55	13.67±1.56	13.68±1.56	13.69±1.56	13.69±1.56	13.69±1.56
Hybrid	RMP	7.51±0.09	5.37±0.28	4.19±0.34	3.52±0.32	3.12±0.30	2.87±0.29	2.71±0.27	2.60±0.25
Method	COPT	6.36±1.13	5.00±0.21	3.30±0.21	3.03±0.16	2.90±0.15	2.82±0.15	2.78±0.15	2.74±0.17
LP		3.88±0.18	2.57±0.36	2.18±0.42	2.07±0.44	5.90±13.04	2.03±0.45	2.03±0.45	2.03±0.45
AIPO-R		3.17±0.16	2.32±0.22	2.07±0.23	1.97±0.21	1.89±0.18	1.83±0.19	1.81±0.18	1.79±0.19
LB		2.43±0.38	2.05±0.44	2.03±0.45	2.03±0.45	2.03±0.45	2.03±0.45	2.03±0.45	2.03±0.45
AIPO [†]		5.76±0.10	3.89±0.09	3.04±0.14	2.53±0.03	2.29±0.16	2.12±0.18	2.00±0.19	1.92±0.19
Pre-defined	vs EM	-29.8% ↓	-31.2% ↓	-30.8% ↓	-31.8% ↓	-30.7% ↓	-30.7% ↓	-31.0% ↓	-31.0% ↓
Noise	vs Laplace	-29.8% ↓	-31.2% ↓	-30.8% ↓	-31.8% ↓	-30.7% ↓	-30.7% ↓	-31.0% ↓	-31.0% ↓
Distribution	vs TEM	-56.4% ↓	-71.3% ↓	-77.7% ↓	-81.5% ↓	-83.3% ↓	-84.5% ↓	-85.4% ↓	-86.0% ↓
Hybrid	vs RMP	-23.3% ↓	-27.6% ↓	-27.4% ↓	-28.2% ↓	-26.7% ↓	-26.4% ↓	-26.4% ↓	-26.0% ↓
Method	vs COPT	-9.4% ↓	-22.2% ↓	-7.7% ↓	-16.6% ↓	-21.1% ↓	-25.1% ↓	-28.1% ↓	-29.9% ↓
vs LP		48.4% ↑	51.6% ↑	39.2% ↑	21.8% ↑	6.8% ↑	4.1% ↑	0.3% ↑	2.3% ↑

Table 8: Utility loss (km) across different perturbation methods where distance is measured using ℓ_1 -norm metric (Mean±1.96×standard deviation).

Rome road map									
Method		$\epsilon = 0.2$	$\epsilon = 0.4$	$\epsilon = 0.6$	$\epsilon = 0.8$	$\epsilon = 1.0$	$\epsilon = 1.2$	$\epsilon = 1.4$	$\epsilon = 1.6$
Pre-defined	EM	0.00±0.00	0.00±0.00	0.00±0.00	0.00±0.00	0.00±0.00	0.00±0.00	0.00±0.00	0.00±0.00
Noise	Laplace	0.00±0.00	0.00±0.00	0.00±0.00	0.00±0.00	0.00±0.00	0.00±0.00	0.00±0.00	0.00±0.00
Distribution	TEM	0.00±0.00	0.00±0.00	0.00±0.00	0.00±0.00	0.00±0.00	0.00±0.00	0.00±0.00	0.00±0.00
Hybrid	RMP	0.00±0.00	0.00±0.00	0.00±0.00	0.00±0.00	0.00±0.00	0.00±0.00	0.00±0.00	0.00±0.00
Method	COPT	22.03±6.11	24.70±12.04	20.81±8.00	16.17±4.77	15.78±9.53	15.81±10.84	14.51±8.92	15.40±9.99
LP		2.26±1.22	4.60±2.94	5.63±1.31	5.28±0.82	5.37±0.41	4.74±1.52	4.62±0.20	4.75±1.01
AIPO[†]		0.00±0.00	0.00±0.00	0.00±0.00	0.00±0.00	0.00±0.00	0.00±0.00	0.00±0.00	0.00±0.00
London road map									
Method		$\epsilon = 0.2$	$\epsilon = 0.4$	$\epsilon = 0.6$	$\epsilon = 0.8$	$\epsilon = 1.0$	$\epsilon = 1.2$	$\epsilon = 1.4$	$\epsilon = 1.6$
Pre-defined	EM	0.00±0.00	0.00±0.00	0.00±0.00	0.00±0.00	0.00±0.00	0.00±0.00	0.00±0.00	0.00±0.00
Noise	Laplace	0.00±0.00	0.00±0.00	0.00±0.00	0.00±0.00	0.00±0.00	0.00±0.00	0.00±0.00	0.00±0.00
Distribution	TEM	0.00±0.00	0.00±0.00	0.00±0.00	0.00±0.00	0.00±0.00	0.00±0.00	0.00±0.00	0.00±0.00
Hybrid	RMP	0.00±0.00	0.00±0.00	0.00±0.00	0.00±0.00	0.00±0.00	0.00±0.00	0.00±0.00	0.00±0.00
Method	COPT	24.96±8.37	18.73±7.19	19.09±3.84	15.94±1.14	15.65±2.10	15.10±5.56	16.09±9.42	14.45±4.93
LP		3.61±0.28	4.39±0.72	5.05±0.20	4.36±0.91	4.49±0.70	4.23±0.72	3.88±0.94	3.20±0.81
AIPO[†]		0.00±0.00	0.00±0.00	0.00±0.00	0.00±0.00	0.00±0.00	0.00±0.00	0.00±0.00	0.00±0.00
New York City road map									
Method		$\epsilon = 0.2$	$\epsilon = 0.4$	$\epsilon = 0.6$	$\epsilon = 0.8$	$\epsilon = 1.0$	$\epsilon = 1.2$	$\epsilon = 1.4$	$\epsilon = 1.6$
Pre-defined	EM	0.00±0.00	0.00±0.00	0.00±0.00	0.00±0.00	0.00±0.00	0.00±0.00	0.00±0.00	0.00±0.00
Noise	Laplace	0.00±0.00	0.00±0.00	0.00±0.00	0.00±0.00	0.00±0.00	0.00±0.00	0.00±0.00	0.00±0.00
Distribution	TEM	0.00±0.00	0.00±0.00	0.00±0.00	0.00±0.00	0.00±0.00	0.00±0.00	0.00±0.00	0.00±0.00
Hybrid	RMP	0.00±0.00	0.00±0.00	0.00±0.00	0.00±0.00	0.00±0.00	0.00±0.00	0.00±0.00	0.00±0.00
Method	COPT	14.73±4.61	13.62±7.11	12.28±4.51	12.39±3.58	12.92±3.37	12.70±4.21	11.54±4.09	10.88±4.13
LP		3.17±0.42	4.32±1.06	4.34±0.64	4.71±0.85	4.56±0.65	4.38±0.31	3.75±0.61	3.93±0.47
AIPO[†]		0.00±0.00	0.00±0.00	0.00±0.00	0.00±0.00	0.00±0.00	0.00±0.00	0.00±0.00	0.00±0.00

Table 9: mDP violation ratio when distance is measured using ℓ_1 -norm metric (Mean±1.96×standard deviation).

Rome road map								
Method	$\epsilon = 0.2$	$\epsilon = 0.4$	$\epsilon = 0.6$	$\epsilon = 0.8$	$\epsilon = 1.0$	$\epsilon = 1.2$	$\epsilon = 1.4$	$\epsilon = 1.6$
COPT	82.50±11.94	73.24±3.94	71.43±2.35	70.98±3.71	70.10±4.47	71.62±1.61	70.17±5.54	69.20±4.31
LP	68.90±21.75	46.45±10.92	41.24±12.05	35.50±9.37	35.62±6.82	102.99±234.98	47.39±42.41	55.12±9.11
AIPO[†]	11.94±9.82	4.31±0.93	3.47±0.44	3.52±0.56	4.11±0.54	4.38±0.66	4.24±0.58	4.85±0.64
London road map								
Method	$\epsilon = 0.2$	$\epsilon = 0.4$	$\epsilon = 0.6$	$\epsilon = 0.8$	$\epsilon = 1.0$	$\epsilon = 1.2$	$\epsilon = 1.4$	$\epsilon = 1.6$
COPT	176.6±54.9	175.0±56.8	174.0±59.8	170.8±51.6	170.3±60.4	167.1±54.5	169.1±53.2	170.1±57.3
LP	111.1±61.2	86.3±47.7	83.0±30.8	72.0±17.8	69.5±12.7	76.4±42.0	71.3±24.3	114.6±54.0
AIPO[†]	44.57±14.34	22.67±4.84	19.55±4.50	16.40±4.50	14.61±3.40	11.88±2.57	11.08±2.65	10.28±1.85
New York City road map								
Method	$\epsilon = 0.2$	$\epsilon = 0.4$	$\epsilon = 0.6$	$\epsilon = 0.8$	$\epsilon = 1.0$	$\epsilon = 1.2$	$\epsilon = 1.4$	$\epsilon = 1.6$
COPT	90.81±5.09	78.51±7.91	79.50±9.21	79.56±7.07	80.05±7.00	76.75±2.74	78.94±5.00	78.94±4.70
LP	102.5±22.4	64.9±29.5	61.4±6.5	74.0±31.6	76.8±32.0	92.4±34.6	92.9±37.9	68.8±52.1
AIPO[†]	80.72±11.24	49.90±4.96	44.28±2.57	40.62±5.42	30.28±5.36	27.44±2.67	21.65±3.47	19.55±3.24

Table 10: Computation time of different perturbation methods when distance is measured using ℓ_1 -norm metric (Mean±1.96×standard deviation).

Rome road map									
Method		$\epsilon = 0.2$	$\epsilon = 0.4$	$\epsilon = 0.6$	$\epsilon = 0.8$	$\epsilon = 1.0$	$\epsilon = 1.2$	$\epsilon = 1.4$	$\epsilon = 1.6$
Pre-defined	EM	8.71 \pm 0.78	8.70 \pm 1.13	8.65 \pm 1.28	8.62 \pm 1.38	8.58 \pm 1.45	8.56 \pm 1.51	8.54 \pm 1.55	8.52 \pm 1.58
Noise	Laplace	8.71 \pm 0.71	8.48 \pm 1.00	8.46 \pm 1.40	8.45 \pm 1.69	8.44 \pm 1.90	8.43 \pm 2.05	8.42 \pm 2.16	8.40 \pm 2.24
Distribution	TEM	8.85 \pm 2.71	8.95 \pm 3.19	8.66 \pm 2.44	8.64 \pm 1.83	8.66 \pm 1.11	8.66 \pm 0.69	8.66 \pm 0.27	8.62 \pm 0.22
Hybrid	RMP	5.94 \pm 0.25	4.96 \pm 0.45	4.28 \pm 0.36	3.85 \pm 0.26	3.58 \pm 0.21	3.40 \pm 0.19	3.28 \pm 0.18	3.19 \pm 0.18
Method	COPT	7.99 \pm 1.53	7.95 \pm 1.04	8.33 \pm 1.50	8.29 \pm 1.57	8.27 \pm 1.59	8.25 \pm 1.61	8.24 \pm 1.60	8.24 \pm 1.60
	LP	4.25 \pm 0.41	2.97 \pm 0.11	2.56 \pm 0.03	2.45 \pm 0.07	2.43 \pm 0.03	2.42 \pm 0.02	2.42 \pm 0.01	2.42 \pm 0.01
	AIPO-R	5.19 \pm 0.23	3.97 \pm 0.21	3.34 \pm 0.17	3.01 \pm 0.12	2.81 \pm 0.07	2.66 \pm 0.03	2.56 \pm 0.05	2.50 \pm 0.01
	LB	1.82 \pm 0.01	1.73 \pm 0.01	1.73 \pm 0.00	1.73 \pm 0.01	1.73 \pm 0.00	1.73 \pm 0.01	1.73 \pm 0.00	1.73 \pm 0.00
AIPO [†]		5.68\pm0.34	4.65\pm0.45	4.02\pm0.22	3.63\pm0.08	3.38\pm0.37	3.14\pm0.25	2.99\pm0.11	2.88\pm0.19
Pre-defined	vs EM	-34.8% \downarrow	-46.5% \downarrow	-53.5% \downarrow	-57.8% \downarrow	-60.7% \downarrow	-63.3% \downarrow	-65.0% \downarrow	-66.1% \downarrow
Noise	vs Laplace	-34.8% \downarrow	-45.2% \downarrow	-52.5% \downarrow	-57.0% \downarrow	-60.0% \downarrow	-62.7% \downarrow	-64.5% \downarrow	-65.7% \downarrow
Distribution	vs TEM	-35.8% \downarrow	-48.1% \downarrow	-53.6% \downarrow	-58.0% \downarrow	-61.0% \downarrow	-63.7% \downarrow	-65.5% \downarrow	-66.5% \downarrow
Hybrid	vs RMP	-4.3% \downarrow	-6.3% \downarrow	-5.9% \downarrow	-5.7% \downarrow	-5.7% \downarrow	-7.6% \downarrow	-8.7% \downarrow	-9.5% \downarrow
Method	vs COPT	-29.0% \downarrow	-41.5% \downarrow	-51.8% \downarrow	-56.2% \downarrow	-59.2% \downarrow	-61.9% \downarrow	-63.7% \downarrow	-65.0% \downarrow
	vs LP	33.8% \uparrow	56.5% \uparrow	56.9% \uparrow	48.1% \uparrow	39.2% \uparrow	29.9% \uparrow	23.7% \uparrow	19.4% \uparrow
	vs AIPO-R	9.4% \uparrow	17.3% \uparrow	20.3% \uparrow	20.8% \uparrow	20.3% \uparrow	18.0% \uparrow	16.7% \uparrow	15.3% \uparrow
London road map									
Method		$\epsilon = 0.2$	$\epsilon = 0.4$	$\epsilon = 0.6$	$\epsilon = 0.8$	$\epsilon = 1.0$	$\epsilon = 1.2$	$\epsilon = 1.4$	$\epsilon = 1.6$
Pre-defined	EM	7.69 \pm 0.74	7.44 \pm 1.30	7.30 \pm 1.58	7.20 \pm 1.73	7.14 \pm 1.82	7.09 \pm 1.88	7.05 \pm 1.93	7.02 \pm 1.97
Noise	Laplace	8.65 \pm 0.93	8.63 \pm 0.92	8.60 \pm 0.91	8.56 \pm 0.90	8.51 \pm 0.88	8.42 \pm 0.83	8.29 \pm 0.71	8.11 \pm 0.43
Distribution	TEM	8.01 \pm 2.22	7.72 \pm 2.27	7.87 \pm 1.94	7.96 \pm 1.11	7.98 \pm 0.62	7.99 \pm 0.35	7.99 \pm 0.12	7.98 \pm 0.13
Hybrid	RMP	5.86 \pm 0.21	5.07 \pm 0.39	4.49 \pm 0.41	4.09 \pm 0.37	3.83 \pm 0.32	3.65 \pm 0.29	3.53 \pm 0.26	3.44 \pm 0.24
Method	COPT	8.06 \pm 2.24	8.06 \pm 2.22	8.06 \pm 2.18	8.07 \pm 2.15	8.07 \pm 2.10	8.07 \pm 2.04	8.11 \pm 1.19	7.35 \pm 0.93
	LP	4.19 \pm 0.24	2.92 \pm 0.13	2.56 \pm 0.14	2.47 \pm 0.11	2.45 \pm 0.07	2.44 \pm 0.09	2.44 \pm 0.03	2.44 \pm 0.05
	AIPO-R	4.97 \pm 0.21	3.94 \pm 0.13	3.22 \pm 0.08	2.83 \pm 0.03	2.59 \pm 0.01	2.43 \pm 0.04	2.31 \pm 0.03	2.24 \pm 0.05
	LB	1.51 \pm 0.05	1.44 \pm 0.02	1.44 \pm 0.03	1.44 \pm 0.01	1.44 \pm 0.00	1.44 \pm 0.01	1.44 \pm 0.00	1.44 \pm 0.00
AIPO [†]		5.42\pm0.76	4.50\pm0.26	3.90\pm0.17	3.43\pm0.17	3.11\pm0.11	2.88\pm0.09	2.71\pm0.21	2.58\pm0.13
Pre-defined	vs EM	-29.5% \downarrow	-39.6% \downarrow	-46.5% \downarrow	-52.4% \downarrow	-56.5% \downarrow	-59.4% \downarrow	-61.5% \downarrow	-63.2% \downarrow
Noise	vs Laplace	-37.3% \downarrow	-47.9% \downarrow	-54.6% \downarrow	-60.0% \downarrow	-63.5% \downarrow	-65.8% \downarrow	-67.3% \downarrow	-68.1% \downarrow
Distribution	vs TEM	-32.3% \downarrow	-41.8% \downarrow	-50.4% \downarrow	-56.9% \downarrow	-61.1% \downarrow	-63.9% \downarrow	-66.0% \downarrow	-67.6% \downarrow
Hybrid	vs RMP	-7.5% \downarrow	-11.2% \downarrow	-13.2% \downarrow	-16.3% \downarrow	-18.9% \downarrow	-21.1% \downarrow	-23.1% \downarrow	-24.9% \downarrow
Method	vs COPT	-32.8% \downarrow	-44.2% \downarrow	-51.6% \downarrow	-57.5% \downarrow	-61.5% \downarrow	-64.3% \downarrow	-66.5% \downarrow	-64.9% \downarrow
	vs LP	29.3% \uparrow	53.8% \uparrow	52.2% \uparrow	38.6% \uparrow	26.7% \uparrow	17.9% \uparrow	11.0% \uparrow	5.8% \uparrow
	vs AIPO-R	9.1% \uparrow	14.1% \uparrow	21.2% \uparrow	21.2% \uparrow	20.0% \uparrow	18.6% \uparrow	17.5% \uparrow	15.2% \uparrow
New York City road map									
Method		$\epsilon = 0.2$	$\epsilon = 0.4$	$\epsilon = 0.6$	$\epsilon = 0.8$	$\epsilon = 1.0$	$\epsilon = 1.2$	$\epsilon = 1.4$	$\epsilon = 1.6$
Pre-defined	EM	13.96 \pm 1.59	13.95 \pm 2.38	13.88 \pm 2.78	13.80 \pm 3.06	13.73 \pm 3.27	13.69 \pm 3.44	13.65 \pm 3.57	13.64 \pm 3.66
Noise	Laplace	13.75 \pm 1.95	13.62 \pm 2.52	13.48 \pm 2.58	13.41 \pm 2.63	13.37 \pm 2.72	13.36 \pm 2.82	13.35 \pm 2.92	13.35 \pm 3.00
Distribution	TEM	13.62 \pm 3.79	13.53 \pm 4.02	13.77 \pm 3.00	13.98 \pm 1.96	13.95 \pm 1.11	13.92 \pm 0.64	13.83 \pm 0.23	13.72 \pm 0.17
Hybrid	RMP	7.69 \pm 0.37	5.58 \pm 0.37	4.55 \pm 0.24	4.00 \pm 0.24	3.69 \pm 0.28	3.50 \pm 0.31	3.38 \pm 0.32	3.29 \pm 0.32
Method	COPT	8.19 \pm 1.63	13.39 \pm 2.91	13.72 \pm 3.30	13.64 \pm 3.55	13.62 \pm 3.64	13.61 \pm 3.72	13.63 \pm 3.75	13.64 \pm 3.77
	LP	4.80 \pm 0.12	3.14 \pm 0.07	2.67 \pm 0.11	2.56 \pm 0.21	2.53 \pm 0.09	2.52 \pm 0.04	2.52 \pm 0.07	2.52 \pm 0.01
	AIPO-R	6.10 \pm 0.21	4.24 \pm 0.05	3.42 \pm 0.08	2.97 \pm 0.12	2.73 \pm 0.03	2.59 \pm 0.01	2.49 \pm 0.01	2.37 \pm 0.09
	LB	2.18 \pm 0.11	2.04 \pm 0.02	2.03 \pm 0.01	2.03 \pm 0.01	2.03 \pm 0.00	2.03 \pm 0.00	2.03 \pm 0.01	2.03 \pm 0.00
AIPO [†]		7.14\pm0.32	5.26\pm0.21	4.32\pm0.11	3.73\pm0.09	3.36\pm0.12	3.10\pm0.17	2.91\pm0.36	2.77\pm0.05
Pre-defined	vs EM	-48.8% \downarrow	-62.3% \downarrow	-68.8% \downarrow	-72.9% \downarrow	-75.5% \downarrow	-77.4% \downarrow	-78.7% \downarrow	-79.7% \downarrow
Noise	vs Laplace	-48.1% \downarrow	-61.3% \downarrow	-67.9% \downarrow	-72.2% \downarrow	-74.9% \downarrow	-76.8% \downarrow	-78.2% \downarrow	-79.2% \downarrow
Distribution	vs TEM	-47.6% \downarrow	-61.1% \downarrow	-68.6% \downarrow	-73.3% \downarrow	-75.9% \downarrow	-77.7% \downarrow	-79.0% \downarrow	-79.8% \downarrow
Hybrid	vs RMP	-7.1% \downarrow	-5.6% \downarrow	-4.9% \downarrow	-6.7% \downarrow	-9.0% \downarrow	-11.6% \downarrow	-13.9% \downarrow	-15.9% \downarrow
Method	vs COPT	-12.8% \downarrow	-60.7% \downarrow	-68.5% \downarrow	-72.6% \downarrow	-75.3% \downarrow	-77.2% \downarrow	-78.6% \downarrow	-79.7% \downarrow
	vs LP	48.7% \uparrow	67.9% \uparrow	61.8% \uparrow	46.0% \uparrow	32.9% \uparrow	23.0% \uparrow	15.6% \uparrow	10.1% \uparrow
	vs AIPO-R	17.2% \uparrow	24.2% \uparrow	26.6% \uparrow	25.6% \uparrow	23.0% \uparrow	19.9% \uparrow	16.9% \uparrow	17.0% \uparrow

Table 11: Utility loss (km) across different perturbation methods where distance is measured using ℓ_2 -norm metric (Mean \pm 1.96 \times standard deviation).

E Discussions

E.1 Why Using d_p -Distance in Interpolation Can Violate mDP

The interpolation mechanism defined in **Definition 6** and analyzed in **Theorem 2** relies on a weighted geometric combination of anchor perturbation probabilities. Intuitively, it aims to ensure that for any non-anchor record \mathbf{x}_a , the interpolated perturbation distribution $z(\mathbf{y}_k \mid \mathbf{x}_a)$ remains close to the perturbations of nearby anchors, especially those with smaller d_p distances. This design is rooted in the fact that tighter d_p distances induce stricter mDP constraints.

A natural question is whether we can enforce (ϵ, d_p) -mDP for a non-anchor record \mathbf{x}_a by simply ensuring that each anchor in $\hat{\mathcal{X}}_m$ satisfies (ϵ, d_p) -mDP with a reference point \mathbf{x}_b (where \mathbf{x}_b can be either anchor or non-anchor). Specifically, if

$$|\ln z(\mathbf{y}_k \mid \hat{\mathbf{x}}) - \ln z(\mathbf{y}_k \mid \mathbf{x}_b)| \leq \epsilon \cdot d_p(\hat{\mathbf{x}}, \mathbf{x}_b), \quad (165)$$

for each anchor $\hat{\mathbf{x}} \in \hat{\mathcal{X}}_m$, does it follow that the interpolated point \mathbf{x}_a also satisfies

$$|\ln z(\mathbf{y}_k \mid \mathbf{x}_a) - \ln z(\mathbf{y}_k \mid \mathbf{x}_b)| \leq \epsilon \cdot d_p(\mathbf{x}_a, \mathbf{x}_b)? \quad (166)$$

Unfortunately, this implication does not hold if the interpolated value $z(\mathbf{y}_k \mid \mathbf{x}_a)$ is computed as a log-convex combination of the anchor values:

$$\ln z(\mathbf{y}_k \mid \mathbf{x}_a) = \sum_{\hat{\mathbf{x}} \in \hat{\mathcal{X}}_m} \lambda_{\hat{\mathbf{x}}, \mathbf{x}_a} \ln z(\mathbf{y}_k \mid \hat{\mathbf{x}}), \quad (167)$$

where $\lambda_{\hat{\mathbf{x}}, \mathbf{x}_a}$ is a convex coefficient associated with anchor $\hat{\mathbf{x}}$. Substituting into the mDP inequality, we obtain:

$$|\ln z(\mathbf{y}_k \mid \mathbf{x}_a) - \ln z(\mathbf{y}_k \mid \mathbf{x}_b)| \quad (168)$$

$$= \left| \sum_{\hat{\mathbf{x}} \in \hat{\mathcal{X}}_m} \lambda_{\hat{\mathbf{x}}, \mathbf{x}_a} \ln z(\mathbf{y}_k \mid \hat{\mathbf{x}}) - \ln z(\mathbf{y}_k \mid \mathbf{x}_b) \right| \quad (169)$$

$$= \left| \sum_{\hat{\mathbf{x}} \in \hat{\mathcal{X}}_m} \lambda_{\hat{\mathbf{x}}, \mathbf{x}_a} (\ln z(\mathbf{y}_k \mid \hat{\mathbf{x}}) - \ln z(\mathbf{y}_k \mid \mathbf{x}_b)) \right| \quad (170)$$

$$\leq \sum_{\hat{\mathbf{x}} \in \hat{\mathcal{X}}_m} \lambda_{\hat{\mathbf{x}}, \mathbf{x}_a} |(\ln z(\mathbf{y}_k \mid \hat{\mathbf{x}}) - \ln z(\mathbf{y}_k \mid \mathbf{x}_b))| \quad (171)$$

$$\leq \epsilon \sum_{\hat{\mathbf{x}} \in \hat{\mathcal{X}}_m} \lambda_{\hat{\mathbf{x}}, \mathbf{x}_a} d_p(\hat{\mathbf{x}}, \mathbf{x}_b). \quad (172)$$

However, this upper bound is not guaranteed to be less than $\epsilon \cdot d_p(\mathbf{x}_a, \mathbf{x}_b)$. In fact, by *Jensen's inequality* [7], the weighted average of the anchor-to- \mathbf{x}_b distances is generally *greater than or equal to* the direct d_p distance between \mathbf{x}_a and \mathbf{x}_b :

$$\sum_{\hat{\mathbf{x}} \in \hat{\mathcal{X}}_m} \lambda_{\hat{\mathbf{x}}, \mathbf{x}_a} d_p(\hat{\mathbf{x}}, \mathbf{x}_b) \geq d_p(\sum_{\hat{\mathbf{x}}} \lambda_{\hat{\mathbf{x}}, \mathbf{x}_a} \hat{\mathbf{x}}, \mathbf{x}_b) \quad (173)$$

$$= d_p(\mathbf{x}_a, \mathbf{x}_b). \quad (174)$$

This inequality holds because the function $f(\mathbf{x}) = d_p(\mathbf{x}, \mathbf{x}_b) = \|\mathbf{x} - \mathbf{x}_b\|_p$ is convex for all $p \geq 1$, and convexity is preserved

under expectation (convex combinations). As a result, even though each anchor satisfies mDP with respect to \mathbf{x}_b , the interpolated record \mathbf{x}_a may *violate* the (ϵ, d_p) -mDP guarantee. This is also demonstrated in empirical results in Table 2.

E.2 Optimal Privacy Budget Allocation

In our current experimental setup, the secret domain lies in two dimensions ($N = 2$). Under this setting, the global ℓ_2 privacy budget constraint, $(\epsilon_1^2 + \epsilon_2^2)^{1/2} \leq \epsilon$, can be reparameterized as $\epsilon_2 = \sqrt{\epsilon^2 - \epsilon_1^2}$. This allows us to discretize the feasible range of $\epsilon_1 \in [0, \epsilon]$ and perform a one-dimensional grid or linear search over candidate allocations. For each candidate, we evaluate the corresponding utility loss by solving the lower-level perturbation problem. This simple procedure allows us to empirically determine the privacy budget allocation that minimizes utility loss while satisfying the global constraint. However, such brute-force grid search becomes computationally expensive in higher dimensions, as the search space grows exponentially with N .

Bi-Level Formulation and Challenges. More generally, the joint privacy-utility optimization can be formulated as a *bi-level program*. In this formulation, the upper-level problem determines the allocation of per-coordinate privacy budgets $\{\epsilon_\ell\}_{\ell=1}^N$ under a global constraint, while the lower-level problem computes the optimal perturbation mechanism that satisfies (ϵ_ℓ, d_1) -mDP constraints and minimizes utility loss. The formal bi-level structure is:

$$\begin{aligned} \min_{\{\epsilon_\ell\} \in \mathbb{R}_+^N} \quad & \mathbb{E}_{\mathbf{x} \sim \pi} [\mathbb{E}_{\mathbf{y} \sim z^*(\cdot | \mathbf{x})} [\mathcal{L}(\mathbf{x}, \mathbf{y})]] \\ \text{s.t.} \quad & \left(\sum_{\ell=1}^N \epsilon_\ell^p \right)^{1/p} \leq \epsilon, \\ & z^*(\cdot | \mathbf{x}) \in \arg \min_z \mathbb{E}_{\mathbf{x} \sim \pi} [\mathbb{E}_{\mathbf{y} \sim z(\cdot | \mathbf{x})} [\mathcal{L}(\mathbf{x}, \mathbf{y})]] \\ \text{s.t.} \quad & |\ln z(\mathbf{y}_k \mid \mathbf{x}_a) - \ln z(\mathbf{y}_k \mid \mathbf{x}_b)| \\ & \leq \epsilon_\ell \cdot |x_{a,\ell} - x_{b,\ell}|, \quad \forall \ell, \mathbf{y}_k, \mathbf{x}_a, \mathbf{x}_b. \end{aligned} \quad (175)$$

While this bi-level structure provides a principled framework for separating privacy budget allocation from perturbation mechanism design, solving it directly is intractable in our setting. This is due to the non-convexity of the lower-level objective function, $\mathbb{E}_{\mathbf{x}, \mathbf{y}} [\mathcal{L}(\mathbf{x}, \mathbf{y})]$, which prevents the application of standard bilevel optimization techniques such as KKT-based reformulations or Benders decomposition.

Alternative: Surrogate-Based Reformulation. As a practical alternative, we can treat the lower-level optimal objective as an implicit function of the upper-level privacy budgets. Let $U(\{\epsilon_\ell\})$ denote the optimal utility loss achieved by the best mechanism satisfying (ϵ_ℓ, d_1) -mDP. Then the original problem reduces to a single-level formulation:

$$\min_{\{\epsilon_\ell\}} \quad U(\{\epsilon_\ell\}) \quad \text{s.t.} \quad \left(\sum_{\ell=1}^N \epsilon_\ell^p \right)^{1/p} \leq \epsilon. \quad (176)$$

Table 12: Summary of mDP Works by Domain, Mechanism, and Approach Type

Reference	Target Domain	Mechanism	Approach Type	Domain Feature
Andrés et al., 2013 [3]	Location Noise	Laplace (Polar)	Pre-defined Noise	Grid Map
Bordenabe et al., 2014 [6]	Location	Optimal Geo-Ind.	Optimization-based	Grid Map
Chatzikokolakis et al., 2015 [12]	Location	Exponential	Pre-defined Noise	Grid Map
Xiao and Xiong, 2015 [34]	Trajectory	Sequential Perturbation	Hybrid	Trajectory
Yu et al., 2017 [37]	Location	Exponential	Pre-defined noise	Grid Map
Oya et al., 2017 [27]	Location	DP Location Obfuscation	Pre-defined noise	Grid Map
Chatzikokolakis et al., 2017 [10]	Location	Bayesian Remapping	Hybrid	Grid Map
Fernandes et al., 2018 [17]	Text Noise	Laplace	Pre-defined Noise	Embeddings
Feyisetan et al., 2019 [19]	Text	Nearest Neighbor + Laplace	Pre-defined noise	Embeddings
Han et al., 2020 [22]	Voice	Angular Distance + Laplace	Pre-defined Noise	Embeddings
Carvalho et al., 2021 [8]	Text	Truncated Exponential	Pre-defined noise	Embeddings
Chen et al., 2021 [13]	Image	PI-Net (Laplace-based)	Pre-defined Noise	Pixel Space
Yang et al., 2021 [35]	Blockchain	Truncated Geo-Ind.	Pre-defined noise	Grid Map
Imola et al., 2022 [23]	Location	Linear Program	Hybrid	Grid Map
Ma et al., 2022 [25]	Location	Personalized Noise	Pre-defined Noise	Grid Map
Zhang et al., 2022 [38]	Location	Group-based Noise	Pre-defined noise	Grid Map
Min et al., 2023 [26]	Location	Reinforcement Learning	Optimization-based	Continuous Space
Yu et al., 2023 [36]	Location	Bilevel Optimization	Optimization-based	Continuous Space
Galli et al., 2023 [21]	Federated Learning Noise	Laplace	Pre-defined Noise	Grid Map
Qiu et al., 2024 [29]	Location	Decomposed LP	Optimization-based	Continuous Space
Qiu et al., 2025 [30]	Location	Benders Decomposition	Optimization-based	Continuous Space

This reformulation enables the use of black-box or surrogate-based optimization methods. Specifically, we can sample multiple candidate allocations $\{\epsilon_\ell\}$, evaluate the corresponding subproblem to obtain utility loss values, and fit a surrogate model (e.g., regression, response surface) to approximate $U(\cdot)$. This approximation can then be used for efficient optimization over the budget space.

E.3 Limitations of the Interpolation Method for High-Dimensional Data

While the interpolation-based method is most effective in low-dimensional continuous domains, its scalability is challenged in high dimensions.

First, the number of anchor records required for interpolation grows exponentially with dimensionality. Specifically, each N -dimensional cube contains 2^N corner anchors. This rapid growth affects both optimization and memory. In particular, the complexity of Anchor Perturbation Optimization (APO) scales quadratically with the number of anchors, i.e., $O(|\hat{\mathcal{X}}|^2)$, and memory usage becomes increasingly expensive. While these costs are manageable in low-dimensional domains, such as mobility data, time-series, and spatial analysis, applying the method to high-dimensional data (e.g., word embeddings) becomes challenging.

Second, the interpolation mechanism relies on computing a log-convex combination over 2^N anchors within the enclosing cube of each input record. For each record, this entails evaluating $\sum_{\gamma \in \{0,1\}^N} \prod_{\ell=1}^N \lambda_{i_m + \gamma_\ell}$ for every output class, leading to 2^N terms. For example, with $N = 20$, over one million terms are required per record. Although computationally intensive in high dimensions, the method remains efficient and highly

scalable in low-dimensional domains, where interpolation is both fast and accurate.

Third, under dimension-wise composition for ℓ_p -norm mDP, the privacy budget per coordinate diminishes with increasing N as $\epsilon_\ell = \epsilon/N^{(p-1)/p}$ for $p > 1$. For example, when $p = 2$ and $N = 100$, each coordinate receives only one-tenth of the total privacy budget. This budget fragmentation reflects a common trade-off in high-dimensional privacy systems, and motivates future work on joint budget allocation strategies that can more effectively scale to high-dimensional domains.

Finally, the overall runtime and memory requirements scale as $2^N \times N \times |\mathcal{Y}|$ and $2^N \times |\mathcal{Y}| \times 8$ bytes, respectively, where $|\mathcal{Y}|$ is the output space size. While these demands grow rapidly with N , they remain practical for a wide range of real-world applications where the data dimensionality is naturally low. In cases where scalability is a concern, potential remedies include anchor pruning, sparse interpolation, dimensionality reduction, and hierarchical grid partitioning.

While our method is best suited for low-dimensional continuous domains, this setting is highly relevant to many applications in mobility, sensing, geolocation, and healthcare. Moreover, the framework establishes a principled foundation upon which scalable extensions for high-dimensional privacy-preserving data release can be developed in future work.

F Summary of mDP Works

Table 12 shows a summary of mDP works by domain, mechanism, and approach type.